DAMAGE THRESHOLD STUDIES OF GLASS LASER MATERIALS

Norman L. Boling, et al

Owens-Illinois, Incorporated

Prepared for:

Advanced Research Projects Agency

31 August 1974

Security Classification

AD/A004 551

DOCUMENT CONTROL DATA - R & D

(Security classification of title, body of abstract and indexing annotation must be entered when the overall report is classified)

1 ORIGINATING ACTIVITY *(Corporate author)*
Corporate Technology Division
Owens-Illinois, Inc.
Toledo, Ohio 43666

2a. REPORT SECURITY CLASSIFICATION

2b. GROUP

3 REPORT TITLE

DAMAGE THRESHOLD STUDIES OF GLASS LASER MATERIALS

4 DESCRIPTIVE NOTES *(Type of report and, inclusive dates)*
Final Technical Report - 1 July 1972 to 31 August 1974

5 AUTHOR(S) *(First name, middle initial, last name)*

N. L. Boling and G. Dubé

6 REPORT DATE	7a. TOTAL NO. OF PAGES	7b. NO. OF REFS
31 August 1974	~~208~~ 210	47

8a. CONTRACT OR GRANT NO.	9a. ORIGINATOR'S REPORT NUMBER(S)
DAHC 15-72-C-0170	
b. PROJECT NO	
c.	9b. OTHER REPORT NO'S) *(Any other numbers that may be assigned this report)*
d.	ARPA Order No. 2050, Program Code P2D10

10. DISTRIBUTION STATEMENT

11. SUPPLEMENTARY NOTES	12. SPONSORING MILITARY ACTIVITY
	Advanced Research Projects Agency

13. ABSTRACT

In Section I, results of studies of Q-switched laser damage to transparent uncoated dielectric surfaces are presented. It is concluded that surface scratches and digs on some conventionally polished glasses are not of prime importance in damage. Rather, contaminants left by the polishing process determine the damage threshold. Removal of these contaminants can be effected by treatment in hot nitric acid or hot water, raising the threshold to as high as 500 J/cm^2 (30 ns). The effectiveness of the treatment is dependent on polishing history.

An analysis of pulse cutoff by the damage site is also presented. It is concluded that the shape of the cutoff is not related to the damage mechanism, but rather to the manner in which the plasma expands across the laser beam.

In Section II, results of experiments on the feasibility of a high energy density laser are reported. Damage-free operation at more than 4.4 GW/cm^2 (70 J/cm^2 in a 15 ns pulse) was achieved. Restraints on higher irradiance operation and possible improvements are discussed.

14 KEY WORDS	LINK A		LINK B		LINK C	
	ROLE	WT	ROLE	WT	ROLE	WT
Laser Damage, Optical Polishing, and Laser.						

DD FORM 1 NOV 65 1473 (BACK)

S/N 0101-807-6821

SPONSORED BY

ADVANCED RESEARCH PROJECTS AGENCY

ARPA ORDER NO. 2050

PROGRAM CODE P2D10

FINAL TECHNICAL REPORT

As of 31 August 1974

By: N. L. Boling and G. Dubé

DAMAGE THRESHOLD STUDIES OF GLASS LASER MATERIALS

CONTRACT NO. DAHC 15-72-C-0170

EFFECTIVE DATE OF CONTRACT: 1 JULY 1972

EXPIRATION DATE OF CONTRACT: 31 AUGUST 1974

CORPORATE TECHNOLOGY

OWENS-ILLINOIS, INC.

TOLEDO, OHIO 43666

PHONE: (419) 242-6543, EXTENSION 33-003

ib

FOREWORD

This report has been prepared by the Corporate Technology of Owens-Illinois, Inc., Toledo, Ohio, under Contract DAHC 15-72-C-0170.

Dr. Norman L. Boling is the Principal Investigator and Program Manager. Dr. George Dubé is the Project Scientist.

The views and conclusions contained in this document are those of the authors and should not be interpreted as necessarily representing the official policies, either expressed or implied, of the Advanced Research Projects Agency or the U. S. Government.

This report is unclassified.

TABLE OF CONTENTS

FIGURES

Figures for Sections I and II are at the end of the respective sections.

I. SURFACE DAMAGE STUDY FIGURES

TABLES

Tables for Sections I and II can be found at the end of the respective sections.

I. SURFACE DAMAGE STUDY TABLE

II. HIGH ENERGY DENSITY LASER SYSTEM TABLES

ABSTRACT

In Section I, results of studies of Q-switched laser damage to transparent uncoated dielectric surfaces are presented. It is concluded that surface scratches and digs on some conventionally polished glasses are not of prime importance in damage. Rather, contaminants left by the polishing process determine the damage threshold. Removal of these contaminants can be effected by treatment in not nitric acid or hot water, raising the threshold to as high as 500 J/cm^2 (30 ns). The effectiveness of the treatment is dependent on polishing history.

An analysis of pulse cutoff by the damage site is also presented. It is concluded that the shape of the cutoff is not related to the damage mechanism, but rather to the manner in which the plasma expands across the laser beam.

In Section II, results of experiments on the feasibility of a high energy density laser are reported. Damage-free operation at more than 4.4 GW/cm^2 (70 J/cm^2 in a 15 ns pulse) was achieved. Restraints on higher irradiance operation and possible improvements are discussed.

I. SURFACE DAMAGE STUDIES

I-1. Summary

This is the final report on contract DAHC 15-17-C-0170 on which work was initiated 1 July 1972, and terminated 31 August 1974. This work has been an extension of work begun under contract DAHC 15-69-C-0303 which extended from 1 July 1969 to 1 July 1972.

Only results obtained since the last semiannual report of 1 July 1973 will be reported herein, with previous data recapitulated only as needed for clarity. The reader is referred to past reports for a complete view of work accomplished under the contract.

The subject of Section I is Q-switched laser damage to glass surfaces. Although it is generally held that a TEM_{oo} mode laser is necessary for accurate, reproducible work on surface damage, we have found that in some circumstances a multimode laser is acceptable. With a multimode glass oscillator-amplifier system, exit thresholds of 140 J/cm^2 (30 ns) were measured on ED-2. With a carefully constructed TEM_{oo} mode laser, thresholds of 125 J/cm^2 were obtained. These thresholds are the same within experimental accuracy. Multimode lasers can suffice for accurate work because gain saturation tends to ''smooth'' the beam profile and because small ''hot spots'' are erased in the far field.

Although basic theory suggests that scratches and digs on the surface should lower the threshold for damage, we have found that defects on ED-2 laser glass after conventional, routine finishing in a commercial shop are not detrimental. In fact, prolonged polishing to reduce the size

and number of surface defects can sometimes result in a lower threshold. We attribute this to increased contaminants introduced into the surface. We conclude that removal of such contaminants is more important than ''superpolishing'' for increasing the threshold. An effective method of removal, for ED-2, appears to be submersion of the surface for several hours in hot nitric acid. The effect of this treatment is dependent on polishing history, but in some cases the entrance threshold is raised permanently from approximately 150 J/cm^2 to almost 500 J/cm^2 without a detrimental effect on the surface optical quality. Treatment in boiling water is almost as effective.

Many materials of current interest will not withstand hot nitric acid or water. We suggest that other high-temperature agents might be effective in greatly increasing the threshold for these materials.

An analysis of pulse cutoff by the damage site is also presented in Section I. We conclude that significant pulse attenuation is always due to a plasma and that the details of attenuation (fast cutoff, slow cutoff, etc.) can be explained by considering the plasma expansion rate and beam size. It is inappropriate to infer a particular damage mechanism from the pulse cutoff.

At the outset of this work several years ago, surface damage to laser glass was held to be a limiting factor in Q-switched operation. Damage thresholds of 30-40 joules/cm^2 (30 ns) were often obtained. In the course of this work and that of many other investigators, laser glass with exit threshold greater than 100 J/cm^2 is now commercially available on a routine basis. This has been accomplished first by simply making

accurate measurements of the threshold, which in some cases had always been over 100 J/cm^2, and second, by learning to avoid certain polishing compounds and/or polishing procedures. With thresholds of over 100 J/cm^2, surface damage is no longer a limiting factor in many glass systems. In those systems where it might be a problem, we now know how to increase the exit threshold to over 300 J/cm^2 (about 500 on the entrance).

Although self-focusing damage was not specifically a subject of this contract, some work on obtaining n_2 from linear parameters is included here, since this work would not have been undertaken in the absence of the contract. The results are included as an appendix in the form of a paper by N. L. Boling, A. J. Glass of Lawrence Livermore Laboratory, and A. Owyoung of Sandia Laboratory.

I-2. Introduction

In Section I we discuss several aspects of laser-induced surface damage. Each subsection is self-explanatory. Two subsections, I-3 and I-4, will perhaps be of the most practical interest. Section I-3 deals with the role of surface geometrical defects in damage, and Section I-4 with the use of hot nitric acid or water to remove surface contaminants. These two subsections are complete in themselves and can be read independently of the rest of the report.

I-3. Experimental Arrangement and the Non-Necessity for a TEM_{00} Laser

The experimental arrangement, including the laser and damage detection techniques, is described in detail in refs. 1 and 2. The laser is

made up of a glass oscillator followed by four amplifiers. It operates in the TEM_{oo} mode and emits several joules in a 30 ns pulse. Measurements at 4 ns have also been made, but unless specified otherwise, results herein were obtained with 30 ns pulses.

Output energies of several joules allow us to do damage testing with a relatively large spot, about 1.8 mm diameter. This yields damage thresholds of practical interest in real systems where large beams are used of necessity. These thresholds are often much different from those obtained with spots of a few microns or a few tens of microns diameter.

Early in this work, it was taken as a truism that a TEM_{oo} laser is required to do accurate, reproducible damage measurements. This was based on reports indicating that very low thresholds are obtained with multimode beams relative to those obtained with TEM_{oo} beams. Consequently, we made a significant effort to design and construct a TEM_{oo} laser for this study. We now believe this was not necessary, although it is still firmly held to be so by many workers.[3] We base this conclusion on damage thresholds obtained with a TEM_{oo} beam vs. those obtained operating multimode with a saturated glass oscillator-amplifier system. For the multimode case, the damaging spot was several mm in diameter, and the energy density was determined as an average across the spot.[4] Damage measurements were made in the far field for both the multimode and single-mode cases. As reported in ref. 4, the multimode exit damage threshold for ED-2 laser glass was approximately 140 J/cm^2. With the carefully designed TEM_{oo} laser, exit thresholds were measured as approximately 125 J/cm^2, with the average across the 1.8 mm spot being

100 J/cm^2. (This lower average value has been accepted by us for reporting purposes in order to keep any error on the conservative side.)

The argument that has been used for the necessity of using TEM_{oo} beams involves small ''hot spots'' often seen in multimode beams. It is argued that the energy density in these hot spots can be as much as an order of magnitude larger than the average density across the entire spot. This is perhaps true at the end of an amplifier where self-focusing, for example, of the beam has occurred; but it is instructive to consider semiquantitatively what happens to these ''hot spots'' in the far field.

Consider a spatially square beam of diameter D_1 and energy density ρ_1 incident on a lens. In this beam is a hot spot of diameter $D_2 \ll D_1$ and energy density ρ_2. D_1 and D_2 are focused to diameters d_1 and d_2 respectively. Elementary arguments show that the relative intensity between the beams D_1 and D_2 incident on the lens is decreased by approximately the factor $(D_2/D_1)^2$ in the focused beams d_1 and d_2. Thus if a 100 micron hot spot in a 1 cm beam has ten times the energy density of the 1 cm beam and these two are focused by the same lens, the intensity of the focused 10 μm beam will be only 10^{-3} that of the focused 1 cm beam. This argument is very crude, of course, but it serves to partially quantify the statement that ''hot spots'' are diffracted out of the test beam very rapidly.

Another reason for the obtainment of similar thresholds in single- and multimode beams is advanced by G. Dubé. When a glass amplifier is operated in the saturated region, hot spots tend to be smoothed over. This was probably the case in the work of ref. 4 where the last amplifier

was operated well in the saturation region. The point we wish to emphasize here is that fairly accurate damage measurements can be made with a large multimode beam when the sample is placed in the far field. In fact, because the average energy density is relatively easy to measure in a large beam, it is probably preferable to do many damage studies with large multimode beams rather than very small (a few microns) single-mode beams where accurate spot sizes are difficult to ascertain.

I-4. Studies of the Relation between Geometrical Surface Defects and the Damage Threshold

In this section, we discuss the relation between surface defects - scratches and digs - and the susceptibility of the surface to damage. More specifically, we are interested in whether or not polishing the surface to a high degree of smoothness affects the damage threshold. Before attacking this question, it is appropriate to have an estimate of just how high the surface threshold can be raised. Obviously, the limit on the surface threshold is that of the intrinsic breakdown level of the material, so the problem becomes that of determining the ratio of surface threshold to intrinsic bulk threshold for so-called ''conventionally polished'' surfaces.

We use the terms ''conventionally polished'' and ''superpolished'' very loosely. By ''superpolishing,'' we generally refer to a ''bowl-feed'' process which, if done carefully, leads to a surface with fewer and smaller scratches and a low rms roughness value. However, the effect of the polishing process on the surface depends on many factors. Among these are the type and size of the grinding materials used,

polishing compound, composition polishing time, amount of water used on the lap, etc. Seemingly insignificant changes in any one of these can lead to large changes in the modified surface layer created by polishing. Because of this complexity, we stress that the terms ''super'' and ''conventional'' are not sufficient to describe polishing. We use them only because they have been used to describe results of other damage studies.

To address the question of bulk vs. surface threshold, we refer to the work of Olness and Swain.[5,6] They investigated the effect of hydrofluoric acid etching on the entrance surface threshold of three commercial glasses. A 5 ns, TEM_{oo} pulse from a glass laser was used. The glasses as they were received from the manufacturer exhibited entrance thresholds of 35 J/cm^2 (7 GW/cm^2). We have made measurements at 4 ns at Owens-Illinois that agree well with these values. Upon etching in HF acid and glycerin for approximately two hours, the threshold increased by a factor of two to three, a significant increase. But when the samples were refinished using barnesite and a pitch lap, the result was even more dramatic. The threshold increased more than an order of magnitude, going as high as 380 J/cm^2 (76 GW/cm^2).

Since these measurements refer to the entrance surface and since the electric vector on the entrance has the same magnitude as in the bulk, these values can be used to indicate a minimum value of the bulk threshold. That is, since Olness and Swain saw no internal damage,[7] we can conclude that the bulk threshold was at least an order of magnitude higher than the conventionally polished surface threshold.

We have found further evidence for this in other work. Feldman has measured a minimum intrinsic bulk threshold of 50-60 GW/cm^2 at 25 ns for laser glasses.[8] At Owens-Illinois, we have regularly been obtaining thresholds of 4 to 6 GW/cm^2 (30 ns), again at least an order of magnitude below the minimum bulk threshold.

On the other hand, recent measurements have been made of the ratio of bulk-to-surface breakdown levels using the same test setup for both measurements.[9] In these measurements, a small beam ($\approx$ 20 μm) was focused first inside the sample and then on the surface. The probability of breakdown in these two positions was measured. For conventionally polished BSC (borosilicate crown) glass, a bulk-to-surface ratio of only 1.7 was obtained. Thus, there is a rather wide discrepancy among reported bulk-to-surface ratios.

One reason for the discrepancy could be that, in the work of ref. 9, shots on which it was judged inclusions were struck were not counted, nor were the levels at which these inclusions damaged reported. That is, only shots on which it was judged that intrinsic damage had occurred were counted. This could lead to the high reported values for surface breakdown (34 GW/cm^2 or $\approx$ 400 J/cm^2 at 12 ns).

Another reason for the discrepancy could lie in the subtleties involved in using very small beams for damage studies, as was done in ref. 9. If we accept as a premise the idea that, for small enough beams, there is no sharp damage threshold, but rather only a probability for damage at a given energy density, it is profitable to analyze an experiment that compares the probability of bulk breakdown to surface breakdown. In such an experiment, damage is due to at least one free electron gaining enough energy to begin an avalanche.

Consider Figure I-1. The laser beam is focused through a microscope lens of focal length f to a spot of diameter d on a sample surface that has no inclusions and is perfectly uniform. Let's suppose in this ideal experiment that the beam profile is square and not Gaussian as in most real experiments. That is, it is possible to associate unambiguously an energy density to any shot that causes damage. In this way we can ascertain the electric field "seen" by the electron that starts an avalanche. One proceeds to hit the sample with a large number of shots at a constant energy level, counts the number of these that cause damage, and then determines the probability $P_S(E)$ of damage at that energy level. Now suppose d is doubled while maintaining the energy density constant, and the experiment is repeated in a second series of shots. It is obvious that, if the beam is small enough to see statistics, the probability for damage will be greater in the second series. The reason for this, of course, is that the probability of damage depends on the initial number of free electrons available to initiate an avalanche in the irradiated volume.

The point of this argument is that, for a beam small enough to see statistics on a uniform surface, the parameter of practical interest is not the probability of damage at a given energy level, which is system-dependent, but rather the probability of damage per unit area of surface irradiated. In fact, even this is over simplifying things. The breakdown occurs not an idealistic two-dimensional surface, but in a surface layer of probably a few hundred angstroms depth. (We consider this depth to be roughly that of the modified surface layer left by the polishing process. It is in this layer that one expects higher free electron

densities due to stresses, impurities, etc.) Thus, one should really consider the probability of damage per unit surface volume as indicated in Figure I-1.

Let us imagine next that the beam is now focused inside the sample to measure the probability of bulk breakdown $P_B(E)$, as in Figure I-2. Again, it is obvious that the number of free electrons in the focal volume V_B is system-dependent, and therefore that $P_B(E)$ is system-dependent.

If we consider the ratio $P_B(E)/P_S(E)$, it might appear that the system-dependence cancels. That this is not the case can be seen by considering that the ratio V_B/V_S (in Figures I-1 and I-2) changes as the focal length of the lens changes. That is, V_B is roughly proportional to f^3, while $V_S \propto f^2$.

Thus, the ideas of electron avalanche and damage probability lead us to conclude that the ratio of bulk-to-surface breakdown levels cannot be measured with very small beams. However, one might make the seemingly obvious argument that, if the sample surface is placed in the middle of the beam waist as in Figure I-3, and the bulk is seen to damage before the surface, then surely the surface breakdown level is at least that of the bulk. After all, the beam has to pass through the surface to get to the bulk! Again, this argument is wrong if one accepts the idea of damage probability. This can be seen by considering again that V_B/V_S (Figure I-3) changes with f. If f is doubled, for example, the number of free electrons in the surface volume is quadrupled, while the number of free electrons in the half of the focal volume in the bulk goes up by about a factor of nine, and therefore $P_B(E)/P_S(E)$ is not constant.

We have gone on at some length with this analysis of small beam results in an attempt to resolve the discrepancy in reported ratios of bulk-to-surface breakdown. On the basis of this analysis and reported large beam results, we conclude that, on conventionally polished laser glass, which exhibits entrance thresholds of 4-6 GW/cm^2 at 30 ns, the surface threshold is at least an order of magnitude below the bulk threshold.

We return to the effect of scratches and digs on the surface threshold. The idea that a scratch or dig should influence the damage threshold stems from the work of Crisp, et al, who showed the importance of considering the local macroscopic field in damage studies.[10] Thus by a straightforward application of Fresnel's equations, they were able to explain the asymmetry between entrance and exit damage thresholds. Bloembergen extended the ideas of Crisp, et al, by observing that the electric field of a laser beam is enhanced at scratches and digs.[11] He therefore concluded that such defects should lead to a lower damage threshold. This lowering of the damage threshold by defects would take place whether damage was due to either avalanche or inclusions. However, because small enough inclusions do not damage, and because free electrons can diffuse out of the high electric field regions around small enough scratches before an avalanche can build up, it was theorized in ref. 11 that defects of less than about 100 Å in their smallest dimension should not lower the threshold.

Before Bloembergen's analysis, Guiliano had conducted surface damage experiments on ion polished sapphire.[12] The sapphire samples were

generally smoother than is often achieved with a conventional polish, and the threshold was indeed higher by a factor of from two to six than on conventional surfaces. These results are often cited as confirmation of the correctness of Bloembergen's analysis. However, an alternative interpretation is that the increased threshold resulted because ion polishing introduces less contaminants than a conventional process.

More recent experimental work on the comparison of intrinsic bulk breakdown to intrinsic breakdown of superpolished surfaces has also seemed to support Bloembergen's analysis.[9] In fact, the work of ref. 9 implies that glass surfaces do <u>not</u> have to be polished very carefully to raise the intrinsic threshold of the surface to that of the bulk. (Again, inclusion damage was excluded in the data.) Close examination of the electron micrographs of superpolished BSC glass in ref. 9 reveals scratches as large as 2000 Å, and yet the intrinsic surface threshold was reported to be the same as that of the bulk. Laser glass can be polished to this degree (< 2000 Å scratches) on a routine basis with ''conventional'' polishing techniques.

Damage thresholds of ''conventionally polished'' and ''superpolished'' fused quartz are also compared in ref. 9. The ''conventional polish'' can only be described as terrible. Defects as large as one micron are clearly visible. The ratio of surface-to-bulk threshold on this was again 1.7. The ''superpolished'' fused quartz again had a surface easily obtainable by routine polishing. Our interpretation of these micrographs and reported results is that no special care in polishing is required to achieve the results presented in ref. 9.

We note that the experiments of ref. 9 were done with a very small beam ($\approx$ 20 μm) and that a probability rather than threshold interpretation was made. The analysis of small beam measurements presented above causes us to question the meaningfulness of the ratios reported. However, such experiments, if the geometry is maintained, should reflect changes in the surface-to-bulk ratio from sample to sample of the same type material.

The two works discussed above (refs. 9 and 11) are consistent with the idea that a smoother surface leads to a higher damage threshold. On the other hand, the work of Olness and Swain[5,6] on HF etched laser glass might lead one to a different conclusion. After deep etching of the commercial laser glasses they tested, which could have been expected to exhibit occasional scratches of a few thousand angstroms when supplied by the vendors, the surfaces were left in extremely rough condition. Defects as large as 3 to 4 microns can be seen in the optical micrographs of ref. 5. In this case then, the change was from a fairly smooth surface to a very rough one, and yet the damage threshold <u>increased</u> by an order of magnitude. This suggests two points. First, increasing the surface geometrical defects does not necessarily decrease the damage threshold. Second, surface contaminants play the major role in determining the damage threshold.

Because of these seemingly conflicting results, we have measured the damage threshold of several samples that have been bowl-feed polished. We note again that a large beam was used in our experiments, so no shots could be discarded because of inclusion damage. Thus, the

thresholds we measure are practical; i.e., they are representative of what one might expect in a real laser system that of necessity utilizes a ''large'' beam.

To ascertain the relative smoothness of the surfaces we have damage tested, electron microscopy was used. Some may object that surface smoothness cannot be quantitatively measured in this way and that an rms roughness measurement would be more appropriate. However, since theory indicates that only defects larger than about 100 Å are detrimental,[11] we are interested only in isolated scratches and digs. Electron micrographs are better suited for this than are rms roughness measurements.

Figures I-4 and I-5 juxtapose two surfaces of ED-2 laser glass. Both have been bowl-feed polished in the same manner, except that the one in Figure I-4 was polished longer in an attempt to further remove scratches. This surface did in fact present a slightly better appearance when viewed in its entirety. Yet the damage threshold on this longer polished surface was only 45 J/cm^2 (1.5 GW/cm^2), while the threshold of the other surface was 90 J/cm^2. These two surfaces, however, were polished with jewelers rouge (iron oxide), which is known to cause low damage thresholds at 1.06 μm.[2] Initial damage is always due to inclusions on rouge-polished surfaces. But two inferences can be drawn from the data. First, longer polishing to get rid of scratches can lead to a much lower threshold. Second, the polishing history, aside from geometrical defects, is of prime importance in damage.

Another set of comparison surfaces is shown in Figures I-6 and I-7. These are fused quartz surfaces polished in the same manner by conventional techniques. The surface in Figure I-7 has been subjected to an acid etch, leaving pits of about 1000 Å. The entrance damage thresholds for the surfaces of Figures I-6 and I-7 were respectively 310 and 360 J/cm^2, about the same within the accuracy of the measurements.

Still another set of comparison surfaces is shown in Figures I-8 and I-9. In Figure I-8 is an ED-2 surface conventionally polished with barnesite. Scratches as large as 1000 Å can be seen. (It is instructive to compare this ''conventional'' surface with the ''superpolished'' BSC glass surface of ref. 9.) Figure I-9 shows a very good bowl-feed polished surface. This sample clearly warranted the description ''superpolished.'' No scratches larger than 100 Å can be seen. The entrance damage thresholds of the two surfaces (Figures I-8 and I-9) were the same, 150 J/cm^2 (5 GW/cm^2).

In those cases described above and in similar other cases, we have been unable to find an example of an increase in threshold due to a decrease in the geometrical surface defects. In fact, the opposite has sometimes been the case. This seems in clear conflict with the basic argument that the field is enhanced at scratches and digs. We offer the following speculations in regard to this conflict:

1. As pointed out by Bloembergen,[11] the degree of field enhancement can only be estimated. Thus the calculations of ref. 11 are only rough estimates. Of the three ideal defects treated, the one which enhances the electric field the most - by a factor of n^2 - is the

''vee'' shaped groove. For this defect the maximum effect on ED-2, with an index of 1.56, would be a lowering of the threshold by a factor of about 5. Given the nature of the calculations, this factor might be much too high.

2. Given that all other conditions are equal, it might be true that a scratched surface will damage before a smooth one. This would not be inconsistent with our experimental results. In the examples we have discussed, the surfaces were always different in ways besides the size of scratches by virtue of having been etched or not, or polished for different times, etc.

3. Free electrons might diffuse out of the high field region faster than estimated in ref. 11. This could make scratches of the size found on most polished surfaces innocuous.

4. If one considers electron avalanche initiated by a free electron to be the mechanism of surface damage, there is a clear theoretical reason why scratches are not as important as might be thought. Consider a single 1000 Å spherical pit struck by the laser beam, for example. By the arguments of ref. 11, the surface with this pit should damage more easily than a perfectly smooth surface. But the field is enhanced in a region of only about 10^{-15} cm^3 around the pit. The probability of finding a free electron in this high field region is small. The extension of this argument is obvious. The density of defects on the surface must be taken into account if avalanche is the breakdown mechanism.

Whatever the case, there are two points that are clear from our experiments. First, surface contaminants are often more important than

scratches and digs in lowering the damage threshold. Second, polishing of laser glass to a degree greater than that readily obtainable by conventional polishing techniques does not raise the damage threshold, and might even lower it through introduction of more surface contaminants.

In closing this section, we note that the surfaces tested and shown in the electron micrographs were carefully selected. In general, the appearance of polished glass surfaces in electron micrographs varies widely, even when the same glass, polishing compound, and polishing techniques are used. This is illustrated in Figures I-10 through I-17 which show ED-2 laser glass polished under various conditions. Note the inclusions readily visible on some of the samples.

I-5. Use of Hot Nitric Acid or Hot Water to Increase the Surface Threshold

I-5.1. Introduction and previous results

Having concluded that rendering a glass surface free of scratches and digs does not generally raise its damage threshold, we have concentrated on surface treatment techniques. These treatments have been based on the premise that surface damage in large beams is due to surface contaminants left by the polishing process.

Acid treatments to raise the surface threshold are, of course, not new. Several investigators have tried them with different acids and varying results. Davit[13] used a solution of sulfuric and hydrofluoric acids and found an increase in the threshold lasting only a few minutes. Sometime ago, we tried very weak solutions of hydrofluoric acid on ED-2 laser glass. No increase in threshold was observed. On the other hand, Yamanaka, et al, have reported a substantial ($\approx 40\%$) threshold enhancement

on barium crown glass after a 10-minute immersion in 10% hydrofluoric acid.[14] They made no comment on the optical quality of the surface after etching. In their work, Olness and Swain [5,6] used a very strong solution of hydrofluoric acid on silicate glasses and the surface was deeply etched. Although they obtained up to a tenfold increase in the threshold, the surface was optically unacceptable.

When one views superpolishing and acid etching collectively, a pattern emerges. Continued polishing to achieve smoother surfaces can lower the threshold. When enough of the surface layer is removed, the threshold can be increased dramatically. These results imply that polishing contaminants are of primary importance in damage, and that a method for removing them without deleterious effects on the optical finish would lead to an increase in threshold useful in practical systems.

I-5.2. Experimental results

We have treated barnesite-polished ED-2 laser glass with hot (just below boiling) 0.4 molar nitric acid. The results have been striking. The entrance threshold is raised from 150 J/cm^2 (30 ns) to as high as 470 J/cm^2. Furthermore, the surface is left in good optical condition, although in some cases the acid exposes subsurface scratches left by polishing. Further yet, the effect appears to be permanent. Acid-treated ED-2 left in the lab environment for almost two months and then cleaned and subjected to a damage test still exhibited a threshold of 470 J/cm^2.

On the other hand, the effect of the hot acid treatment varies with polishing history. The increase in threshold for the ED-2 barnesite-polished glass given above was 320 J/cm^2. This was for a set of samples

all polished in the same manner in a particular polishing shop. The increase was consistent from sample to sample in this set. However, for ED-2 polished by different techniques, including bowl-feed and different polishing compounds, the increase in threshold varied from almost zero to 270 J/cm^2. The variation in results for ED-2 is indicated in Table I-1. (The listed thresholds are accurate to within ± 25%.)

These results clearly indicate the importance of the polished surface layer. That this is the case is not surprising when one considers the complexity of the process we simply label "polishing." The earliest discussion of the polishing problem appears to be by Robert Hooke.[15] It has been a subject of speculation by such luminaries as Newton and Lord Rayleigh, yet no satisfactory explanation of the polishing process has yet been devised. There is still contention over whether polishing is a result of abrasion by ever-finer particles, a melting and resolidifying of the surface with intermediate flow filling in scratches, or even a chemical process.

An example of how the surface is affected by the details of polishing is found in a paper by Bennett and King.[16] They used ellipsometry to measure the thickness and refractive index of the surface layer on fused quartz. After polishing by a given process, they found the modified surface layer to be 100-200 Å thick with an index 0.005 ± 0.010 above the bulk value of 1.46. By changing only the amount of water on the pitch lap, they found the surface layer could be several hundred angstroms thick with the outer part having an index as high as 1.50.

Let us return to the effect of the hot nitric acid bath on polished glass surfaces. Figures I-18 and I-19 show respectively "before" and

''after'' electron micrographs of a treated surface. The glass in this case is EY-1, an Owens-Illinois Faraday rotator glass. ED-2 shows a similar effect after nitric acid treatment. The acid treatment causes a surface graininess. One might expect this to lead to increased surface scattering. Although we have not done quantitative scattering measurements, visual observation of a He-Ne beam passing through before and after surfaces indicates no increased scattering. As is well known, visual observations can be a sensitive test for differences in scattering properties.

When ED-2 is polished with diamond, the increase in threshold after acid treatment is negligible (see Table I-1). Electron micrographs of acid-treated surfaces polished with diamond show some tendency toward graininess but not as much as in the barnesite-polished case where there is a large increase in threshold. This is still another indication of differences in the modified surface layer left by polishing.

We have subjected glasses other than ED-2 to hot nitric acid. The results for barnesite-polished EY-1 were good, with the entrance threshold increasing from 120 J/cm^2 to 400 J/cm^2. The surface was left in good optical condition (see Figure I-19). The acid does not remove scratches. A large scratch was visible in the sample of Figure I-19 (not shown in the figure). It is possible that this scratch was exposed by the acid bath. It is known that what appears to be a very smoothly polished surface often has subsurface crevices that have been covered over in the polishing process. These crevices can be exposed with mild acid etches.

Other glasses treated were fused quartz; E-11, a high index bismuth glass; and FK-6, a Schott fluorosilicate glass. The barnesite-polished fused quartz showed no increase in threshold. The entrance threshold was 300 J/cm^2 for the treated and untreated samples. No other polishing process was tried on the fused quartz. The nitric acid badly damaged the E-11 surface, leaving myriad cracks. The same was true for FK-6. The FK-6 surface could be removed in flakes after acid treatment.

I-5.3. Theory

We turn now to speculation about why the hot acid bath can be so effective in increasing the threshold. The effectiveness of the treatment is time-dependent; Figure I-20 shows the entrance threshold vs. time in the acid bath for barnesite-polished ED-2. The threshold begins at about 160 J/cm^2, rises rapidly for the first few hours, and then approaches an asymptotic value. The shape of this curve and the times involved suggest that the increase in threshold is related to a diffusion process. To further explore this, we examine the mathematics of diffusion.

The diffusion equation is

$$\frac{\partial C}{\partial t} = D \frac{\partial^2 C}{\partial x^2} \qquad (1)$$

where C is the concentration of the atomic species of interest, t is the time of diffusion, x is the diffusion distance, and D the diffusion coefficient. As a system, we take our 1 cm^3 glass samples submerged in nitric acid. This approximates a semiinfinite solid in contact with a semiinfinite liquid, and the appropriate solution of (1) is

$$C = C_o \left(1 - \text{erf} \frac{x}{2\sqrt{Dt}}\right) \qquad (2)$$

where C_o is the concentration of the species of interest in the liquid. Arbitrarily, setting $C/C_o = 1/2$ we obtain

$$X_{1/2} \simeq \sqrt{Dt} \qquad (3)$$

or

$$X_{1/2} \alpha \sqrt{t}$$

$X_{1/2}$ is the distance into the glass surface at which the concentration C is one half C_o.

The fractional change in untreated surface threshold $\Delta(DT)/DT$ is plotted in Figure I-21. We see that indeed the fractional change in threshold follows $\sqrt{t}$ very well, except the point at 24 hrs is far off the curve. This is not surprising, since one does not expect the threshold to increase indefinitely as diffusion progresses.

To further check the reasonableness of a diffusion process, we set $t = 10^4$ sec and $x = 1000$ Å in eq. (3). We choose this value of t because the threshold is approaching a maximum after about 3 hrs. 1000 Å is reasonable for the modified surface layer left by polishing. The value then obtained for D is 10^{-14} cm^2/sec. The diffusion coefficient in water for a glass similar to ED-2 is 10^{-16} cm^2/sec. Thus 10^{-14} cm^2/sec is reasonable when one considers that D for glasses typically changes two or three orders of magnitude between 25°C and 100°C.

This strong dependence of D on temperature might also explain why we have seen large increases in the threshold through acid treatment at

98°C while others have not when using acid at room temperature. It also suggests that treatments at higher temperature, say 150°C in a pressure cooker, might be effective in decreasing the strong dependence on details of polishing.

A peculiar aspect of acid-treated ED-2 shows up in the damage morphology. Figure I-22 shows an optical micrograph of an exit damage site. One can see what appears to be a thin film on the surface. This film has been partially stripped away by the plasma accompanying the damage. Interference micrographs show that this film is about 400 Å thick. The film does not occur on untreated ED-2, or on treated or untreated EY-1 or fused quartz. Normal cleaning of the undamaged surface with lens tissue does not appear to damage the film. We will not speculate about the nature of this film other than to say that one might expect nitric acid to leach Li ions from ED-2, leaving a silica-rich surface layer. This would be consistent with a diffusion process.

Boiling water is almost as effective as hot nitric acid in increasing the surface threshold of barnesite-polished ED-2. Twenty-four hours in boiling water raised the entrance threshold of ED-2 to 360 J/cm^2. However, no film appears around the damage sites on water-treated samples.

In all this discussion of diffusion, we have said nothing about what is diffusing. This is because we don't know. It might be polishing contaminants, but since most atoms of polishing compounds are large, diffusion would be very slow relative to, say, diffusion of lithium. We leave open the possibility that evidence for a relation between the increase in threshold and diffusion is misleading. The hot nitric acid and hot water might simply be very effective cleaning agents.

I-5.4. Conclusions and implications

We have found a 24-hour treatment in hot (98°) nitric acid or boiling water can greatly increase the surface threshold of laser glass. The effectiveness of the acid treatment is highly dependent on polishing history of the surface. These results are consistent with the view that surface contaminants left by polishing are of primary importance for surface damage. The results are also consistent with those of Section I-3 where it was shown that longer polishing to achieve a smoother surface can lower the damage threshold.

We do not completely understand why a hot acid or water treatment is so effective, but the data suggest diffusion plays a role. Because of this, and because acid at room temperature is not effective, we suggest that treatments at still higher temperature may remove the dependence on polishing history.

We have dealt mostly with laser glass in these studies, since that was our charter under the contract guiding the work. Surface damage on laser glass can be a practical problem unless care is taken to avoid rouge polish. However, we have determined that ED-2 laser glass produced in an optical production shop normally has an exit threshold of well over 100 J/cm^2 for large beams (30 ns). In most glass systems, self-focusing leads to damage before the surface threshold is reached. For most purposes, therefore, a surface treatment to raise the threshold is not required. (This may not apply to some systems, such as rangefinder oscillators where surface damage can be important.)

Perhaps the greatest potential use for the results presented here is for other types of laser materials where surface damage is still a problem. Much effort is being expended, for example, on 10.6 μm window materials. Many of these materials cannot be subjected to boiling water or hot nitric acid without deleterious effects. However, other hot liquid agents might prove effective.

Another area of concern is damage to glass surfaces by flashlamp light. This is particularly important in some of the large disk lasers being used or constructed for fusion studies. We have found that thorough cleaning can greatly decrease susceptibility of laser glass to flashlamp damage. We are not sure that this damage is due to remnants of polishing compound, but if it is, the treatments discussed here might be effective.

I-6. Analysis of Laser Pulse Cutoff by Damage Site

In studies of laser-induced damage to dielectrics, a commonly observed phenomenon is cutoff of the laser pulse as it passes through the damage site. The shape of the pulse transmitted through the damage site - that is, the wave form seen on the photodetector - takes many forms. Sometimes the pulse is attenuated in less than the response time of the detector (usually less than one nanosecond); sometimes it is gradual, taking place over 15 ns of a 30 ns pulse, for example; and often there is no perceptible attenuation at all, even when damage has occurred.

The transmitted pulse shape has been used to infer the mechanism of damage in some studies.[11,17] If the cutoff is sharp, the mechanism was inferred to be electron avalanche. Inclusion damage was inferred

from a gradual attenuation. It is difficult to understand how an inclusion can lead to significant attenuation under the conditions described in ref. 17. In that work, a 20 μm diameter beam was used. Inclusions that lead to damage in a Q-switched pulse are often much less than a micron in diameter. Such an inclusion would intercept much less than one percent of the power in the 20 μm beam, an amount too small to be detected on a photodiode-oscilloscope arrangement.

One might argue that it is not the inclusion but the damaged area resulting from the inclusion explosion that intercepts a significant part of the beam. This is feasible, since sound, and therefore mechanical damage, can traverse a 20 μm beam during a Q-switched pulse. However, it has been shown that inclusions can lead to craters as small as one micron in diameter.[18] Again the cross-sectional area of such a crater does not intercept enough energy from the beam to cause significant attenuation.

It was also shown in ref. 18 that inclusion damage can occur without an accompanying plasma. Thus, one cannot argue that an inclusion initiated plasma is responsible for pulse cutoff.

Because so much emphasis has been placed on interpretation of attenuated pulses, we present an analysis of the phenomenon. To begin, we assume that the plasma that often accompanies surface damage is responsible for any <u>significant</u> interception of the damaging pulse. That is, we take inclusion attenuation to be physically unreasonable. The damaging beam is taken to be of Gaussian cross section. The temporal dependence of the pulse is approximated by a half sine wave. A plasma is born at a point

at $\bar{R}$ on the surface sometime during the pulse. (A cylindrical coordinate system with origin at the Gaussian beam center is used.) The plasma electron density is greater than the critical value for the laser frequency, which renders the plasma opaque to the laser beam. The plasma spreads from its point of origin with a speed v, intercepting an increasing fraction of the instantaneous beam power passing through the surface. The problem is to calculate for this system the total power as seen by the photodiode, placed beyond the damaging surface, at time t.

The power density at any point $\bar{r}$ on the surface is given by

$$\rho(\bar{r},t) = \rho(0,t = \pi/2w)(\sin wt) \exp\left(-\frac{r^2}{c^2}\right) \tag{5}$$

Integrating eq. (5) in space, we obtain the total power at time t.

$$P_T = \rho(0,\pi/2w)(\sin wt) \int_0^{2\pi}\int_0^{\infty} \exp\left(-\frac{r^2}{\sigma^2}\right) r \, dr d\theta \tag{6}$$

$$= \pi\sigma^2 \rho(0,\pi/2w) \sin wt$$

Now we calculate the power P_I intercepted by the spreading plasma at time t and subtract this from eq. (6) to obtain the power incident on the photodetector. To calculate P_I, we translate the coordinate system center to $\bar{R}$ where the plasma originates. The new coordinates are taken as $\bar{r}'$ and θ', and

$$\bar{r} = \bar{R} + \bar{r}' \tag{7}$$

Thus the power density at $\bar{r}'$ is given by

$$\rho(\bar{r}',t) = \rho(-\bar{R},\ t = \pi/2w)(\sin wt)\ e^{-\frac{(\bar{R}+\bar{r}')^2}{\sigma^2}} \tag{8}$$

$$(\bar{R}+\bar{r}')^2 = R^2 + 2\ r'R\cos\theta + r'^2 \tag{9}$$

$$P_I(t) = \rho(-\bar{R},\pi/2w)(\sin wt)\int_0^{vt'}\int_0^{2\pi} \tag{10}$$

$$\exp -\frac{(R^2 + 2\ r'R\cos\theta + r'^2)}{\sigma^2}\ r'\ dr'\ d\theta$$

The limit vt' is the radius to which the plasma has expanded at time t. (We have assumed that breakdown [plasma initiation] occurs at the pulse peak; that is, at $t' = t + \pi/2w$. That this is not always the case does not concern our analysis here.) Note that integration over θ is equivalent to integration over θ'.

Subtracting eq. (10) from eq. (6), we have the power P(t) incident on the diode.

$$P = \rho(0,\pi/2w)\sin wt\left[\pi\sigma^2 - \exp\left(-\frac{R^2}{\sigma^2}\right)I(t)\right]\ , \tag{11}$$

where

$$I(t) = \int_0^{vt'}\int_0^{2\pi} \exp -\left(\frac{r'^2 + 2\ r'R\cos\theta}{\sigma^2}\right)r'\ dr'\ d\theta \tag{12}$$

From eq. (11), we see that the deviation of the photodetector pulse from a half sine wave depends on v, R, and σ; that is, upon the plasma

expansion rate, the distance from the beam center at which breakdown occurs, and the beam size.

It is possible that eq. (12) can be integrated over r' and/or θ in closed form to obtain a more tractable expression, but we do not see the solution. Certainly eq. (11) can be evaluated numerically for several cases of interest, but we leave this to anyone else that might be interested. Instead, we will discuss semiquantitatively the wave forms that could be generated.

First, we ask what are reasonable values of the plasma expansion rate v. This has been measured in two experiments.[19,20] In both of these, rates of approximately 10^6 cm/sec were found for Q-switched pulses. However, these measurements were generally made well above the breakdown threshold. This leads us to take 10^6 cm/sec as an upper limit on v for two reasons. First, v can be expected to depend on the rate at which the laser pulse deposits energy into the plasma. Second, although we have assumed in our analysis that breakdown occurs at a single point, this is decreasingly likely to be true at power levels above the breakdown threshold. The result would be an apparently greater expansion rate in the experiments of 19 and 20. As a lower value of v, we somewhat arbitrarily choose 10^5 cm/sec.

With these values of v we can consider what wave form might be obtained when a 20 μm diameter Gaussian beam is used, as in the work of ref. 17. First, suppose that breakdown occurs at beam center and that $v = 10^6$ cm/sec (10 μm/ns). The result would be an almost total cutoff of the pulse in less than one nanosecond, the pulse form attributed to intrinsic breakdown in ref. 17 (see Figure I-23).

Suppose that $v = 10^5$ cm/sec (1 μm/ns) and breakdown occurs at beam center. Then the pulse attenuation will be as shown in Figure I-24. A fairly fast cutoff occurs at first because the plasma is intercepting the most intense part of the beam. This is followed by a more gradual attenuation as the plasma intercepts the less intense beam edges. This pulse form might be attributed to inclusion produced damage.[17] (It is worthy of note that, in the work of ref. 17, plasmas assumed to be associated with inclusions were usually less intense. One could infer from this that these plasmas were not as hot as those attributed to intrinsic breakdown, and therefore v would be smaller.)

It is obvious from these examples that, by choosing appropriate values of v, R, and σ, one can generate a wide variety of attenuated pulses. Thus with large beams in which the power density is near threshold, one expects to see almost no attenuation, and in fact in our studies with a 1.8 mm beam this is the case. At the other extreme, with a small beam of power density well above the threshold, where breakdown would occur at several places in the beam, one expects to invariably see a very rapid attenuation.

In this section, we have attempted to analyze the myriad pulse forms seen in damage work. The major points we have made are:

1. Pulse attenuation is almost certainly due to a plasma;
2. The myriad forms of attenuation observed can be easily explained by considering the plasma expansion rate in conjunction with beam size and power; and

3. It is not generally appropriate to relate pulse forms to the basic damage mechanism, especially when the mechanism is inclusion damage where a plasma is often not present.

I-7. Damage Morphology - Comments on Ring Structure on ED-2

Damage morphology takes many forms, depending on material, pulse width, etc. We discuss only one aspect of damage morphology here; the frequent appearance of a ring structure around damage sites on ED-2. A typical ring that can appear on either the entrance or exit surface is shown in Figure I-25. The ring consists of material deposited on the surface. This deposit cannot be removed by hand rubbing with acetone or isopropyl alcohol. The form of the structure varies; sometimes it consists of a single ring, sometimes of multiple noncircular rings (Figure I-26) and sometimes of multiple concentric rings (Figure I-27). The ring diameter can range from approximately the diameter of the damaging beam, about 1.8 mm in our studies, to several times that size. Generally, the diameter increases with the energy of the beam. Although the effect is not easily discernible in the micrographs, the surface inside the rings always exhibits a rippling or "orange peel" effect. Occasionally, some cracking of the surface is seen.

Since the rings can be much larger than the damaging beam, it can be concluded that they are caused by the plasma accompanying damage and not by the laser beam. This is supported by the absence of rings when damage occurs without a plasma.

Rings are especially prominent on ED-2 laser glass, but are not manifested on some other materials. On fused quartz, for example, we

never observe them. They are fairly easily seen on FK-6, a Schott fluorosilicate glass.

We have offered the following explanations of these rings in another place.[21] The initial plasma is formed in the region of the damaging beam. Its temperature is greater than 10^5 K as it begins to expand over the surface, and it heats the surface as it comes into contact with it. It is this heating that causes the ripple effect. The plasma is cooled by expansion and by contact with the cooler surface. As the plasma cools to an appropriate temperature, one or more of its components condense onto the surface, forming a ring of material.

We still think this explanation of the ring formation is valid. However, in ref. 21, we attempted to explain the multiple ring structure by attributing each ring to a different plasma component that condensed at a different temperature, and therefore at a different radius. We now believe the multiple rings are associated with mode beating on the damaging pulse. Thus the pulse shown in Figure I-28 led to a single ring, while the pulse in Figure I-29 led to a multiple structure similar to that of Figure I-27.

By this theory, the plasma is ''driven'' by the laser pulse. The plasma temperature easily follows the power peaks on the pulse. The radius of a particular ring depends on the temperature of the plasma in its inchoate stage. The temperature in this stage is in turn a function of the laser beam power intercepted (absorbed) by the plasma.

This explanation of the ring structure is supported by the number of rings and peaks on the laser pulse. In Figure I-27, for example,

seven rings can be seen. In Figure I-28, there are nine peaks on the laser pulse. These two observations are consistent if we assume that breakdown occurred near the third peak, leaving one ring for each succeeding peak after the third. From this we infer that the outer ring is associated with a peak near the middle of the pulse and the inner rings with the following lower power peaks.

Further support of our interpretation of the rings is found in the distance between adjacent rings. In Figure I-27, the distance between adjacent inner rings is approximately 0.05 mm. The time between peaks on the laser pulse is 6 ns. The plasma expansion rate inferred from this is approximately 10^6 cm/sec. Since the rings in Figure I-27 are about the same size as the damaging beam, this is in good agreement with measured expansion rates. If the rings were much larger in diameter, this relation between initial plasma expansion rate and distance between rings would not hold, since the plasma cools rapidly as it expands.

As shown in Figure I-26, the ring structure is not always circular. We attribute this to breakdown in two well-separated regions of the laser beam so that two plasmas are present. This noncircularity would not occur if a very small beam were used.

Finally, we point out a characteristic of some rings for which we have no explanation. This is the sawtooth structure seen in Figure I-30. Perhaps this is due to temperature differences along the periphery of the expanding plasma, but this is strictly conjecture.

I-8. References

1. N. L. Boling, L. Spanoudis, and P. R. Wengert, Semiannual Technical Report, ARPA Order 1441 (Dec. 1971).

2. N. L. Boling, G. Dubé, and M. D. Crisp, Damage in Laser Material, NBS Special Publ. 387, A. J. Glass and A. H. Guenther, eds. (U.S. Gov't Printing Office, Washington, DC, 1973).

3. A. J. Glass and A. H. Guenther, Appl. Opt., 12, 637, April 1973.

4. R. W. Beck, Damage in Laser Materials, NBS Special Publ. 341, A. J. Glass and A. H. Guenther, eds. (U.S. Gov't Printing Office, Washington, DC).

5. D. J. Olness, J. Appl. Phys., 39, 6 (1968).

6. J. Swain, Damage in Laser Glass, ASTM Spec. Tech. Publ. 469, A. J. Glass and A. H. Guenther, eds. (1969).

7. Personal communication with J. Swain of Lawrence Livermore Laboratory, Lawrence, Calif.

8. Personal communication with A. Feldman of NBS, Gaithersburg, Md.

9. D. W. Fradin and M. Bass, Appl. Phys. Letters, 22, 152 (1973).

10. M. D. Crisp, N. L. Boling, and G. Dubé, Appl. Phys. Letters, 21, 364, 15 Oct. 1972.

11. N. Bloembergen, Appl. Opt., 12, 661 (April 1973).

12. C. R. Guiliano, R. W. Hellwarth, and C. R. Rickel, Semiannual Report 2, ARPA Order No. 1434 (Jan. 1972).

13. J. Davit, Damage in Laser Glass, ASTM Spec. Tech. Publ. 469, A. J. Glass and A. H. Guenther, eds. (1969).

14. C. Yamanaka, T. Sasaki, M. Hongyo, and Y. Nagaa, Damage in Laser Materials, NBS Spec. Publ. 356, A. J. Glass and A. H. Guenther, eds. (U.S. Gov't Printing Office, Washington, DC, 1971).

15. E. Rabinowicz, Science Journal, p. 45, Jan. 1970.

16. J. M. Bennett and R. J. King, Appl. Opt., 9, 236, Jan. 1970.

17. M. Bass and D. W. Fradin, IEEE J. Quantum Elec., QE-9, 890, Sept. 1973.

18. N. L. Boling and G. Dubé, Appl. Phys. Letters, 23, 658, 15 Dec. 1973.

19. N. L. Boling and R. W. Beck, Damage in Laser Materials, NBS Spec. Publ. 356, A. J. Glass and A. H. Guenther, eds. (U.S. Gov't Printing Office, Washington, DC, 1971).

20. C. R. Guiliano, Damage to Laser Materials, NBS Spec. Publ. 372, A. J. Glass and A. H. Guenther, eds. (U.S. Gov't Printing Office, Washington, DC, 1972).

21. N. L. Boling, M. D. Crisp, and G. Dubé, Appl. Opt., 12, 650 (April 1973).

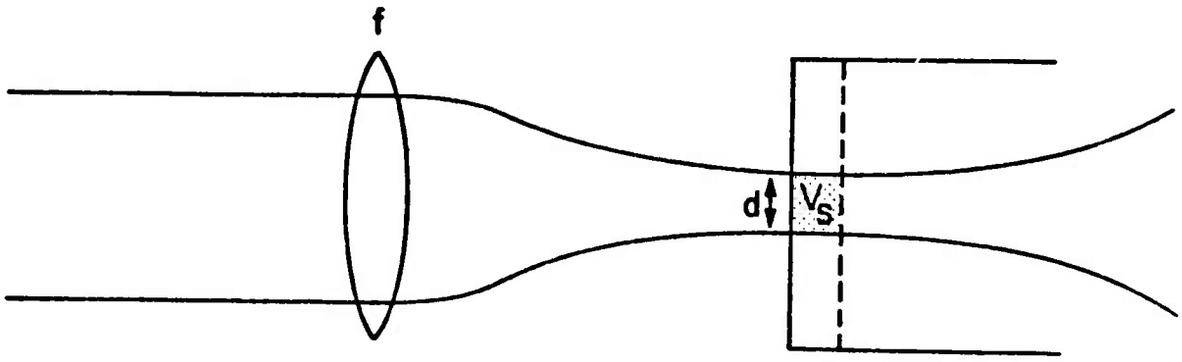

Figure I-1. Damaging beam focused on surface volume V_S

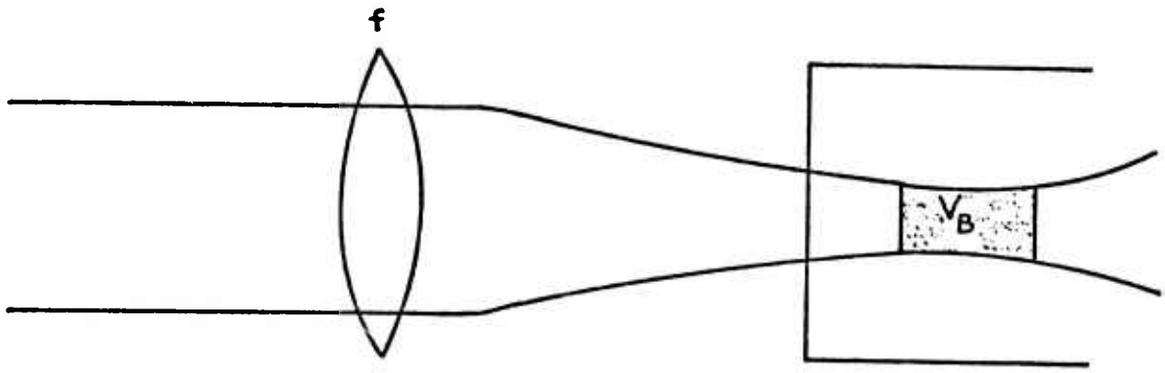

Figure I-2. Damaging beam focused into interior

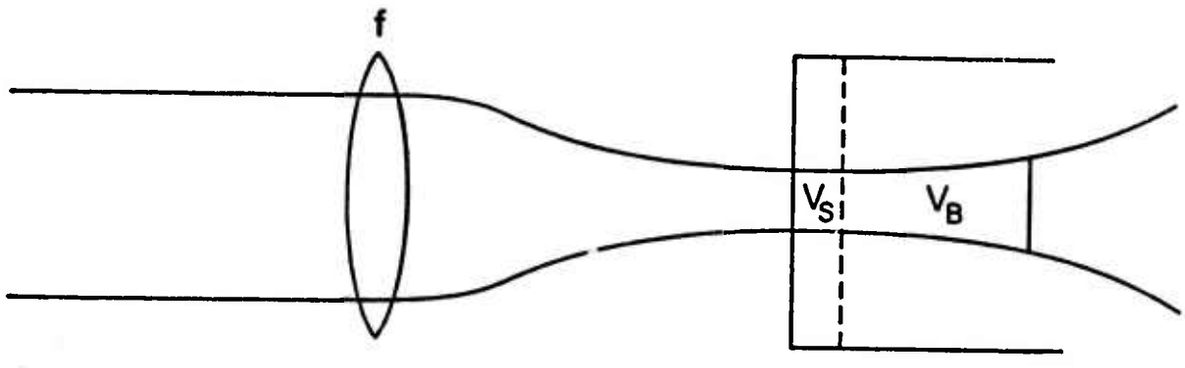

Figure I-3. Damaging beam focused to measure surface and bulk breakdown

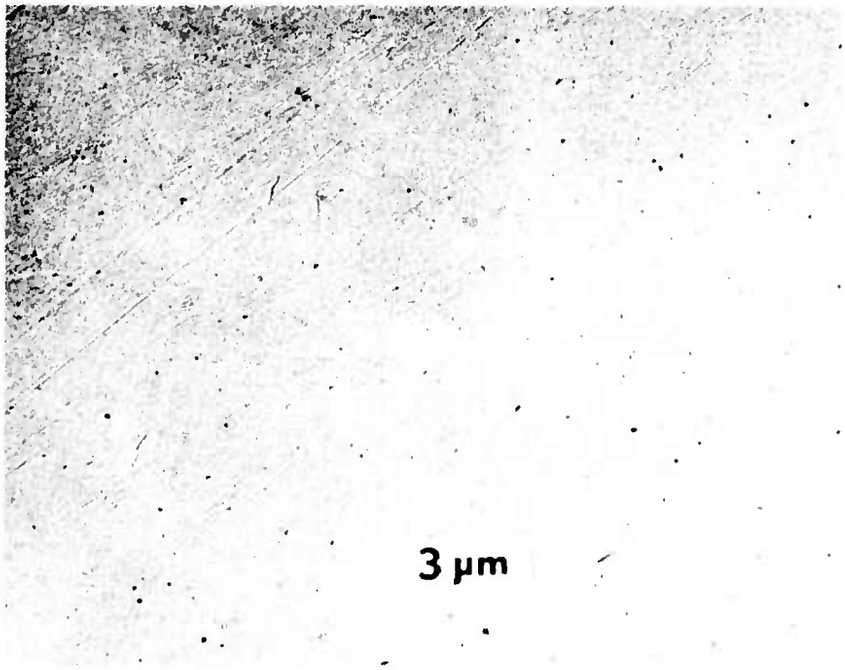

Figure I-4. Bowl-feed polished ED-2 laser glass - long polishing time - rouge polish

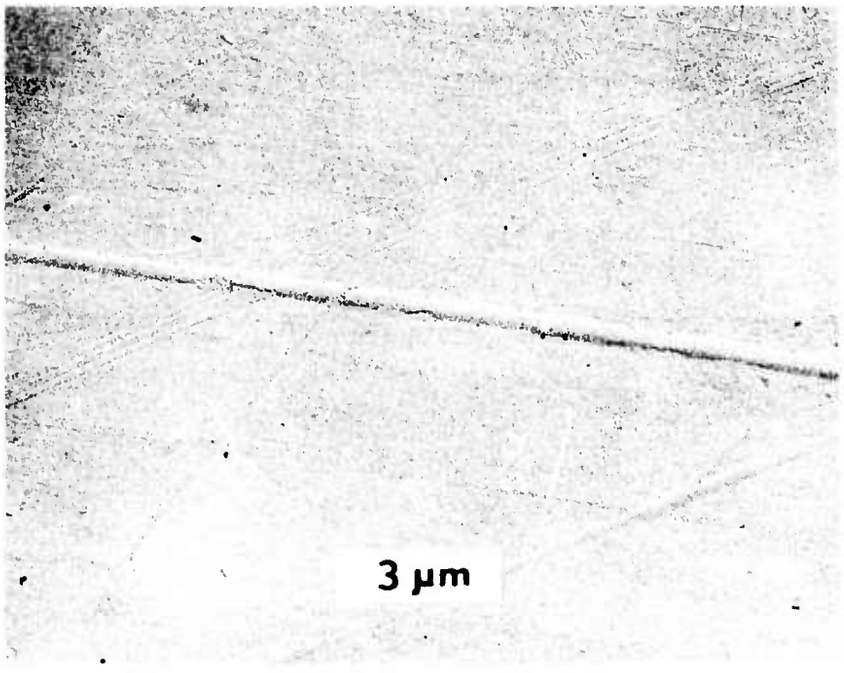

Figure I-5. Bowl-feed polished ED-2 laser glass - short polishing time - rouge polish

Figure I-6. Conventionally polished fused quartz

1 μm

Figure I-7. Conventionally polished fused quartz after acid etch

1 μm

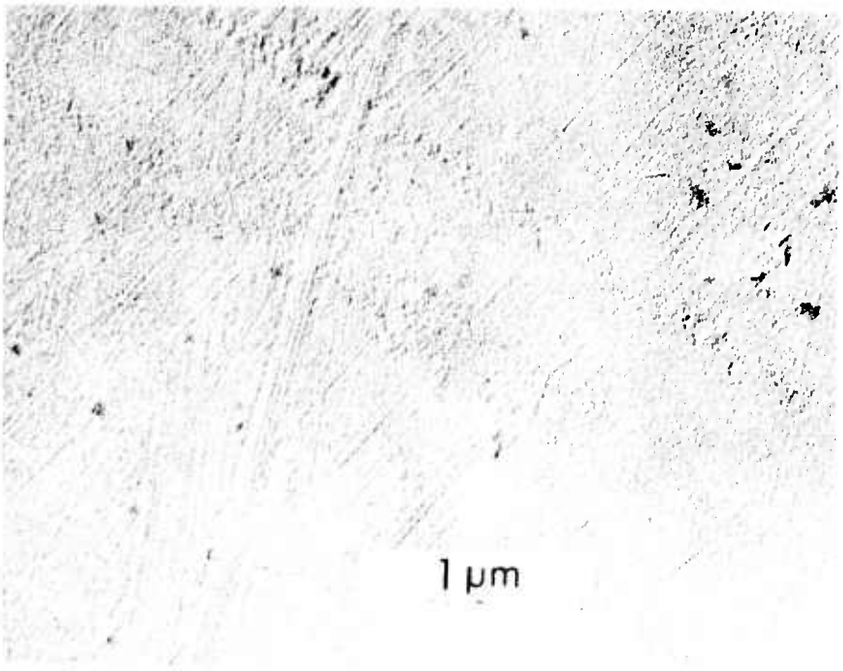

Figure I-8. Conventionally polished ED-2 laser glass - barnesite polish

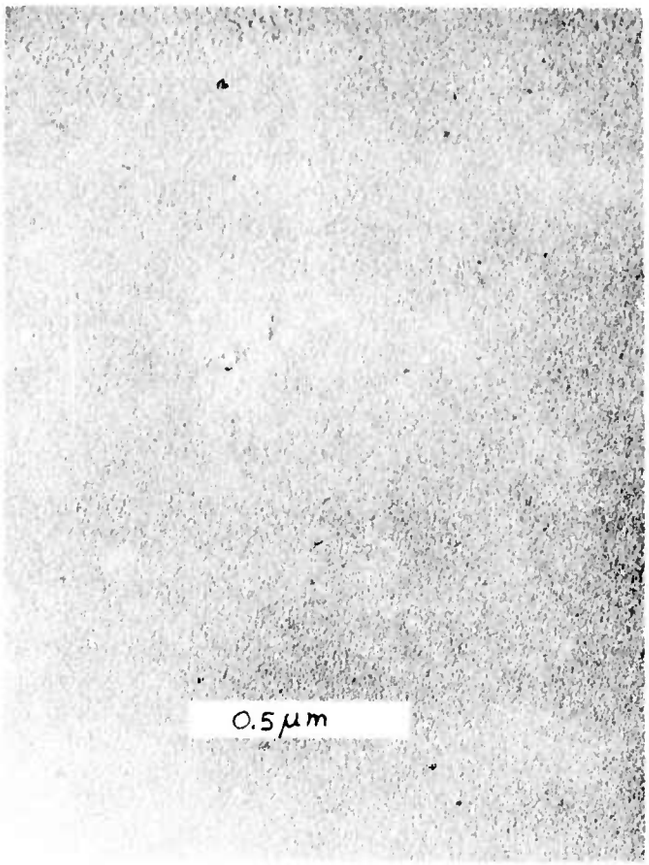

Figure I-9. Bowl-feed polished ED-2 laser glass

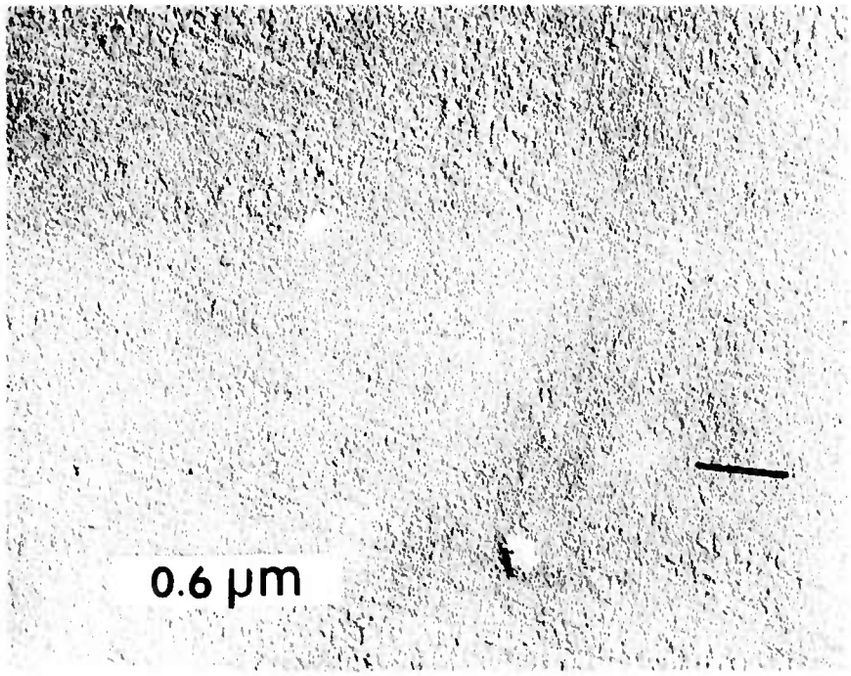

Figure I-10. ED-2 bowl-feed - rouge polished - long polishing time

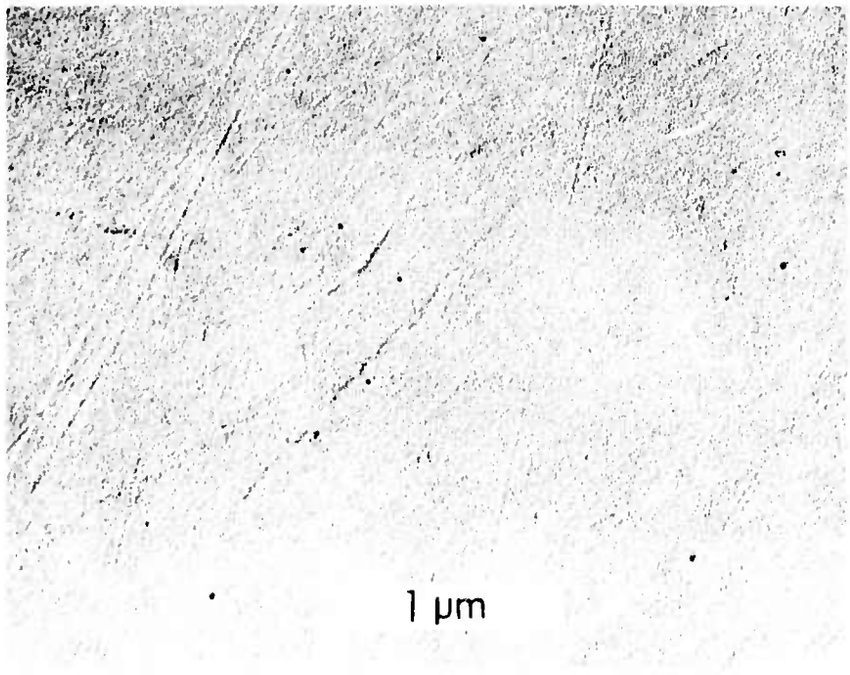

Figure I-11. ED-2 bowl-feed - rouge polished - short polishing time

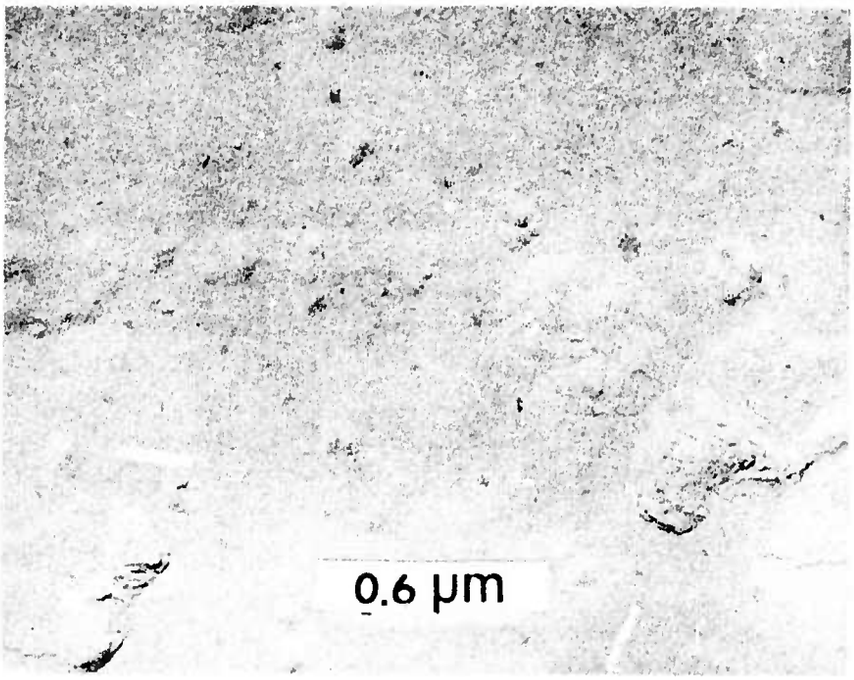

Figure I-12. ED-2 conventional polish with rouge

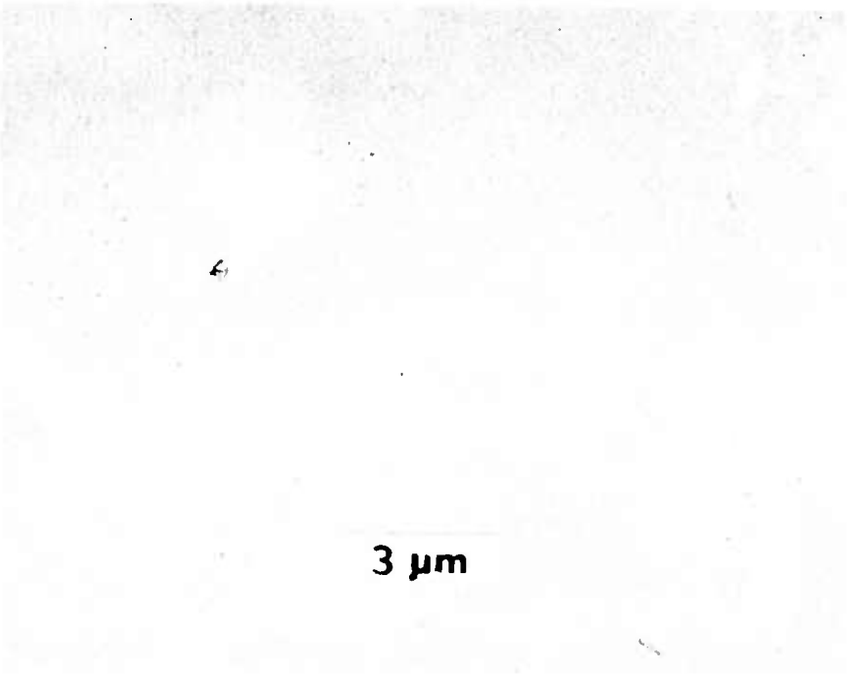

Figure I-13. ED-2 conventional polish with barnesite

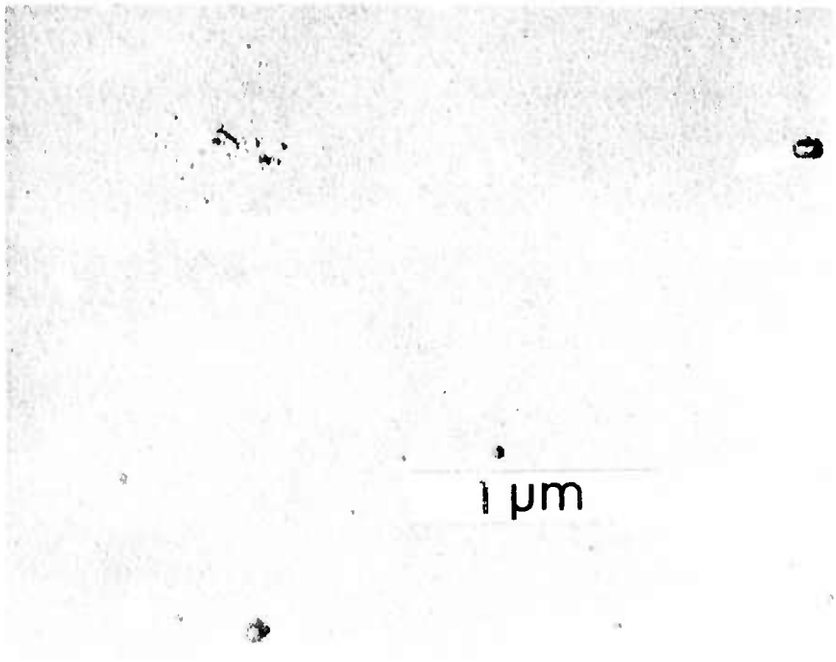

Figure I-14. ED-2 conventional polish with barnesite - crystalline structures may be platinum

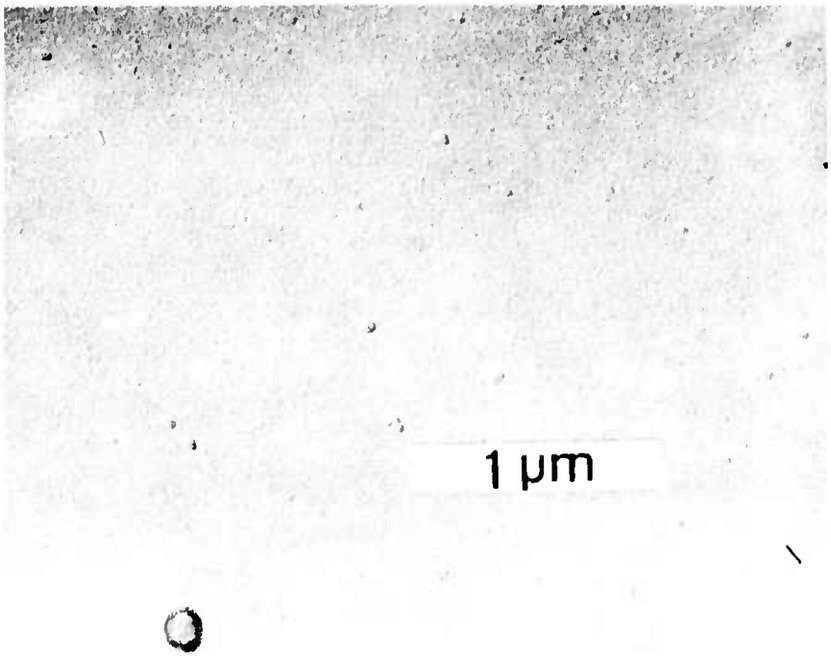

Figure I-15. ED-2 bowl-feed - barnesite polished

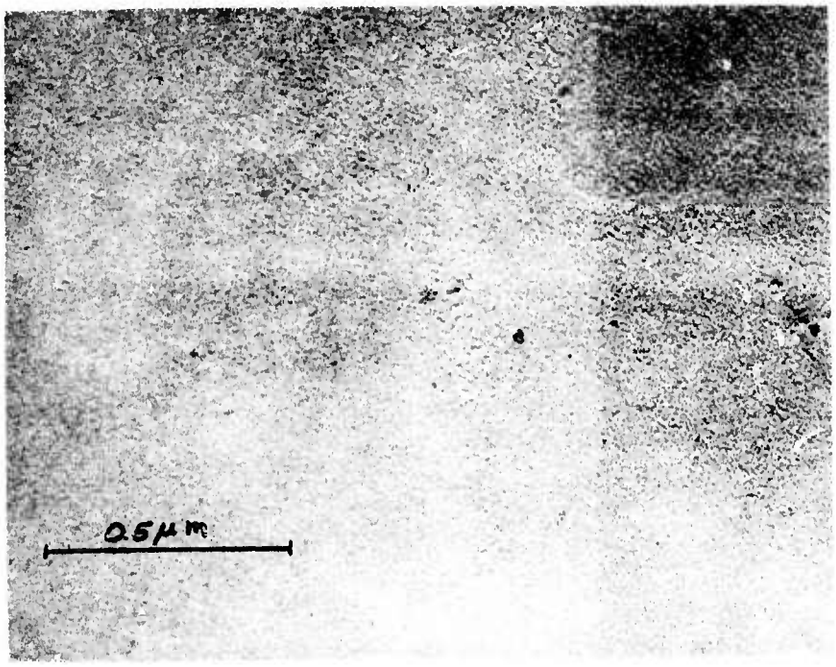

Figure I-16. ED-2 bowl-feed - Cerox polished

Figure I-17. ED-2 bowl-feed - Cerox polished

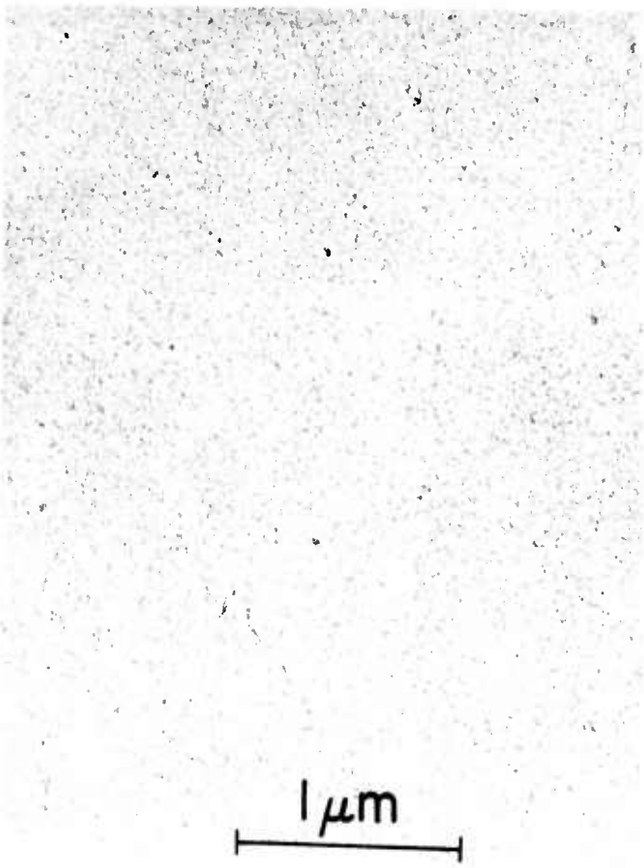

Figure I-18. Polished glass (EY-1) surface before hot acid treatment

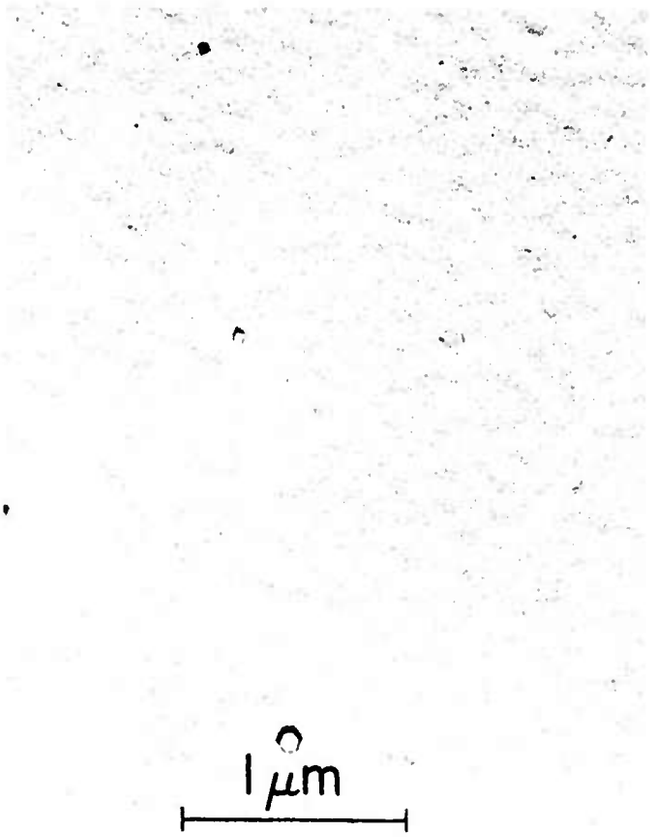

Figure I-19. Polished glass (EY-1) surface after hot acid treatment

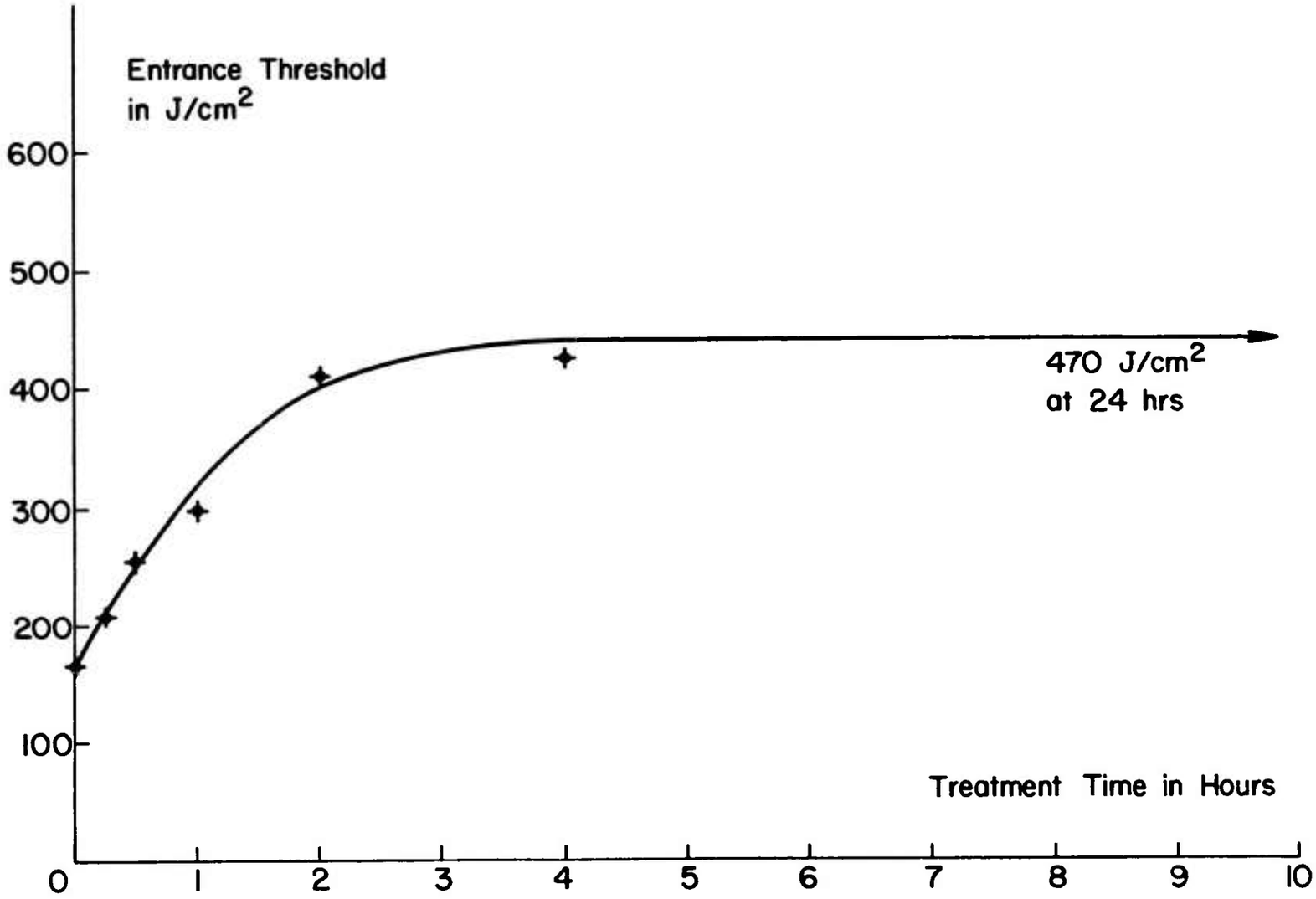

Figure I-20. Entrance threshold vs. time in acid bath for barnesite polished ED-2

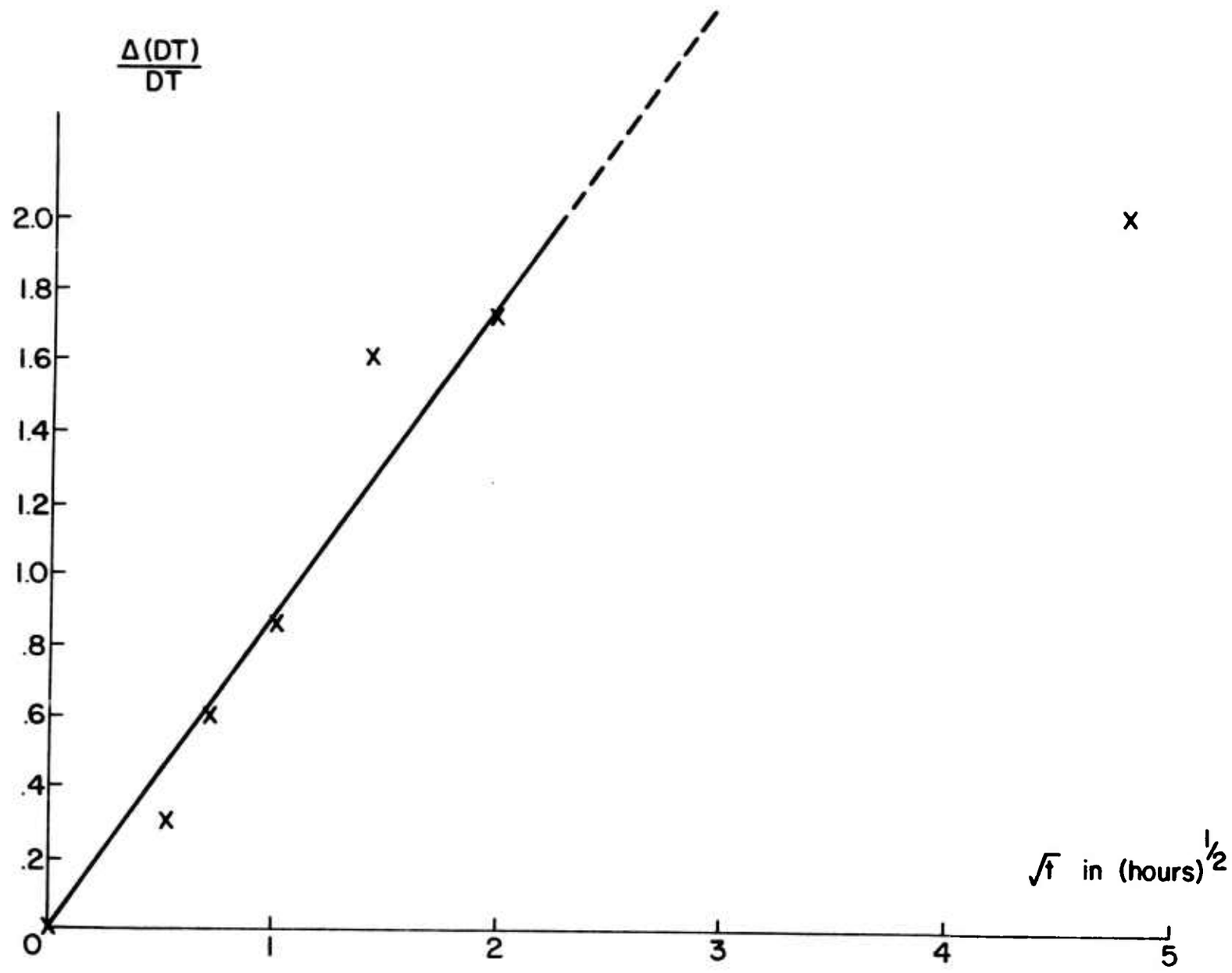

Figure I-21. Fractional change in the entrance threshold of ED-2

Figure I-22. Damage on acid-treated ED-2

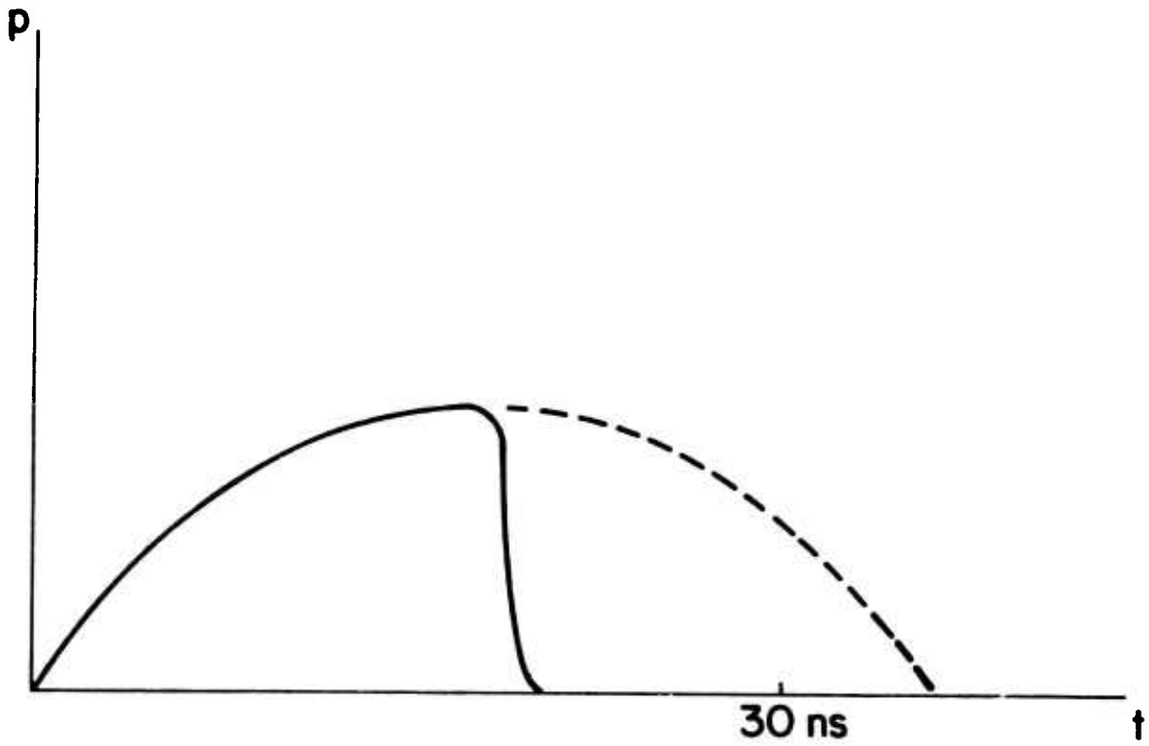

Figure I-23. Form of pulse attenuation when plasma expansion rate is 10^6 cm/sec

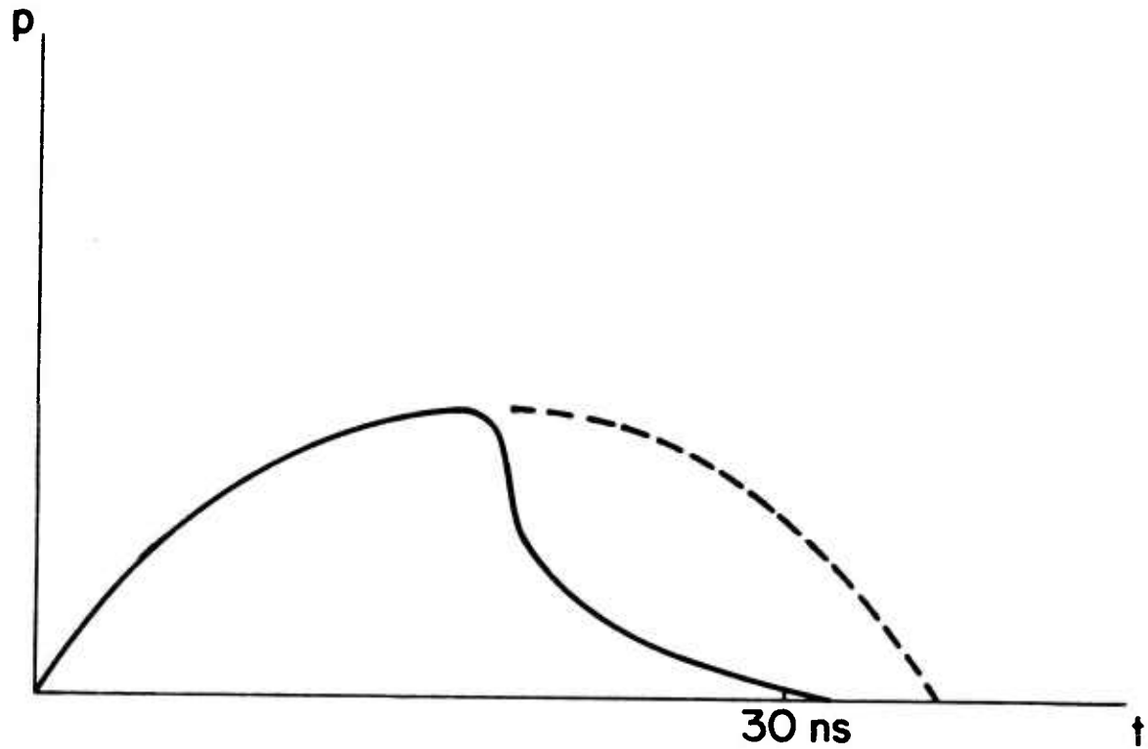

Figure I-24. Form of pulse attenuation when plasma expansion rate is 10^5 cm/sec

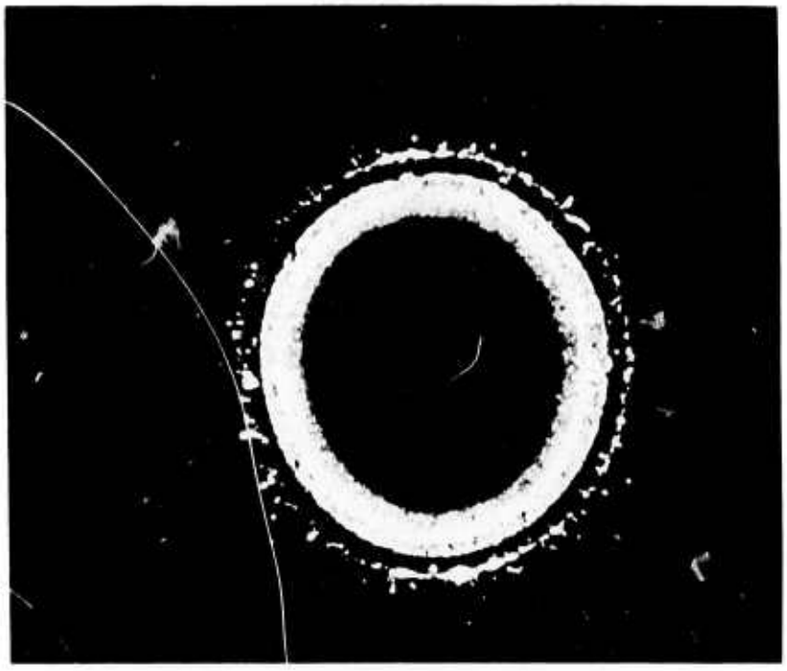

Figure I-25. Ring of material deposited around damage site on ED-2. Ring diameter is about 3 mm.

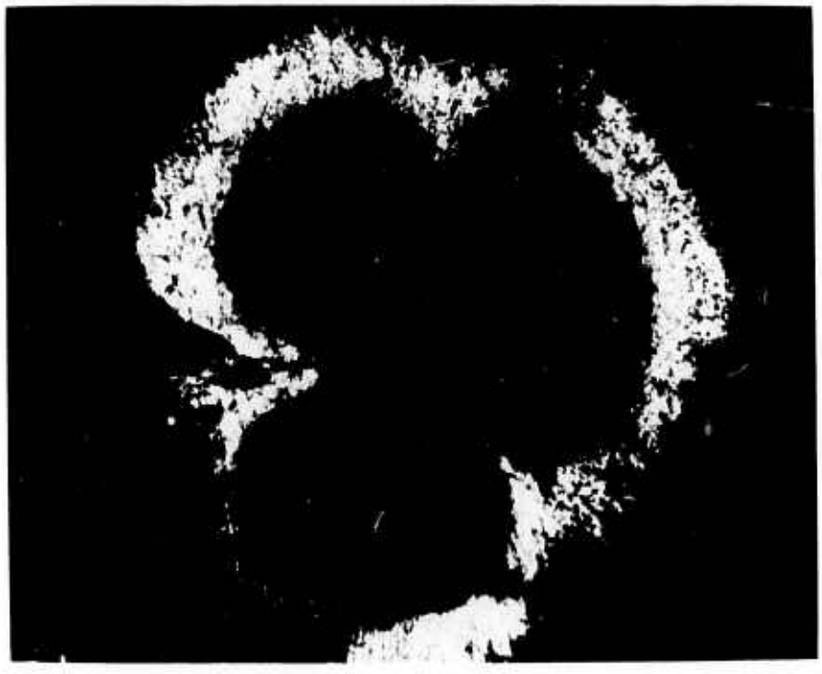

Figure I-26. Noncircular damage ring on ED-2. Diameter is 2.5 mm.

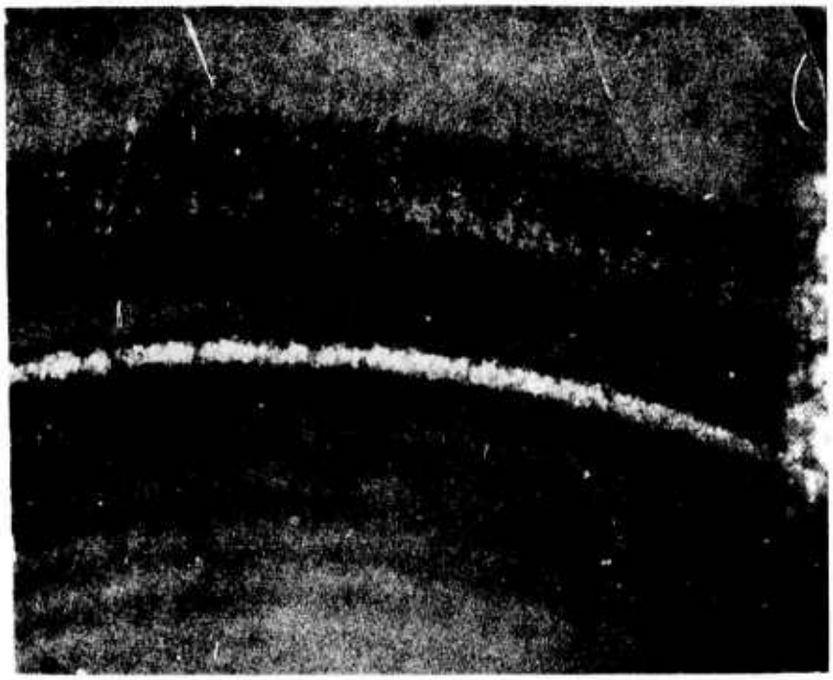

Figure I-27. Multiple ring structure on ED-2. Distance between adjacent inner rings is approximately 0.05 mm.

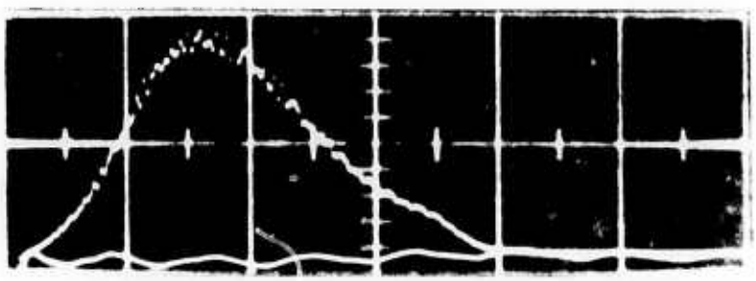

Figure I-28. Pulse form associated with a single damage ring. 20 ns/division.

Figure I-29. Pulse form associated with multiple rings. 20 ns/division.

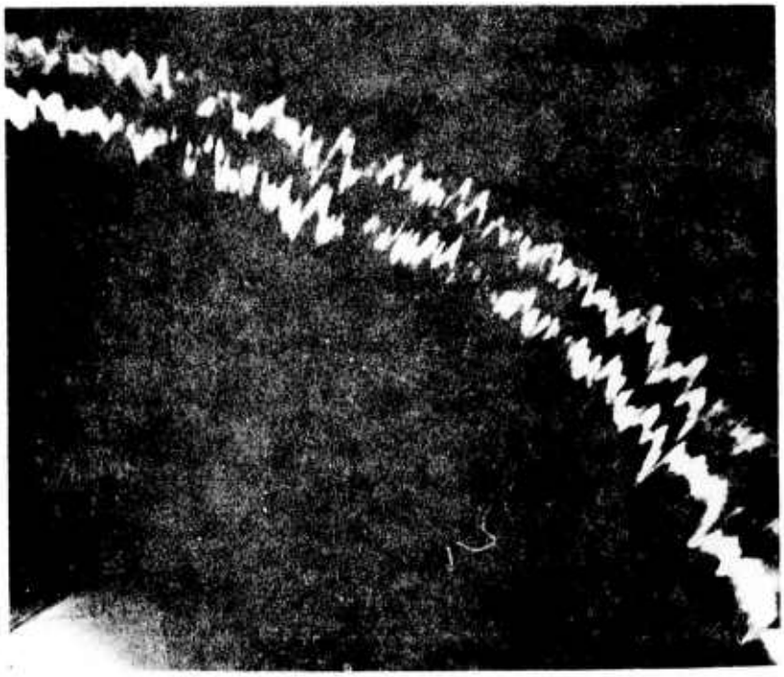

Figure I-30. Sawtooth structure on damage ring distance between rings in approximately 0.1 mm

Table I-1

Effect of Hot Acid Treatment on ED-2
Polished by Several Processes

Polishing Technique	Entrance Threshold before Acid Treatment	Entrance Threshold after Acid Treatment
Barnesite with pitch lap - Shop 1	150 J/cm^2	470 J/cm^2
Cerox and pitch Shop 1	180	525
Cerox and pitch Shop 2	180	250
Cerox - Bowl-feed Shop 3	140	375
Diamond - Shop 2	200	210
Rouge (iron oxide) Shop 1	60	270
Rouge (bowl-feed) Shop 4	45	150

II. HIGH ENERGY DENSITY LASER SYSTEM

II-1. Summary

1. Using TEM_{oo} narrow bandwidth 15 ns pulses, we achieved output irradiances of more than 4.4 GW/cm^2 (70 J/cm^2) with no damage. In terms of irradiance, this is 140% of the contract goal of 3.1 GW/cm^2 or 100 J/cm^2 in a 30 ns pulse.
2. Using multimode broad bandwidth 30 ns pulses, we achieved output irradiances of 2.2 GW/cm^2 (70 J/cm^2) with no damage to the amplifiers but with damage to a collimating lens. We achieved 1.9 GW/cm^2 (59 J/cm^2) with no damage at all, but the highest repeatable multimode output irradiance without any damage was approximately 1.4 GW/cm^2 (45 J/cm^2).
3. In both cases, higher irradiances could only be achieved by sharper focusing of the beam which led to self-focusing damage. With shorter amplifier rods and greater preamplification, even greater output irradiances should be possible.
4. In no case was an amplifier rod surface damaged, unless self-focusing damage occurred also. Surfaces of passive components nearly normal to the beam were frequently damaged and limited the extent of the experimental part of this study. This damage could be eliminated but was not, due to delays in the delivery of certain items and a shortage of time. In high-power nanosecond lasers, surface damage is a problem, but a solvable problem. Self-focusing is the current limit to the performance of such lasers.

5. At 70 J/cm^2, it did not seem to matter whether the 15 ns pulse envelope was temporally smooth or spiky (displaying irregular subnanosecond substructure).

6. At least in the case of nanosecond pulses of irradiance greater than the amplifier saturation irradiance there seems to be no great need to use single spatial mode or narrow bandwidth pulses to prevent damage.

7. Amplifier spontaneous emission kept us from using as much preamplification as we had originally planned on in the single-mode experiments. Greater isolation should have been provided.

8. A Faraday isolator should have been used to prevent damage due to backward traveling reflections.

9. All positive lenses of focal length f form a tertiary (twice-reflected) focus located approximately 0.15 f from the lens. This twice-reflected focus can be intense enough to cause damage.

10. The concept of total internal reflection apodizers appears worthy of further research. Other areas considered worthy of further research are outlined in Section II-5.3.

II-2. Introduction

II-2.1. Preliminary remarks

In order to minimize confusion, we begin by stating several of the definitions, assumptions, and convention used in this section of the contract report.

Pulse lengths in time (t_p) are full width at half maximum (FWHM) values. For purposes of calculating peak powers (P), we assume all pulses are Gaussian in time. This means that

$$P = 0.94 \frac{E}{t_p} \qquad (1)$$

where E is the energy in the pulse.

The symbol "ρ" is used to indicate J/cm^2 which we call "energy irradiance." Irradiance refers to W/cm^2. The word intensity is used only loosely. If we say a pulse is more intense, that may refer to power (W), irradiance (W/cm^2), energy (J), energy irradiance (J/cm^2), or other parameters that would apply in that particular context.

We also wish to acknowledge the technical assistance of D. Wahl and T. Phillips.

II-2.2. Goals

The goal of this phase of the contract was to demonstrate a Nd:glass laser that operated at an energy irradiance of 100 J/cm^2 in a 30 ns pulse. The feeling was that we had already shown that the surface damage threshold of typical laser glasses was at least 100 J/cm^2, so one should be able to operate actual lasers at these irradiances (3.1 GW/cm^2). All the previous experiments, however, were done with small, isolated, passive glass samples at the focus of a 1.5 meter lens.[1] The goal of this portion of the contract was to show that the same damage thresholds could be expected in actual laser systems using large pieces of active (optically pumped) Nd laser glasses. Thus we hoped to show actual laser operation at 100 J/cm^2, not just passive resistance to damage at 100 J/cm^2. Recent studies by Bliss, et al, have shown that there is indeed a difference in damage resistance between pumped and unpumped samples and that this difference is consistent with current theories of small-scale self-focusing.[2]

Given a goal of 100 J/cm^2, one still has not specified the total energy in the laser output. Originally we hoped for ≈ 100 J, but financial and technical constraints made us decide to concentrate on 100 J/cm^2 and treat the total energy as a secondary concern. Our philosophy also was to not do anything that couldn't be readily applied to existing Nd:glass lasers. The 100 J/cm^2 would be attempted under conditions as near as practical to those found in operating lasers. For example, 100 J/cm^2 in a highly focused or defocused beam would not be in the spirit of this contract. We wanted 100 J/cm^2 at the output of a practical laser system.

Frankly, we experienced some indecisiveness in starting this work because we felt that the limiting factor in 30 ns lasers was self-focusing damage, not surface damage - and this contract was to focus specifically on surface damage. One could also question the wisdom in seeking 100 J/cm^2 in a laser material that saturates at approximately 6 J/cm^2. At energy irradiances several times the saturation level, the extraction of energy from the laser amplifier becomes very nearly complete and further increases in energy irradiance become counterproductive due to the inevitable losses of scattering and absorption. Consider a laser pulse of total energy E_o that is to be amplified to $E_o + 3\ W_o$, where W_o is the energy stored in an amplifier of cross-sectional area A and length ℓ. Four cases will be considered (see Figure II-1). We further assume that the incident energy irradiance in cases a and b is 100 J/cm^2, thus in cases c and d the energy irradiance is 33.3 J/cm^2. If we neglect all losses and assume that at both 33.3 and 100 J/cm^2 complete energy

extraction takes place, the output in all four cases is $E_o + 3\ W_o$. Now let us consider the losses. Let each surface have a loss of "s" % and let the laser material have a loss coefficient of γ. The output in each case is listed in Table II-1. We calculated some numerical values using: $(E_o + 3\ W_o) = 109\ J/cm^2$

$$\ell = 3\ cm$$

$$s = 0.1\% = 0.001$$

$$\gamma = 0.002\ cm^{-1}$$

(The 5.33 exponent in Table II-1 arises in case c because one beam sees four surfaces, while two beams see six.)

The advantage of large apertures and lower irradiances is clear, although more rigorous calculations would be necessary to accurately evaluate the trade-off's involved. Because of these losses and pulse-shaping effects, it is seldom advisable to operate at energy irradiances more than five times the saturation energy irradiance.[3] For ED-2 laser glass, the saturation energy irradiance (ρ_s) is approximately 6 J/cm^2, so the contract goal of 100 J/cm^2 is more than sixteen times ρ_s.

Nonetheless, there is a variety of valid reasons why one might want to operate at 100 J/cm^2. The maximum aperture size may be limited by technical or financial constraints. Also the pumping (storage efficiency of small aperture Nd:glass amplifiers is higher than the pumping efficiency of large aperture disk amplifiers.[4,5] Pumping or storage efficiency is the ratio of the energy stored in the (Nd) amplifier to the energy stored in the pumping capacitor banks. So even if high irradiance

operation leads to less efficient energy extraction, the total system efficiency and/or cost effectiveness could be higher due to the increased pumping efficiency. Attempts at 100 J/cm^2 operation may also lead to further improvements applicable to other laser systems and/or other optical components. All things considered, there are indeed valid reasons for seeking a 100 J/cm^2 laser.

II-3. Theory

II-3.1. Measurements

An important question in this study was: "what is the best way to measure irradiances of 100 J/cm^2 in 30 ns pulses?" These measurements require careful attention to both temporal and spatial effects. We consider temporal effects first. Figure II-2 illustrates the possible problems. If the pulse has low irradiance wings in time (or space), the total energy in these wings may be large enough to give misleading measurements. For example, the flashlamp and Nd:fluorescent lifetime assure that the amplifiers will be in a condition of rather high gain for about 1 ms. During this time, amplified spontaneous emission (ASE) will be emitted along the optic axis. It will be divergent, but if the energy detector is close to the amplifiers and has a large area, it will measure this energy. The temporal resolution of the calorimeters used in this study, and many other energy detectors cannot indicate whether the energy was deposited in 1 ms or 30 ns. Also, the dynamic range of photodiodes or other pulse length measuring devices is nowhere near large enough to indicate the presence of low-intensity wings. For example, let us assume that the ASE is only 10^{-5} the irradiance of the 30 ns pulse peak

($I_w/I_p = 10^{-5}$). The total energy then will be (30 ns) x (3 GW) plus (1 ms) x (3 x 10^{-5} GW). No photodiode will detect wings of 10^{-5} and yet 25% of the total energy would be in these wings.

Several things can be done to minimize these temporal difficulties. One step is to fire the amplifiers without a laser pulse and see if any ASE is detected. A few complications arise though when one asks what is the fair thing to do with the oscillator during these tests. If it is simply blocked off from the amplifiers, the ASE is likely to be affected by the oscillator output mirror (which in standing wave oscillators must be perpendicular to the optic axis) and by the fluorescence of the oscillator rod. The technique used in this work was to block off the light between the oscillator rod and the nonoutput mirror. Even this affects the ASE because we purposely used a leaky Pockels cell to Q-switch the oscillator. Another solution is to temporally gate the detector and/or the transmission through the amplifiers. Integrating photodetectors are another possibility, but linearity and dynamic range can still be a problem. Faraday isolators can help by insuring that the oscillator output mirror does not increase the ASE. Another approach (used in this work) is to make the 30 ns pulse smaller in area than the area of the ASE. In our case, we sampled a 1 mm diameter. The ASE was emitted (rather uniformly we assume) over 2.85 cm^2. This is 363 times the area of the 1 mm hole. So less than 0.3% of the ASE enters the detector. If the ASE is 10 J, it would make less than a 4% error in a 100 J/cm^2 measurement. Note also that these temporal complications are much worse in the case of subnanosecond pulses.[6]

Next, we turn to the spatial problems involved in measuring 100 J/cm^2. The problem is the same except that now the wings refer to space instead of time. One obvious solution is simply to use an aperture. But, if an aperture were simply placed in a 100 J/cm^2 30 ns laser beam, two serious problems would arise. First, the aperture and/or the plasma caused by the laser-induced damage to the aperture would reflect part of the beam back towards the oscillator. In a system such as ours, with no isolation, this could be disasterous. Second, if a plasma develops, it may limit the transmission of the later parts of the pulse through the aperture. One solution is to use filters and/or beam splitters to reduce the irradiance before it strikes the aperture. We used beam splitters in our work to limit the energy irradiance on the aperture to less than 3 J/cm^2. We looked for a plasma-limiting-transmission effect and saw none. With a beam splitter reflectance of about 4%, less than 1.6×10^{-3} of the energy reflected by the aperture is returned to the amplifiers.

Use of the 1 mm aperture still does not insure the correct temporal interpretation of irradiance measurements. We had hoped to calibrate a fast photodiode so that the photodiode could measure the peak power of the pulse that passed through the 1 mm aperture. In attempting to establish the responsivity of our photodiode, we found that the spread in our measurements was ± 20%. We considered this too large a spread and abandoned the idea of measuring irradiance or energy irradiance with a photodiode. We decided it would be best to use a 1 mm aperture, beam splitter, and a calorimeter to measure energy irradiances. The photodiode

would be used to establish the pulse length and check for double pulsing or spurious signals.

Before settling on a beam splitter-aperture-calorimeter detection system, we had to estimate the size aperture we would need. Our calorimeters had responsivities of about 200 μv/J and we figured that a 10 μv signal would be easily and accurately recorded. So at least 5×10^{-2} J had to pass through the aperture. At 100 J/cm^2 and with a reflectivity (R) of 4%, this implies an area of 1.25×10^{-2} cm^2 or a diameter of 1.26 mm. We used apertures of 1.5 and 1.0 mm diameter during this work. We used quartz ($R \simeq 3.3\%$) and ED-2 ($R \simeq 4.7\%$) beam splitters.

Having fixed the minimum aperture size needed to make measurements, we next asked what effect the beam size will have on these measurements. Clearly, if the beam size is smaller than the aperture, the measurements will be in error. Consider a Gaussian irradiance pattern

$$\rho(r) = \rho_o \, e^{-(r/r_o)^2} \tag{2}$$

where ρ_o is in J/cm^2. The energy passing through an aperture of radius a is given by

$$E + \pi\rho_o r_o^2 \left[1 - e^{-(a/r_o)^2}\right] \tag{3}$$

If one divides this by the aperture area, one gets an average energy irradiance $\bar{\rho}$ given by

$$\bar{\rho} = \rho_o \left(\frac{r_o}{a}\right)^2 \left[1 - e^{-(a/r_o)^2}\right] \tag{4}$$

Figure II-3 shows the error in energy irradiance ($1 - \bar{\rho}/\rho_0$) as a function of r_0/a. In order to keep the error less than 5%, r_0/a should be > 3. If the aperture diameter is 1 mm, then the 1/3 (irradiance) diameter of the beam should be at least 3 mm.

Another constraint on the beam diameter (b) is that the beam must be large enough to avoid whole beam self-focusing. To first order the self-focusing length (Z) of a beam is given by[7]

$$Z \simeq \frac{b}{4}\sqrt{\frac{n}{\Delta n}} \tag{5}$$

where n is the refractive index (1.55) and $\Delta n = n_2 E^2$ is the change in index caused by the intense light beam. n_2 for our laser glass is about 2×10^{-13} in esu units. At an irradiance of 3 GW/cm^2, $\Delta n \simeq 2 \times 10^{-7}$. In order to insure $Z > 40$ cm, the length of our last amplifier rod, we find that we must have a beam diameter greater than 0.6 mm. Thus whole beam self-focusing should not be a problem in these experiments in which the beam diameter is greater than 1 mm. We note also that all our experiments were done with beams containing at least one hundred times the (self-focusing) critical power for ED-2 laser glass.[7] In the self-focusing sense, our experiments were both large beam and high power. (Recent experiments by Bliss, et al, have indicated that, under conditions similar to ours, there may be whole-beam self-focusing.)[2]

Another effect we considered was that of slight misalignments of the aperture of diameter a and thickness t (Figure II-4). It can be shown that

$$a' = a \cos \theta - \frac{t}{a} \sin \theta \cos \theta \qquad (6)$$

Approximating the area of the transmitted beam as $\pi a a'$ (elliptical), Figure II-5 gives the error in irradiance (area) due to various misalignments in degrees in one and both planes for one of our apertures which had t = 1.1 mm and a = 1.0 mm. Also shown is the error for an aperture of zero thickness. We note that it should be easy to keep the errors less than 5%, but that thin (tapered) apertures reduce any error even further.

The final amplifier rods used in this research all had Brewster angle ends. We define the output irradiance to be measured in an imaginary plane called the exit plane. This plane is perpendicular to the laser beam, located in air and as close to the laser rod as possible (Figure II-6).

At the beginning of this study, it was widely held that self-focusing thresholds could be raised appreciably if a diverging beam were passed through the amplifiers.[8] We therefore tried to design our experiments so a diverging beam propagated through the last amplifier. We wish to point out, however, that a slight divergence can have a drastic effect of irradiance. For simplicity, we consider a top-hat irradiance pattern propagating with half-angle divergence α (Figure II-7). The area of the beam A_2 at a distance L from the plane where the beam has area A_1 is given by

$$A_2 = A_1 \left(1 + \frac{\alpha L}{r_1}\right)^2 \qquad (7)$$

where r_1 is the radius of area A_1 ($A_1 = \pi r_1^2$).

Let us now calculate the change in irradiance of a beam with irradiance α through our final amplifier. The minimum distance between the negative lens on the input side of the final amplifier and the exit plane of the amplifier is 45 cm. Due to mechanical restraints (protrusion of the amplifier base), the distance in practice was 60 cm. If we assume

$$\alpha = 0.001 \text{ (1 mR)}$$

$$L = 60 \text{ cm}$$

$$r_1 = 0.15 \text{ cm} \qquad (r_2 = 0.21 \text{ cm})$$

we have

$$A_2 = A_1 (1.96)$$

So if the exit plane is to experience 100 J/cm^2, the negative lens must experience more than 166 J/cm^2. (With 30 cm of pumped amplifier length, the amplifier can add no more than 30 J/cm^2 to the beam irradiance.) It may well be possible to make lenses capable of withstanding 166 J/cm^2, but most lenses available today will not withstand this high level of irradiance (> 5 GW/cm^2). In retrospect, we did not become aware of this problem as early in the study as we might have liked. However, some of our experimental results, and recent theoretical work of others, indicate that divergence of the beam is not an important parameter for avoiding small-scale self-focusing.[9]

Note that, because of the strong effect α (divergence) has on the irradiance of small-diameter beams, it is all the more important to

measure the irradiance at the plane of interest. In our case, the plane of interest is the exit plane of the final amplifier. We had previously decided that the measurements must be made through a small aperture in order to be accurate. We also had previously described why this aperture could not be located in the exit plane. The seemingly conflicting requirements of placing the aperture in the exit plane but not in the exit beam were solved by using a beam splitter and a lens to form an image of the exit plane on the aperture (Figure II-8). Unit magnification was used throughout this work.

II-3.2. Design considerations

In the course of this work, we were forced to alter our experimental program for two reasons. One had to do with unanticipated damage to passive components and the other with unanticipated gain limitations. Because of this, we'll spend a few paragraphs considering general limitations and restraints in the design of high-power laser systems.

II-3.2.1. Gain and energy irradiance limitations

First we'll consider some gain limitations. We ask the question, besides damage, what limits are placed on the gain and/or irradiance of amplifier systems. Several possibilities present themselves. At some gain value, the amplifier system will turn into an oscillator due to reflections from targets, oscillator output mirrors, or other components. At some gain value, the single-pass amplification of spontaneous emission will defeat any attempts to store energy in the amplifiers. At some irradiance value, the losses of the amplifier will make further increases in energy irradiance impossible. At some gain value, the

inevitable backscattering of amplified spontaneous emission will turn the amplifier into a bulk-feedback oscillator - even without any reflecting surfaces. Other practical limitations may arise from the backscattering of the amplifier laser pulse.

Frankly, we initially thought of this amplifier system as a rather small amplifier system. It only had three 3/4'' diameter laser rods. The total volume of pumped glass was 256 cm^3, less than 5% of the pumped glass volume in the large glass lasers used in fusion research. In terms of small signal gain, however, our system is quite equivalent to the larger systems. Our small signal gain could be more than 8×10^6.

Consider the gain necessary to turn the amplifiers into an oscillator. At one end of the system, the reflector is the output mirror (etalon) of the oscillator. At the other end, reflections could come from walls, targets, apertures, or lenses. The gain (G_o) and reflectances must be such that

$$G_o^2 R_1 R_2 < 1 \qquad (8)$$

where R_1 is the reflectance of the oscillator output etalon ($\approx 35\%$) and R_2 is the reflectance at the output end of the amplifier. If we assume $G_o \simeq 2 \times 10^6$, we must have

$$R_2 < 7 \times 10^{-11}$$

If the laser target were a perfectly diffusing reflecting wall, the distance from the wall to the laser would have to be > 700 meters to insure $R < 7 \times 10^{-11}$ back into the laser. In any case, it would be difficult

to insure $R < 7 \times 10^{-11}$. So gains of $> 10^6$ may not be feasible in unisolated lasers only 300 cm long. A Faraday isolator will stop any oscillations and any amplified pulse reflections from damaging the oscillator, but it will not stop amplified spontaneous emission (ASE). Saturable absorbers will help on all counts but they are inefficient and may distort the beam.

Next, consider the spontaneous emission emitted at one end of a laser system. Spontaneous emission is emitted into 4π steradians, and only a small fraction of this will be along the axis of the system. However, this portion of the energy will experience high gain. To a good approximation, this fraction can be given by the area of the last amplifier (or equivalent limiting aperture) divided by 4π times the square of the length of the amplifier chain. This gives the solid angle (Ω) of the spontaneously emitted light that gets amplified. In other words, it gives the fraction of the emitted light that will experience high gain along the axis of the laser amplifier chain.

It seems reasonable then to expect amplified spontaneous emission (ASE) problems whenever the system small signal gain times Ω exceeds one. This condition means that there is enough gain that the light leaving the amplifier at the output end consists mostly of ASE, rather than simply spontaneous emission. As an example, we'll consider our system of three amplifiers; all of equal size. In this case, $A = 2.85$ cm^2 and $L \simeq 368$ cm

$$\Omega \simeq 1.67 \times 10^{-6}$$

The small signal gain (G_o) near the edges of our three amplifiers is more than 1×10^7, so

$$G_o = 19 > 1$$

(Experimentally, we found that ASE was indeed a problem.) We have applied this $G_o\Omega$ rule to other high-gain laser systems known to not have an ASE problem, and found that in these cases $G_o\Omega < 1$. In Figure II-9, we have attempted to show how increasing the aperture of the final amplifier makes Ω larger but that this increase can be reduced by using beam-expanding lenses. In any configuration, increasing the distance between amplifiers will decrease Ω.

Next, we note the effect of losses in the amplifiers. Consider, as before, a section of amplifier of area A and length ℓ. Let the stored energy in the amplifier be W_o. The stored energy density (S) then is $W_o/A\ell$; in most glass laser systems $0.2 < S < 1.0$ J/cm^2. As before, we let the amplifier material have a loss coefficient of γ cm^{-1}. In most glass lasers, $0.001 < \gamma < 0.005$ cm^{-1}. For the moment, we neglect any surface losses. If the incident energy is E_o, the energy lost (E_l) will be given by

$$E_l \simeq \left(1 - e^{-\gamma \ell}\right) E_o \qquad (9)$$

The energy added (E_a) can never be more than the total stored energy W_o. At a certain incident energy (E_c), the energy lost will equal the maximum possible energy that could be added and further gain will be impossible. This will occur when

$$E_1 = E_c \left(1 - e^{-\gamma \ell}\right) = W_o \tag{10}$$

or in terms of energy irradiance

$$\rho_1 = \rho_c \left(1 - e^{-\gamma \ell}\right) = S\ell \tag{11}$$

Because $\gamma \ll 1$, we can approximate

$$e^{-\gamma \ell} \simeq 1 - \gamma \ell \qquad \text{for } \ell < 50 \text{ cm} \tag{12}$$

Then we have

$$\gamma \ell \rho_c = S\ell \tag{13}$$

or

$$\rho_c = S/\gamma$$

Using the range of γ and S values mentioned previously, we have

$$40 < \rho_c < 1000 \text{ J/cm}^2$$

Even at 40 J/cm^2, the energy extraction from an amplifier should be nearly complete, thus it is reasonable to treat the energy added as equal to the total stored energy.

Next, we consider surface losses. If each surface transmits (1-q), then the energy lost becomes

$$E_1 \simeq E_o \gamma \ell + E_o 2q \tag{14}$$

The expression for ρ_c becomes

$$\rho_c = \frac{S}{\gamma + 2\ q/\ell} \tag{15}$$

Next we calculate ρ_c for two cases, a typical small-diameter rod amplifier and a typical large-diameter disk amplifier. The values of the parameters used and the resulting ρ_c are listed in Table II-2. One point is that the large disk lasers used in fusion research are not well suited for attempting operation at 100 J/cm^2. Other points are that the losses must be small and the stored energy high if one is to achieve 100 J/cm^2 operation. Note that, since we assumed complete extraction, these ρ_c values are upper limits. As we mentioned in the introduction, operation at 100 J/cm^2 probably will not maximize gains, but other constraints such as overall efficiency or limited aperture sizes may make 100 J/cm^2 operation desirable.

Next, we consider the backscattering of an amplified laser pulse. For high-gain systems, one can approximate the backscattered signal (E_o) by

$$E_b \simeq \frac{E_o \gamma e}{2g}^{2g\ell} = \frac{E_o \gamma G_o^2}{2g} \tag{16}$$

where E_o is the input pulse energy, γ is the backscattering coefficient (in cm^{-1}), g is the small signal gain coefficient and ℓ is the pumped length of the amplifier. All transparent materials scatter light and some of this light is backscattered into a narrow enough cone that it does not escape from the amplifier.

In our case, we have $g \simeq 0.16$ cm^{-1} and $\ell = 30$ cm per amplifier, thus

$$\frac{E_b}{E_o} = \gamma\ 4.6 \times 10^4 \qquad \text{(one amplifier)}$$

$$\frac{E_b}{E_o} = \gamma\ 1.0 \times 10^{13} \qquad \text{(three amplifiers)}$$

Now the value of γ is affected by the solid angle (Ω) that can be accepted. In the case of three amplifiers, we have $\Omega \simeq 1.6 \times 10^{-6}$. For one amplifier, $\Omega \simeq 3 \times 10^{-3}$.

Scattering loss coefficients in ED-2 laser glasses[10] are about 1.6×10^{-6} cm^{-1} Ω^{-1}. For a first approximation, then

$$\gamma_3 \simeq (1.6 \times 10^{-6})(1.6 \times 10^{-6}) = 2.56 \times 10^{-12}\ \text{cm}^{-1} \qquad \text{(three amplifiers)}$$

$$\gamma_1 \simeq (1.6 \times 10^{-6})(3.1 \times 10^{-3}) \simeq 5 \times 10^{-9}\ \text{cm}^{-1} \qquad \text{(one amplifier)}$$

So for three amplifiers

$$\frac{E_b}{E_o} \simeq 25.6$$

and for one amplifier

$$\frac{E_b}{E_o} \simeq 2.3 \times 10^{-4}$$

Here again it appears that gains of 10^6 (three amplifiers) will require isolation, since few oscillators would benefit from a return signal 25 times its output. These calculations are only first-order approximations, but they do indicate that one should expect difficulties when the small signal gain approaches 10^3.

Scattering from surfaces can increase the magnitude of this backscatter problem. Total backward scattering (not including specular reflection) from ED-2/air interfaces is $R \approx 10^{-5}$.[11]

In this case

$$\frac{E_b}{E_o} \simeq RG_o^2 \left(\frac{\Omega}{2\pi}\right) \tag{17}$$

For one amplifier

$$\frac{E_b}{E_o} \simeq (10^{-5})(10^4)\ \frac{3 \times 10^{-3}}{6.28} \cong 4.7 \times 10^{-5}$$

For three amplifiers

$$\frac{E_b}{E_o} \simeq (10^{-5})(10^{12})\ \frac{1.6 \times 10^{-6}}{6.28} \lesssim 2.54$$

Here again, gains of 10^6 could, it appears, cause trouble.

Reflections from amplifier rod surfaces must also be considered. The Fresnel reflection of 100 J/cm^2 for ED-2/air interfaces will be more than 4 J/cm^2. If the beam is converging and the surface is nearly normal to the beam, this 4 J/cm^2 light could be amplified and focused to a point inside an amplifier. Even if the beam is diverging and the surface is not normal to the beam, the total internal reflections from the rod barrel may form caustic foci that could cause damage. Note also that, even if these caustics do not directly cause damage, the refractive index perturbations at the caustic may cause self-focusing damage further downstream. At 100 J/cm^2, it is clear one does not want backward traveling

reflections. Faraday isolators will help but they cannot protect an amplifier from its own reflections. Anti-reflection coatings would help if damage-resistant coatings can be produced. Making the final amplifier exit surface a Brewster angle surface should also help - but not completely eliminate the problem. Because of surface scattering and imperfect polarization of the beam, there will always be some reflection at the Brewster angle surface. Because Brewsters angle is $> 45°$ - this reflected light will not immediately be traveling in a backward direction. It will however be traveling backward after five reflections ($R \approx 6 \times 10^{-6}$) and experience total internal reflection at the rod barrel/water interfaces. The off axis and diffuse (rod barrels are fine ground) nature of this light should make it not a major problem unless a focused caustic causes damage. Note that the first reflection from the barrel makes a line focus that intercepts the Brewster angle surface. It may be wise to spoil the reflection of the barrel near the output end of Brewster angle rods.

One way to eliminate or greatly reduce the problems created by the reflections from amplifier rod ends is to use a clad laser rod and cut the ends of the rod a few degrees from normal. The cladding material index matches and makes optical contact with the laser rod to eliminate reflections. The cladding also absorbs the laser light to prevent it from reentering the laser rod after reflection from the cladding/air interface. The primary purpose of the cladding generally is to eliminate parasitic oscillations and increase pumping efficiencies. However, the cladding can also serve a valuable purpose by absorbing the laser light

reflected from the amplifier exit face - thus preventing damage from caustics, as well as increasing the efficiency. Solid cladding by samarium-doped glass has been used, but it is difficult to maintain optical contact without stressing the laser rod. The author has been developing liquid claddings for both rods and disks.[12] With liquids, no stresses can develop and the same liquid can cool the laser rod. McMahon[13] has recently demonstrated significant increases in gain by using a liquid cladding on laser rods.

Finally, we ask at what gain value the laser will become a bulk-feedback oscillator. The ASE starting in the middle of a rod will reach a certain intensity by the time it reaches the end of the rod. Some of this ASE will be backscattered and amplified as it returns toward the center of the rod. The condition for oscillation is that, at the center of the rod, the returning (backscattered) ASE be more intense than the original ASE. We have seen that backscattering is on the order of 10^{-12}, so gains of at least 10^{12} will be required. This gain limit is much higher than the other gain limits already treated. Thus, bulk feedback oscillations are probably unobservable in Nd:glass lasers.

II-3.2.2. Damage resistance of Brewster angle surfaces

It is well established that a surface at Brewsters angle (θ_B) will have a higher surface damage threshold than the same surface at normal incidence. This is not surprising since the same beam energy is spread over a larger surface area in the Brewster angle case. The increase in area is given by

$$1/\cos \theta_B = 1.84$$

Since the irradiance decreases by $(1.84)^{-1}$, one might expect the damage threshold to increase by 1.84. However, this may be a naive view.

The work of Crisp, et al,[14] strongly suggests that it is the value of the oscillating electric field on the surface that determines damage thresholds. Application of Fresnel's equations show that, on a Brewster angle surface, the p polarized electric vector is reduced to $1/n$ of its in-air value. At normal incidence, the electric vector on the exit face (neglecting gain) is $4n/(n+1)^2$ times its in-air value. The increase in damage threshold of Brewster surfaces over normal surfaces should then be given by

$$\left[\frac{4n^2}{(n+1)^2}\right]^2 = 2.18 \qquad \text{for } n = 1.55 \tag{18}$$

This is appreciably different from the 1.84 factor in surface area. Note, however, that there are qualitative differences between the Brewster angle case and the normal incidence case. Only tangential electric fields are present in the normal incidence case. For p polarized light in the Brewster angle case, normal and tangential fields are present. There does not appear to be enough experimental evidence to establish whether normal and tangential fields have the same effect on surface damage. The author believes that it would be fruitful to conduct such experiments.

Nonetheless, it is well established that Brewster angle surfaces are more damage resistant than normal surfaces. (Our experiments made this painfully obvious.) We have already discussed how problems due to

reflections from the amplifier faces also suggest that Brewster angle faces be used. So it seemed quite reasonable to make the final amplifier a Brewster angle configuration. Both final amplifiers used in our experiments had Brewster angle (parallel) ends.

Recently, Bloembergen (Appl. Opt., 12, 661 [1973]) showed that theoretically scratches should enhance surface electric fields and thus lower damage thresholds by as much as $1/n^2$. In theory, this applies only for scratches perpendicular to the electric vield. For scratches parallel to the electric field, no effect should exist. In all our experiments, linearly polarized light was used with its electric fields horizontal. In order to minimize any effects of scratches, all cleaning of rod surfaces was done using only horizontal motions. Thus, any scratches caused by the cleaning process would be parallel to the electric field and thus should not lower the damage threshold of the surface. In order to check the necessity of taking this extra precaution, we purposely scratched two glass samples with straight scratches and tried to show that the damage threshold was lower for electric fields perpendicular to the scratches. No such effect was found, within our experimental error. Admittedly, only two samples were tested, but this failure to demonstrate the effect of the scratches is consistent with the conclusions reached in Section I; namely, that in practice scratches do not appreciably lower the damage thresholds of glass surfaces. Possible reasons for this are given in Section I.

II-3.2.3. Maintaining a smooth irradiance profile

The importance of creating a ''clean'' beam and keeping it clean as it propagates through an amplifier chain was recognized long ago.

Whatever the damage mechanism is, hot spots in the beam will cause damage at lower average irradiances. Practical lasers must be concerned with total efficiencies and therefore it is normally desirable to uniformly fill the entire clear aperture of the laser with an irradiance that is just below the damage level.

Historically, the first problem was how to create a beam without hot spots. Most techniques for creating a clean beam had the practical disadvantage of reducing the total energy or power in the beam. Q-switched oscillators restricted to the TEM_{oo} mode were generally limited to outputs of 0.1 J or less. Without mode control, much higher total outputs were available, but one could never be sure that hot spots were eliminated. Similarly, pinhole spatial filters could be used to clean up a beam outside of the oscillator, but again the total power or energy was reduced. Later on, there was some interest in maximizing the efficiency and total output of TEM_{oo} oscillators by careful cavity design. Sometimes a nice side effect is that such cavities are highly stable. That is, the spot size is relatively insensitive to changes in cavity parameters due to flashlamp-induced stress, temperature effects, n_2 effects, etc.

There are ways of producing smooth irradiance distribution, and once this is done, one must concentrate on increasing the total power of the beam. A common attitude is that one need not worry about the energy that was wasted in cleaning up the beam because one can simply add more amplifiers to make up the energy. At a certain amplifier gain value, however, isolation will become necessary, so there is good reason to want a large oscillator output.

A top-hat irradiance distribution of diameter equal to the laser amplifier's clear aperture and height (irradiance) just below the damage threshold would maximize the extraction of energy from the laser amplifiers. The smooth irradiance patterns referred to earlier, however, are bell-shaped. There are several ways to transform a bell-shaped irradiance pattern into a top-hat irradiance pattern. Two passive ways are: (1) to simply use a small aperture to pass only the central peak, and (2) to pass the bell-shaped pattern through a filter that transmits less in the center than at the edges. Both of these techniques, of course, cause further reductions in total energy. A third way is to pass the bell-shaped pattern through an amplifier that has higher gain near its edges than along its axis. Almost all Nd:glass rod amplifiers meet this criterion. Even if the amplifier has uniform small signal gain, the center of a bell-shaped pattern will saturate sooner than the edges and barring damage, the pattern will become more top-hat-like as it propagates through the amplifiers.

This point seems worth elaborating a bit. If one can avoid damage, the saturation of an amplifier may smooth over any irregularities in the beam irradiance. We emphasize this because at 100 J/cm^2 in a 30 ns pulse, we are well over the saturation energy irradiance for ED-2 (generally considered to be ≈ 6 J/cm^2). This is in contrast to the 0.1 ns Nd:glass lasers which must operate at < 1 J/cm^2 to avoid self-focusing damage.

Unfortunately, the abrupt truncation of the top-hat distribution leads to undesirable diffraction effects. The apertures used to truncate

the beam create diffraction patterns downstream that make the irradiance not uniform. The depth of modulation in these diffraction rings can be reduced by making the truncation less severe, that is, by returning to a bell-shaped irradiance pattern. In many practical laser systems then there is a trade-off between the top-hat distribution which maximizes energy extraction and a bell-shaped distribution that minimizes diffraction rings. If damage and output radiance are of no concern, the top-hat distribution would seem to be the best choice. However, the largest interest in Nd:glass lasers is in the subnanosecond region where self-focusing-type damage is a problem and diffraction rings should be avoided.

If one asks the question, what spatial irradiance distribution propagates to its far field such that no diffraction rings form, the answer is, a Gaussian irradiance distribution. Unfortunately, any distribution available to us in the lab can at best be a truncated Gaussian. Several references have considered the diffraction rings formed by varying degrees of truncation.[15] As a rule of thumb, diffraction effects are minimal if the aperture is at least four times the 1/e (intensity) size of the Gaussian beam.

So, it appears that no ideal solution to the diffraction problem exists. We must then ask, what's the best practical solution? This problem is similar to the apodization problem in image-forming optics. We would like, however, to point out two important differences. These differences should make one think twice before one simply borrows results known from apodization theory. The first difference is that the

amplifier chain has gain, and this gain is not uniform across the amplifier aperture. Even if a uniformly pumped amplifier is used, saturation of the gain will alter the final intensity distribution, in both amplitude and phase. The second difference is that in image-forming apodization one is concerned with reducing or eliminating the diffraction rings with the additional constraint that the central lobe not be significantly broadened. This apparently means that only real (uniphase) transmission filters are of use in image-forming apodization.[16] Phase plate filters have one valuable feature in that their transmission is 100%. It might be worthwhile to study theoretically phase plate apodization for high-power laser beam propagation. Such a study was considered beyond the scope of this contract.

Nonetheless, it seems reasonable to borrow several conclusions from the apodization literature. One such conclusion is that any transmission distribution, T(r), that smoothly drops off towards the edge of the (circular) aperture reduces the relative intensity of the diffraction rings in the far field. Further conclusions seem to be that the more derivitives of T(r) that go to zero at the edge, the better. One method of making "clean" beams involves making the intensity go to zero in a ring of some diameter and then placing another aperture of this diameter at that spot. The most common of these techniques is to use an Airy disk spatial filter (Figure II-10). In this device, the first positive lens serves as a focusing lens and limiting aperture that forms at its focus an Airy disk pattern. Strictly speaking, this is true only if it is illuminated with a uniform plane wave. In practice, the pattern at

the focus is very similar to an Airy disk. More than 80% of the total energy is contained in the central lobe, making this device highly efficient. A (pinhole) aperture just big enough to pass only the central lobe is then placed at the focus. At this plane then there is an intensity distribution which drops smoothly to zero at the edges of the pinhole aperture. Another positive lens then recollimates (or focuses) this light. Recall, however, that even in theory, the far field diffraction pattern of the light is not fringeless. Note also that lenses can be eliminated by placing the second aperture in the far field of the first aperture.

During the course of this contract, there was a great deal of interest in the laser community in designing and producing apodizers or soft apertures for use in high-power laser systems, especially Nd:glass lasers. Again, the goal is to achieve a high total transmission while still eliminating diffraction rings downstream. As a result of this work at Livermore, Los Alamos, the University of Rochester and elsewhere, some more specific criteria have evolved. In order to maximize the total transmission, the transmission of the apodizer should be 1.0 from its center out to perhaps 3/4 of its clear aperture. From there, its transmission should decrease smoothly to $\leq 10^{-4}$ at the edges. Computer calculations have indicated that such an apodizer should work very well. Appendix B is a copy of a letter we prepared on the subject of such apodizers. Many types of apodizers have been considered and late in this work we thought of what may be a new type of apodizer suitable for use with high-power lasers; we call it the total internal reflection (TIR) apodizer (see Appendix B).

Early in this work, we considered many ways of creating and keeping a clean beam. In the next several pages, we will briefly discuss a few of what we think are new contributions arising from this work.

To start, we mention an obvious fact, but one that is seldom put to advantage. A spatially incoherent beam does not create diffraction patterns. Thus, one way to avoid diffraction rings is to use a spatially incoherent beam. We will say more about this later.

We also considered trying to use two or more complimentary diffraction patterns such that the peaks of one fell on the valleys of the other - resulting in a more uniform irradiance. We considered splitting the beam in two, exposing each beam to a different aperture, and then recombining the two beams (the two diffraction patterns). We considered designing stepped semitransparent apertures so the resultant diffraction patterns would be complimentary. None of the above approaches seemed attractive enough to continue investigating. The complimentary diffraction patterns only seemed to help for a narrow range of distances from the aperture(s) and seemed to offer no advantage over continuous (smooth) apodizers.

Nonplanar (concave) dye cells can also be used to apodize a beam. In unrelated work, the author has developed a class of liquids that strongly absorb (absorption coefficients up to 10 cm^{-1}) 1.06 μm light and index match typical glasses.[12] Figure II-11 shows one design considered during this work. Figure II-12 shows the transmission as a function of distance from the optic axis for two values of absorption coefficients. Without going to highly aspheric surfaces, it is difficult

to achieve both a high average transmission and complete attenuation at the edges. No such apodizer was used in our experiments.

Another method we considered for eliminating diffraction ripple was to use a limiting aperture of irregular (random) shape. The idea was that the diffraction pattern from such an aperture would be blurred out so that no steep intensity gradients would result. We made several irregularly shaped apertures (Figure II-13) by hand and used a He-Ne laser to produce diffraction patterns which were observed visually. Our conclusion was that, while the diffraction pattern was more irregular, it still contained steep intensity gradients.

Historically, the first self-focusing to be considered was the whole-beam collapse type. More recently, small-scale or instability mode self-focusing has been recognized and studied. This evolution is quite understandable since early lasers had modest total outputs, irradiances necessary for nonlinear effects like self-focusing required small beam diameters. As total outputs increased, the same irradiance could be produced in larger beams making it easier to observe the small-scale (angel hair) type of self-focusing in damage. The instability theory warns that small-scale (< 1 mm) perturbations of the irradiance patterns will grow rapidly and quickly lead to damage. Even without intentional perturbations, a beam propagating through any material will develop its own perturbations due to the inevitable random disordering on a local scale. Nonetheless, it seems entirely reasonable

to avoid perturbing the beam whenever possible. Thus, we carefully selected our laser rods to be as free as possible of any scattering centers (see p. 101).

Another possibility for keeping a clean beam is to eliminate the nonlinear refractive index of the Nd:glass. The possibility of achieving such a glass is in doubt. A zero or negative n_2 has not been demonstrated. Defocusing has been demonstrated but only at near resonance where saturated anomalous dispersion can lead to time-integrated intensity dependent self-defocusing. Such a technique might find use even if a laser glass with positive n_2 is inevitable. By placing a self-defocusing material between stages of self-focusing materials, the deleterious effects of self-focusing might be reduced. No such material was available to us so this technique could not be pursued.

Another possibility for cleaning up a beam would be a pseudo-saturable absorber. This device would offer low transmission to hot spots and high transmission to weaker irradiances (the opposite of a saturable absorber). Possibly a two-step absorption process with the middle level lifetime longer than the pulse width would result in a pseudosaturable absorber. Here again no suitable material was known to us and at 15 or 30 it was not clear that we would need such a device.

Another technique we considered we called lensless spatial filtering. This technique relies on the Fresnel diffraction pattern of a lensless aperture rather than the Fraunhoffer diffraction of a lens. As in the Airy disk spatial filter, the first element makes a diffraction pattern with a dark (zero irradiance) ring of diameter F, the second element is an aperture with diameter F. In both types of spatial filters, the irradiance in the plane of the second element (aperture) is bell-shaped with zero irradiance at the edges. As already mentioned, this irradiance distribution (if uniphase) will propagate with reduced diffraction ring effects.

Figure II-14 shows the distances needed to estimate the Fresnel diffraction effects used in lensless spatial filtering. Given any a and b (a may be negative for converging incident light), the plane of the aperture will contain a certain number of Fresnel zones. The radius of these zones is given by

$$s_m = \sqrt{\frac{m\lambda ab}{a+b}} \tag{19}$$

In the plane of b, the irradiance can be estimated at any point (on or off axis) by placing the center of the aperture over the Fresnel zone pattern referred to above. Each Fresnel zone carries an equal amount of energy (given uniform incident irradiance) and is out of phase with its neighboring zones. So if the imaging aperture passes an odd number of zones, the spot at the center of the aperture will be bright; if the imaging aperture passes an even number of zones or equal areas of two adjacent zones, the spot will be dark.

If we want to pick b and/or s in order to insure a dark ring in the plane of B, we must have

$$s_2 - s_1 = s = \sqrt{\frac{\lambda ab}{a+b}} \tag{20}$$

If the incident irradiance is bell-shaped, s must be smaller. In the limit of zero irradiance at the edges of s, the conditions become

$$s = \frac{1}{2}\sqrt{\frac{\lambda ab}{a+b}} \tag{21}$$

This corresponds to an imaginary aperture that, when placed a distance $s_1 + s_2/2$ off axis, passes only a portion of the second Fresnel zone. Any aperture smaller in radius than $1/2\sqrt{\lambda ab/a+b}$ should produce a dark ring with radius approximately equal to s_1.

Let us assume

$\lambda = 1.06 \times 10^{-4}$ cm

$a \to \infty$

beam size < 2 mm (typical oscillator output) and solve for b, we find

$$\frac{1}{2}\sqrt{\frac{\lambda ab}{a+b}} < s_2 = s_1 < \sqrt{\frac{\lambda ab}{a+b}} \tag{22}$$

or

$$\frac{1}{2}\sqrt{\lambda b} < s_2 - s_1 < \sqrt{\lambda b}$$

or

$$3.77 \text{ meters} < b < 15.1 \text{ meter}$$

With a table length of about 4 meters, the use of a lensless spatial filter appeared marginal in our case. Nonetheless, we pursued its properties a bit more because we feel that there may be cases where its use would be warranted.

The advantages of a lensless spatial filter are: (1) no lenses are required, (2) because there is no focusing, the chances of damage to apertures or air sparking are low, and (3) the overall transmission can be high. The disadvantages are: (1) in many cases, it requires large separations of apertures, and (2) it is probably less successful at cleaning up a bad beam than a pinhole spatial filter - it requires a reasonably good beam to start with.

We note that, for an aperture of radius s, the far field is generally given by

$$\frac{\pi s^2}{\lambda b} \ll 1 \qquad (23)$$

or

$$b \gg \frac{\pi s^2}{\lambda}$$

In the case discussed above, $\pi s^2/\lambda$ is 11.8 meters, so the b necessary to insure a dark ring is <u>not</u> equivalent to going to the far field of the aperture. We hasten to point out that the Fresnel zone approximation is only an approximation. Our experiments with He-Ne lasers indicate that the Fresnel-zone approach gives good qualitative agreement (number of dark rings, etc.) but that more detailed calculations must be used to get good quantitative agreement. For example, our simple approach does not allow for the general spreading of the light as it propagates.

One can shorten the distance between the two apertures by using a converging beam. For example, if a = -1.16, we have

$$0.34 \text{ meters} < b < 1.37 \text{ meters}$$

a much more workable distance. However, now one must use two lenses to focus and recollimate the beam and the possibility of air sparking exists. One would, however, keep the advantage of minimizing the chance of damage to either aperture. Figure II-15 shows an irradiation (diffraction) pattern produced by lensless spatial filtering of a collimated He-Ne beam. In this case, $a = \infty$, $b = 847$ cm, $s \simeq 1.0$ mm, and $s_2 - s_1 \simeq 0.96$ mm.

In conclusion, we felt that lensless spatial filtering was a technique with some merit, but that it was not suitable for our experiments.

Whenever a lens is used as an optical element in a high-power laser system, one must be careful that focused reflections from the lens surfaces do not cause optical damage or otherwise perturb the beam. This seems rather obvious, but we believe we have discovered at least one case where these precautions are not generally taken.

Perhaps the most obvious thing to avoid is reflections from a concave surface (Figure II-16). If the first surface is concave, a source at a distance x_o from the apex will be imaged at x_1, where

$$x_1 = \frac{rx_o}{r - 2x_o} \tag{24}$$

so as

$$r < x_o < \infty$$

then $$r < |x_1| < r_2$$

If the second surface is concave, the position of x_1 will of course depend on the first surface reflection as well as the second surface reflection.

Returning for the moment to the concave first surface, we estimate the irradiance at x_1 given an incident irradiance I_o. The image at x_1 will, of course, suffer from spherical aberration. In order to calculate an upper limit, we assume a diffraction limited focus in which 80% of the total energy is contained in a circle of radius $1.2\,\lambda x_1/D$ where D is the lens or beam diameter, whichever is lesser. The irradiance at x_1 is then approximated by

$$I_{x_1} = \frac{0.8 I_o \frac{\pi}{4} D^2 R}{\pi\left(\frac{1.2\lambda x_1}{D}\right)^2} = \frac{0.8 I_o D^4 R}{5.76\lambda^2 x_1^2} \tag{25}$$

where R is the reflectivity of the surface for $\lambda = 1.06 \times 10^{-4}$ cm.

$$\frac{I_{x_1}}{I_o} = \left(\frac{RD^4}{x_1^2}\right) 1.23 \times 10^7 \quad \text{all distances in cm} \tag{26}$$

For example, consider a 4-meter focal length negative lens of 3 cm diameter such as might be used to add divergence to a laser beam in order to fill up larger succeeding amplifiers. In this case, $r \simeq f$ if the lens is biconvex. If the incident light is collimated, $x_1 \simeq 2$ meters and

$$\frac{I_{x_1}}{I_o} = R\ 2.48 \times 10^4$$

If the lens is uncoated, $R \simeq 0.04$ and

$$\frac{I_{x_1}}{I_o} = 1.0 \times 10^3$$

Even as an upper limit, this is a large number. If the lens is AR coated so $R = 10^{-3}$, we have

$$\frac{I_{x_1}}{I_o} = 24.8$$

still a large number. Note also that permanent damage at x_1 is not the only danger. The local high intensities at x_1 can cause refractive index perturbations that will perturb the laser pulse if the pulse is longer in space than $2x_1$. For the case considered above, this would mean a pulse length of greater than 130 ns. If the coherence length is greater than $2x_1$ ($\Delta\lambda < 2.75 \times 10^{-3}$ Å), an interference pattern will be formed at x_1. This should further perturb the material (air or whatever) at x_1. The current emphasis on small-scale self-focusing should make these secondary foci important considerations.

One nice feature of these single reflection foci is that a slight tilt of the lens can often move x_1 away from damageable elements without adding troublesome aberrations to the beam. The properties of these foci are well known, our main purpose in detailing these properties is to compare them with the foci to be discussed next.

Next we'll consider a less obvious but potentially more troublesome focus formed on the downstream side of any positive lens, regardless of its shape factor. This focus is due to light twice-reflected

inside a positive lens. For simplicity, we consider a plano-convex lens (Figure II 17). We have shown that

$$x_3 \simeq \frac{f(n-1)\, x_o}{x_o(3n-1) - f(n-1)} \tag{27}$$

where f is the focal length of the plano-convex lens, x_o is the object distance, n is the refractive index of the lens, and x_3 is the image distance.

If the incident light is collimated

$$x_3 \to \frac{f(n-1)}{3(n-1)} \tag{28}$$

for n = 1.5, this becomes

$$x_3 \simeq 0.14\ f$$

One common use for positive lenses is as the second element of a beam-expanding afocal telescope. In this case, x_o = f and

$$x_3 = \frac{f(n-1)}{2n} \tag{29}$$

for n = 1.5, this becomes

$$x_3 \simeq 0.17\ f$$

We see then that x_3 is not a strong function of x_o for practical cases. We have experimentally verified eq. 27 for plano-convex lenses. The focus and interference patterns near the focus are easily visible using a He-Ne laser. No theoretical work was done on more complicated lenses,

but our experiments on plano-convex, meniscus, and biconvex lenses indicate that for $x_o = \infty$

$$0.12 < \frac{x_3}{f} < 0.15$$

Before calculating the upper limit to the irradiance at these foci, we wish to point out several important qualitative differences between these two reflection foci. First, one cannot move the focus out of the beam by tilting the lens. Second, in order to have interference effects at x_3, the coherence length (or lengths) of the laser pulse need only be twice the optical thickness of the lens. If $n = 1.5$ and the lens is 1 cm thick, this corresponds to $\Delta\lambda \leq 0.37$ Å. This makes it more likely that interference patterns will further aggravate any small-scale self-focusing problems.

As before, we estimate the irradiance at x_3 to be

$$I_{x_3} = \frac{0.8 I_o \frac{\pi}{4} D^2 R^2 (1-R)^2}{\pi\left(\frac{1.2\lambda x_3}{D}\right)^2} \qquad (30)$$

$$= \frac{0.15\gamma\, D^4 R^2 (1-R)^2\, I_o}{\lambda^2 x_3^2}$$

if $\lambda = 1.06 \times 10^{-4}$

$$\frac{I_{x_3}}{I_o} = 1.23 \times 10^7 \frac{(1-R)^2 R^2 D^4}{x_3^2}$$

assuming $x_3 \simeq 0.14\ f$

$$\frac{I_{x_3}}{I_o} = 62.75 \times 10^7 \frac{(1-R)^2 R^2 D^4}{f^2} \qquad (31)$$

We'll consider two cases numerically, one lens typically used in a beam expander, and one typically used to recollimate the beam. In the first case, we take

$$f = 15 \text{ cm}$$

$$D = 3 \text{ cm}$$

x_3 in the second case we take

$$f = 700 \text{ cm}$$

$$D = 10 \text{ cm}$$

In both cases, we consider R = 0.04, and 0.001. The results are listed in Table II-3.

These are upper limits, but they clearly show that this twice-reflected foci can cause problems. Note also that, if an interference pattern occurs at x_3, the peak intensity will be four times higher than in the case of incoherent addition of intensities at x_3. The authors do not know of a particular case where damage could be attributed to this twice-reflected focus, but we would not be surprised to find such a case.

Another technique for keeping a fringe-free or clean beam is to start with a clean beam and simply keep the beam small compared to any apertures (amplifiers) it must pass through. The price paid of course is that only the central portion of the amplifiers is used, resulting in inefficient operation. Since total energy and efficiency were not parameters to necessarily be optimized in our experiments, the small beam approach could be used. To a certain extent, it was.

In summary, our work on getting and keeping a clean beam turned up three new techniques or findings, lensless (Fresnel) spatial filtering, TIR apodizers, and the twice-reflected foci of positive lenses. Next we outline the two basic experiments performed under this portion of the contract.

II-3.3. Planned experiments

Two basic types of experiments were planned. One sought a single longitudinal mode and single spatial mode oscillator and clean beam propagation through the amplifiers. The goal for the other experiment was no-spatial mode control but single longitudinal mode. However, we could only do no-spatial mode control with no longitudinal mode control. The ideas behind the no-spatial mode control experiment were basically that spatially incoherent beams would not make (stationary) diffraction rings and that the random superposition of hundreds or thousands of spatial modes, coupled with the saturation of the amplifiers, would result in a smooth irradiance (no hot spots).

The idea behind the TEM_{oo} experiment was also to use a no-hot-spot irradiance, but the method of achieving this was different. In this experiment, a TEM_{oc} oscillator would be used and special care would be taken to keep the beam clean (free of hot spots) as it propagated through the amplifiers. The narrow bandwidth assured that there would be no temporal hot spots (intense subnanosecond spikes).

A check of the commercial literature showed that no one offered a single longitudinal mode Q-switched Nd laser. One firm offered a narrow bandwidth (< 0.01 A) Q-switched Nd:YAG oscillator. This bandwidth

contains at most only a few longitudinal modes - so it appeared that one might achieve single-mode operation. The energy output is only 20 mJ which means that considerable amplification would be necessary.

Our choices then were to either buy the oscillator mentioned above, or design and build our own oscillator for reliable high-energy single-mode operation. Consistency and reliability are definite requirements in any system designed to be operated just under the damage threshold. We gave some thought to building a unidirectional traveling wave oscillator because we felt that such an oscillator could achieve high-energy single-mode operation. Damage to components would be minimized because steep angles of incidence could be used and standing wave anti-nodes would be avoided. Also the traveling wave feature should enhance energy extraction and single longitudinal mode operation. We decided, however, that designing, building, and optimizing such a device was simply too large an undertaking.

Unfortunately, we could not study only the effect of spatial mode differences. In order to avoid temporal hot spots (subnanosecond structure on the 15-30 ns pulse envelope), we wanted to use a single longitudinal mode oscillator with a bandwidth limited pulse length. The oscillator used for the no-spatial mode control experiments was a Nd:glass oscillator and had neither spatial nor longitudinal mode control. Consequently, its output contained thousands of longitudinal modes.

In the chart below, we studied cases (A) and (D). With the equipment we have at hand, we could also study cases (B) and (C). For case (B), we could remove the 1.8 mm mode selecting aperture from our YAG

oscillator and if necessary add further frequency narrowing components. For case (C), we could use our original TEM_{oo} glass oscillator and/or use our YAG laser with the output etalon replaced by a dielectric mirror. In principle then we could use our Nd:YAG oscillator to study all four mode conditions.

	Spatial Modes	Longitudinal Modes
(A)	1	1
(B)	$\gg 1$	1
(C)	1	$\gg 1$
(D)	$\gg 1$	$\gg 1$

We felt that this would be a very worthwhile study in both nanosecond and the picosecond pulse lengths. If multimode beams experience the same damage thresholds and limitations as single-mode beams, considerable savings could result due to the higher total outputs, higher efficiencies, and lower costs available in the multimode case.

II-4. Experiments

We describe the clean beam (single mode) experiments first and begin by describing the properties of the components used in this portion of our research.

II-4.1. Single-mode experiments

II-4.1.1. Oscillator characterization

A commercially available Pockels cell Q-switched Nd:YAG laser oscillator was purchased (with company money) for use in this phase of the contract. It is a Holobeam Model No. 356. It is advertised to feature TEM_{oo} and single longitudinal mode (or very close to it)

operation with a pulse energy of 30 mJ. A temperature-controlled two-piece air-spaced etalon is used as the output mirror to narrow the spectral content of the output. A bias-closed Pockels cell is used to Q-switch the laser and a 1.8 mm diameter aperture is used to limit the output to the TEM_{oo} mode.

A great deal of time was spent on the optimization and characterizing of this oscillator. To study its transverse mode pattern, we used zap marks on black Polaroid film, TV viewers, and shearing interferometers. To study its longitudinal mode structure, we used fast (< 1 ns) detectors and a 1-meter grating spectrograph. Once optimized, the oscillator performed very reliably for several months except for a few electrical malfunctions in the cooling system controls.

We found that only by purposely making the Pockels cell "leaky" could we obtain narrow bandwidth emission. Figure II-18 shows the temporal profile of the pulse as a function of Pockels cell voltage. The half-wave voltage was measured to be 4.9 kV. At lower voltages, the energy is lower but the pulse is smooth. We believe that the leaky Pockels cell operates like a slowly opened Q-switch in helping to narrow the spectral output.[10] We made no direct measurements that would establish single longitudinal mode operation, but the temporal profiles were consistently smooth once the oscillator was optimized. In hundreds of shots, only a few shots were not temporally smooth and all of these shots showed a temporal profile that could be explained as the beating of two adjacent modes. By detuning the temperature of the temperature-controlled etalon, we could demonstrate nonsingle mode operation. We

could make the output spectrum so broad that a spectrometer of ≈ 1/2 Å resolution could display the difference. In this experiment, we used a 1-meter grating spectrograph with a ground glass in the film plane. The infrared sensitive TV system was then focused on the ground glass and displayed the spectrum. As described in earlier reports,[21] one line of the TV scan could be displayed on an oscilloscope and photographed. Figure II-19 shows an obviously broad spectrum and what we believed to be a single-mode spectrum.

The output of the oscillator was nearly linearly polarized. The ratio of the intensity of light polarized with its E vector horizontal to the intensity of light polarized with its E vector vertical was 16.6:1. The lack of complete polarization is probably due to birefringence in the YAG rod and the temperature-tuned etalon.

In summary, a reliable TEM_{oo} narrow bandwidth (probably single longitudinal mode) oscillator was used. Its output pulse contained approximately 25 mJ in 15-20 ns. The energy repeatability was approximately ± 15%. This oscillator was quite reliable for several months, but its dependability and consistency dropped toward the end of this work. We have not pursued the causes of this reduced consistency. Because the oscillator was not isolated from the amplifiers, multiple longitudinal mode (spiky) outputs were more likely when the amplifiers were pumped intensely.

II-4.1.2. Characterization of the amplifiers and related equipment

Three identical amplifier heads were purchased from Apollo Lasers Inc. Each held a 3/4'' diameter rod and pumped approximately 30 cm of

the rod. Each head had two helical flashlamps and could discharge up to 10,620 J total. Mounts were designed and built to hold the amplifiers, oscillator, and numerous other components. These mounts were designed to keep the beam 15 cm above the table top. Fifteen cm was felt to be the minimum practical value. Shorter heights were not compatible with the oscillator and amplifier construction and higher distances would exaggerate any vibration problems. All components were placed on a 356 x 116 x 1.9 cm stainless-steel sheet. This sheet was not vibration-isolated, but did make a convenient working surface. Figures II-20 to II-22 show various components of the system.

Figure II-23 shows the FWHM and zero-to-peak times of the amplifier flashlamps at various voltages. Figure II-24 shows the central small signal gain for both a Brewster/Brewster angle rod and a 4°/4 rod. We believe the Brewster angle rod shows higher gain because of parasitic oscillations inside the rods. Figure II-25 shows the energy storage and small signal gain across the aperture of an amplifier pumped at 9 kV. The small signal gain through the edges of all three amplifiers is twelve times as great as the small signal gain through the center of all three amplifiers. We will comment later on how this complicates isolation and beam propagation.

Figure II-26 shows the experimental arrangement used to determine the lens effect of a pumped amplifier on the laser pulse. An etalon element was used as a shearing plate interferometer[19] to produce fringes that were viewed with a TV-videotape system. Figure II-27 shows a photograph of the TV display and the oscilloscope display for a typical

experiment. From the fringe spacing, we calculated the effective focal length of an amplifier for the laser pulse. We estimated that the amplifier acts like a negative lens with a focal length of 14 meters. Figure II-28 shows how the fringe spacing changed as a function of time. We found that a few seconds after the flashlamp pulse, the rod behaved as a positive lens. Figure II-29 shows the fringe spacing as a function of flashlamp voltage. As expected, the lens effect becomes more intense with increased pumping intensity. We felt these studies were important because we would be dealing with weakly focused beams and a slight lensing in an amplifier might be significant. In retrospect, it would have been interesting to study the lens effect at various positions in the aperture of the amplifier and at higher pumping voltages.

In order to minimize any damage or small-scale self-focusing caused by inclusions or inhomogeneities in the rods, we tried to find rods free of any scattering centers or inhomogeneities. A 15 mw He-Ne laser beam ($\approx$ 2 mm diameter) was passed along the rod axis and scanned manually so as to cover the entire area of the rod. The barrel of the rod was coated with index-matching oil so that any scattering centers could be more easily seen through the side (barrel) of the rod. About six rods were examined and three were found to be scattering center-free. The other rods had two to five scattering centers. One of the scattering center-free rods was damaged beyond repair during finishing. The other two scattering center-free rods were used in the first and last amplifiers of the mode-controlled (clean beam) experiments. The last (high irradiance) amplifier had

Brewster angle surfaces. The other two rods used in the mode-controlled experiments had 4° surfaces (4° off the normal). All rods were Owens-Illinois ED-2.2 (2 weight percent Nd) rods. All demonstrated surfaces flat to $\lambda/10$ homogeneity or better than $\lambda/8$.

In summary, each amplifier head could give small signal gains of more than 100 and behaved as a 14-meter negative lens. The lens effect remained rather constant during the peak gain of the amplifier. Neutral density filters would be used to reduce the gain at the amplifiers, while keeping the pumping intensity constant at 9 kV. Total pumped volume was 256 cm^3 and storage efficiency was about 1.1%.

The beam is expanded before it enters the first amplifier to maximize the gain of the first amplifier. In order to achieve 100 J/cm^2 in the third amplifier, the beam must be contracted. We decided to do this by focusing the beam-expanding telescope and using one negative lens between the second and third amplifiers (Figure II-30). Another way would have been to use another afocal beam-contracting telescope between the second and third amplifiers. We felt that the fewer lenses the better due to the problems of unwanted reflections. We tested a few home-made beam expanders and found that we could keep aberrations down to a few λ. However, the vibrations of our table became quite apparent during these tests and this convinced us that a one-piece mounting for the two lenses would be necessary. Thus, we purchased a commercially available 6:1 beam expander (General Photonics).

It is perhaps worth noting that one must be careful in applying simple lens design formulas to such a system. Figure II-31 illustrates

one potential pitfall. The Gaussian optics formulas measure focal length from the principal plane. In an afocal (or nearly afocal) system, the principal plane can be far removed from either of the lenses. For example, if $f_1 = 5$ cm, then a magnification (m) of 6 means that d (the separation of the lenses) must be 25 cm. If we ask for a focal length of 300 cm, we have

$$f = \frac{f_1 f_2}{f_2 + f_1 - d} \qquad \text{or} \qquad f_2 = 29.5$$

But the physical location of this focus will be $\ell' = mf = 1800$ cm from the lens.

Our early experimental efforts were aimed at learning how to observe the spatial profile of the beam and after that learning how to keep the beam clean and smooth as it propagates through the beam expander, amplifiers, and negative lens.

We used zap marks and the TV videotape system to record beam profiles. We found that the TV monitoring system could detect diffraction rings and that we could keep the beam relatively free of diffraction rings be carefully aligning the telescope and the first amplifier. Except in the first amplifier, the beam was smaller than the limiting apertures and alignment was not critical. In all cases, the beam was intercepted by a ground glass screen and the TV camera was focused on the screen from the back side (Figure II-32). This is in contrast to the previous method of using the TV system in which the beam was intercepted by the active surface of the TV camera (no lens or screen was used).[21] We felt that the screen system was more versatile in that

any size beam could be studied at any desired magnification. Figure II-33 shows a photograph of a burn pattern taken after the first amplifier. Figure II-34 shows a TV display of the beam taken after the third amplifier. This photograph is included to show that diffraction rings could be detected and displayed, it is not typical.

We found that a 2.5 mm diameter aperture placed between the oscillator and the telescope prevented extraneous light in the outer regions of the beam. The aperture did not seem to affect the central part of the beam. With the TV system, we also could observe that the position of the beam waist (or the size of the beam at any particular point) was a function of the pumping intensity of the amplifiers. The simple lens formula indicated that the two amplifiers, each acting like a 14-meter negative lens, could shift the focus of the beam by almost one meter.

We also used the TV system to carefully align the first amplifier. This was done by placing a tissue-paper screen over the ends of the amplifier rod. A white light shown through the rod illuminated the clear aperture of the amplifier. When the laser pulse irradiated the screen, we could display (single frame still) the laser pulse and the rod aperture on the TV monitor. This allowed for very accurate alignment.

We could also observe that small signal and large signal diffraction patterns were different and that a beam that gave fringes in one plane sometimes did not show fringes in a plane farther or closer to the oscillator.

The flashlamp light created a lot of noise on the TV pictures. Normal shielding did not help much because the TV system is more sensitive to visible light than infrared light. A thin film band pass filter

did not work well because it introduced lines or fringes in the picture. In order to block the visible light and still keep the picture quality, we prepared a water solution of KI_3[22] and placed a 5 cm cell of this solution between the TV and the screen (or in front of the screen). This solution was opaque to visible light but transmitted about 30% of the 1.06 μm light.

One of our early studies involved purposely damaging a (passive) rod placed where the third amplifier would be. We hoped to see a beam break-up prior to catastrophic damage and to study what effect catastrophic damage might have on the rest of the system. We did not see any predamage break-up of the beam - but only a few experiments were run; we studied only the near field, and the energy density was increased in large steps. We did, however, discover that there was significant scattering of the laser pulse from the damage sites. The backward scattered light was amplified, focused by the positive lens of the telescope, and damaged the negative lens of the telescope. A Faraday isolator would have prevented this damage. In pursuing the forward scattering, we found that, even in the absence of damage, there was significant forward scattering. This scattering caused us at one point to think that we were observing pulse broadening in the final amplifier. We finally determined that our detector was picking up forward scattered light from both the third and the second amplifiers (Figure II-35). In later experiments, the detector was shielded from all amplifiers.

We have no direct reason to believe that this forward scattered light could be used as a precursor to damage, but it would be interesting

to investigate this possibility. The light seems to be more intense than passive scattering calculations would suggest - perhaps a plot of relative scattered intensity versus beam irradiance would demonstrate a kink or bend at an irradiance level below the damage level. It is certainly true that significant scattering will occur for free electron densities below the free electron density necessary for damage. The growth of free electron densities (electron avalanche) is a very nonlinear process, but it still seems possible that, by monitoring the forward scattered light, one might be able to tell when one was approaching damage threshold irradiance. It is often observed in large glass lasers that the beam spreads appreciably at high irradiances.[23] In the past, it has not been clear whether this spreading occurred because of damage or before damage. A careful study of forward scattering might reveal a precursor to damage. If so, this would be a significant finding whose benefits would not be restricted to Nd:glass lasers.

Figure II-36 shows oscilloscope displays of a damaging pulse. Note the reflected pulses of high intensity. By measuring the temporal spacing of these pulses, we determined that they were indeed reflected from the damage sites and the oscillator. A Faraday isolator would eliminate the intense pulses and prevent them from causing further damage.

In all our experiments, visual observations by two observers using a bright microscope light were used to search for damage. In only two cases out of twenty did the two observers not agree on whether or not there was damage.

After damaging the expendable rod, we noted that the AR coatings on the second amplifier rod were damaged in several areas. We had had only one rod AR coated because we wanted to see how the coatings held up and how they affected the other properties of the rod. Interferograms of the rod before and after coating showed obvious differences - perhaps indicating that the rod became very hot during the coating process. Coupled with the facts that the coating damaged and the gain (energy storage) did not seem to improve (we had hoped that the AR coating would increase energy storage by reducing the parasitic oscillation problem), we decided to not AR coat any of the amplifier rods. Thus, because of reflections, the final amplifier exit surface would almost have to be a Brewster angle surface. If a nearly normal surface were used, an intense pulse would be backscattered and focused inside the amplifier.

II-4.1.3. Single-mode experimental results

We replaced the second amplifier rod and the negative lens in the telescope and proceeded to the setup shown in Figure II-37. The exit plane was imaged on the ground glass and the area of the beam at the FWHM points was determined from oscilloscope display of the TV picture. ρ was determined by dividing the total output energy by the area calculated above. Readings as high as 157 J/cm^2 were recorded, which made us suspicious of our measurement technique. We decided that a 1 mm aperture should be used at least to calibrate the TV system and perhaps even to replace the TV system.

When the 1 mm aperture was placed some 62 cm beyond the exit plane, we registered $\approx$ 45 J/cm^2 (never more than 50 J/cm^2). ρ at the exit

plane can only be estimated because the divergence of the beam was not accurately known. In any case, this was still not a direct measurement of ρ at the exit plane. Our plan was to increase ρ by simply using a stronger negative lens placed closer to the third amplifier. Also the measurement scheme would use a simple positive (f = 31 cm) lens to focus the exit plane of the amplifier on the plane of the 1 mm aperture. The calorimeter would be placed directly behind the 1 mm aperture. In order to obtain some sort of visual display of the beam quality, darkened Polaroid film (paper) was placed over the 1 mm aperture with a hole in it slightly greater than 1 mm in diameter to let the 1 mm portion (center) of the beam pass through the aperture. The beam patterns on the film showed whether or not the beam was centered on the 1 mm aperture and also indicated (approximately) the diameter of the beam. Roughly 0.2 J/cm^2 is required to burn this film so when a quartz beam splitter is used, the full diameter of the burn pattern indicates the beam diameter at the 6.1 J/cm^2 level. No TV monitoring was done when the above measurement scheme was in use.

Our first round of experiments had gone so smoothly that we relaxed our concerns over damage to the final negative lens. No damage occurred in the first experiments, so we thought it would be rather straightforward to increase ρ at the lens. We found, however, that every attempt to increase ρ at the lens resulted in damage, mostly surface damage to the lens. We tried several different types of readily available lenses and also tried using the hot nitric acid treatment on some of these lenses. This hot nitric acid treatment developed under this contract

(see Section I) had been very successful in raising the damage threshold of some glass surfaces. All our efforts were to no avail, we continued to damage the negative lens. We ordered some custom-made fused quartz lenses, but the manufacturer lost these lenses and by the time they were remade and shipped, time had run out.

On two shots with the (damaged or damaging) negative lens in place, we did achieve more than 60 J/cm^2 with no damage to anything except the negative lens.

Finally we removed the negative lens and pumped only the first and third amplifiers. If all three amplifiers were pumped, we encountered air sparking in front of the third amplifier and several joules of amplified spontaneous emission. Using only two amps, we obtained > 70 J/cm^2 on several ($\approx$ 6) shots with no apparent damage. At 75 J/cm^2, there was some doubt as to whether there was self-focusing damage or not and, at 94 J/cm^2 (5.9 GW/cm^2), there was definitely self-focusing damage. Unfortunately, we could only achieve these irradiances by pumping the amplifiers at more than 9 kV. This meant that the divergence and size of the beam in the third amplifier may have changed slightly because we had not characterized the beam properties under these conditions. Thus we cannot be sure that the beam was diverging - it may have been focused inside the amplifier or beyond the amplifier due to the unknown lensing effect of the first amplifier. So again, it may be possible to do better than 70 J/cm^2 (4.4 GW/cm^2) when more preamplification is provided. We could not achieve more preamplification because of isolation problems. Figure II-38 shows oscilloscope traces and burn patterns for

two > 70 J/cm^2 shots that did not cause damage. Figure II-39 shows two damaging shots - note again the intense reflected pulses propagating back and forth through the entire system.

The spot size in these final clean beam experiments was estimated (on the basis of the burn patterns in the plane of the 1 mm aperture) to be about r_o = 1.55 mm. So, if the beam irradiance was Gaussian, the actual peak irradiance given by Figure II-5 would be 74 J/cm^2 instead of 70 J/cm^2.

Since we don't know how Gaussian the beam was, we'll claim only $\gtrsim$ 70 J/cm^2 in a 15 ns pulse (4.4 GW/cm^2). In terms of irradiance (W/cm^2), this is 142% of the contract goal. In terms of energy irradiance, this is 70% of the contract goal, but in a pulse half the length of the contract goal (100 J/cm^2 in a 30 ns pulse or 3.1 GW/cm^2). In Section II-5.1, we will compare these results with the prior state of the art.

It is interesting to note that $\gtrsim$ 70 J/cm^2 operation was achieved with pulses that had smooth temporal profiles and with pulses that had irregular substructure on the 15 ns pulse envelope (Figure II-38). When the amplifiers were pumped intensely, the oscillator output was more likely to be temporally irregular. One should be careful in trying to draw conclusions from such limited experiments, but it does appear that subnanosecond spikes do not appreciably lower the damage threshold.

With the diagnostics used in these experiments, we cannot say whether the self-focusing was whole-beam or small-scale in nature. Bliss[2]

has reported whole-beam self-focusing in similar rods at similar irradiances and beam diameters, but with picosecond pulse lengths.

It is also interesting to note that the Polaroid burn patterns indicate fringes near the periphery of the beam (Figure II-38). Recall that this burn pattern periphery corresponds roughly to the 6 J/cm^2 energy irradiance level. This may be an indication that, at higher energy irradiances, the saturation of the amplifiers smooths out the irradiance pattern. Of course, it could also indicate that fringes can only be detected by the film when the irradiance is near the film burn threshold.

II-4.1.4. Final examination of amplifier rods

Upon the termination of these experiments, the three laser rods used in the mode-controlled experiment were reexamined for scattering centers, optical homogeneity (Mark-Zender interferometer and polarimeter) and flatness of surfaces.

The first amplifier rod showed no scattering centers before or after the experiments. The rod experienced approximately 1500 shots with a maximum irradiance (exclusive of pulses reflected from damage sites) of approximately 60 Mw/cm^2. The second amplifier rod had two scattering centers before the experiments and four scattering centers after the experiments (the original two plus two more). No size or shape could be attributed to these scattering centers because they are so small. All we can say is that, under intense illumination and careful observation, they scatter light. The maximum irradiance through this amplifier (exclusive of irradiation from light reflected off damage sites) was approximately 700 Mw/cm^2. It is possible that two scattering centers were missed during our first examination, but it also is possible that two scattering centers were below our detection thresholds before the experiments and

grew as a result of the intense laser irradiation. The third amplifier received tracking damage in several areas. This tracking damage consisted of large damage sites several millimeters apart and sometimes, but not always, connected by thin filaments. It is possible that those sites connected by filaments resulted from temporally smooth pulses, while those sites not so connected resulted from the intense spikes on irregular pulses. We cannot say for sure because no detailed examination was made after or during each damaging shot.

Mark-Zender interferograms of all three rods before the experiments showed $\leq \lambda/4$ distortions. After the experiments, all three rods had developed about a $\lambda/2$ sphericity. Figure II-40 shows interferograms of the first amplifier rod before and after the experiments. The other two rods gave similar results. The sphericity is such that the emerging wavefront diverges. By testing all six surfaces for flatness, we have ascertained that the sphericity is not due to any changes in surface figures. The sphericity corresponds to a change in refractive index of approximately 1×10^{-6} at the edge of the rod compared to the center of the rod.

Since the passive sphericity of the rods changed with use, it would be interesting to again determine how the sphericity is affected by the pumping of the rods. The change in passive sphericity is small compared to the measured change in sphericity induced by the pumping - but the pump-induced sphericity may change with use also.

Polarimeter studies of the first two amplifier rods showed a compression of about 80 mm. An accurate measurement of the stress was not made before the experiments.

In conclusion, the optical properties (sphericity) of all three rods changed in a similar manner. This similarity leads us to believe that the changes were due to the pumping and/or water cooling of the rods rather than any action of the laser light. There is some indication that the action of the laser light did create or enlarge two isolated scattering centers in one of the laser rods.

II-4.2. Multimode experiments

II-4.2.1. Description of experiments

In this portion of the contract, we tried to determine the practical damage threshold for a laser pulse with little or no spatial or longitudinal mode control. The idea was that the (hopefully) random superposition of a great number of spatial and longitudinal modes would add up and average out to a very uniform irradiance pattern. In the case of longitudinal modes, the addition of many modes does not generally result in a uniform temporal envelope. Irregular spikes are detected even with 1 ns response time detectors. Faster detectors would, we feel certain, show irregular picosecond and even subpicosecond spikes. Without a better understanding of the exact damage mechanisms, it is difficult to say what effect a given temporal substructure will have on damage thresholds. It would be interesting to study damage with a laser pulse of narrow bandwidth (ideally one longitudinal mode) but many spatial modes. This could be approximated by removing the aperture from the YAG oscillator used in this project. This same YAG laser could be used to study damage thresholds of single and multiple longitudinal mode pulses, both TEM_{00}. This too would be interesting.

In the case of spatial modes, the superposition of many modes also does not result in a perfectly uniform irradiance. However, the spatial incoherence of such a beam should make diffraction rings less of a problem. Time-integrated measurements (zap marks) indicate that a fairly smooth profile can be obtained by using a large aperture oscillator. Also in this time region (30 ns), passage through the saturated amplifiers may smooth out certain spatial irregularities - making the output more uniform than the input.

II-4.2.2. Description of equipment

The laser system used in this portion of the project was the same one used in previous ARPA work done here at O-I.[24] All rods were ED-2.3 Brewster angle rods 3/4'' in diameter. The pumped length of all rods was 20 cm and there were three amplifiers and a Pockels cell Q-switched oscillator (Figure II-41).

The oscillator was modified by replacing the 2 mm mode selecting aperture with a 7.5 mm aperture. Previous experience with this oscillator had shown that the 2 mm aperture was the largest aperture which would allow TEM_{oo} mode outputs. Outside of the oscillator a 4.5 mm aperture was used to transmit the most uniform portion of the oscillator output. Various lenses were used to try to get a nonconverging small diameter beam through the last amplifier (Figure II-41.)

At first, we intended to use a Pockels cell beam chopper to reduce the 30 ns pulse to a 15 ns pulse so we could compare our results directly with the 15 ns pulses used in the YAG oscillator experiments. We found, however, that reflections from the spark inside the spark-gap (used to trigger the Pockels cell) induced a $\approx$ 3 ns modulation of the

beam chopper output. Due to saturation of the amplifiers, the final output pulse contained most of the energy in the first 3 ns. This was unsuitable so we used the 30 ns oscillator pulse. This of course was the original contract goal, but did not allow for direct comparison with the 15 ns YAG pulses.

II-4.2.3. Multimode experimental results

No neutral density filters were used in the multimode experiments, irradiances were controlled by the positioning of the lenses and the pumping intensity of the amplifiers. We did achieve output energy irradiances of 70 J/cm^2 (Figure II-42) with no damage to the amplifiers, but damage to the second lens. This is half the maximum irradiance achieved in the single-mode narrow bandwidth experiments.

The length of the final multimode amplifier was 38 cm vice 42 cm for the single-mode final amplifier. Apparently we can conclude that using single-mode narrow bandwidth pulse does not improve self-focusing damage thresholds by more than a factor of two. Considering the greater energies and efficiencies available in the multimode case, a factor of two might favor multimode operation in many lasers.

More intense pumping of the amplifiers did not increase the irradiance, although it did of course increase the total output energy (up to 20 J). With such a ''sloppy'' beam, it is difficult to be precise about characterizing the beam. Using burn patterns in the plane of the 1 mm aperture, we estimate the beam radius to be $r \approx 2.3$ mm. We determined by two methods that the beam had a half-angle convergence of about 2 mR. One method used two beam splitters some 80 cm apart to compare burn patterns. The other method measured average irradiances in the exit plane

and 55 cm after the exit plane, where energy irradiances of up to 118 J/cm^2 were measured. We were rather surprised to find that a converging beam of more than 1 GW/cm^2 did not self-focus, but recent self-focusing theory indicates that the convergence or divergence of the beam is not a critical parameter.

It is significant to note that, in over a hundred experiment shots in this system, the final amplifier was damaged about seven times. We never saw surface damage on the Brewster angle exit face of the amplifier except where it was at the end of a track of internal damage. The normal surfaces of beam splitters and lenses were extensively damaged and caused a premature end to these experiments. One must conclude that, in systems of this type, surface damage is the weak link in the system. One must also conclude that there is indeed a terrific advantage in going to Brewster angle surfaces.

II-4.2.4. Advantages of multimode operation

Although the multimode experiments were not as decisive as we would have liked, they did indicate that multimode nanosecond pulses may propagate through amplifiers nearly as well as TEM_{oo} narrow bandwidth pulses. If the damage thresholds of materials is identical for both types of pulses, there is a great practical advantage to using the multimode approach. That advantage is, of course, that more total energy is available in the multimode case. The laser used in our multimode experiments had a total output of about 15 J largely because we purposely apertured the beam to minimize alignment problems. This same system with a different multimode oscillator has produced 140 J in a 60 ns pulse when its full aperture was used.

In comparison, our clean beam system used 80% more pumped volume of laser glass, pumped harder, and still produced only about 12 J total. The simplicity and efficiency of the multimode technique are quite attractive. Of course, it must truly be multimode, the superposition of just a few modes will not result in uniform irradiances. Also the time-dependence of multimode hot spots and damage mechanisms should be better understood before one states that multimode damage thresholds are equivalent to TEM_{00} mode damage thresholds.

II-5. Discussion

II-5.1. Comparison with prior state of the art

Most of the recent work on Nd:glass lasers has concentrated on subnanosecond (or at least less than 3 ns) pulses currently of interest in fusion research. In the late sixties and early seventies, there was a good deal of work on 30 ns Nd:glass lasers and it is interesting to compare our work with this earlier work. Table II-4 lists the ρ and pulse length values reported by various labs. The last column estimates the peak irradiance. Direct comparison of these data with our work is unfair in many cases because the central ρ may have been higher than the average values used in the table. However, most of the work at that time was aimed at achieving top-hat irradiance distributions that filled the amplifier, so we still feel that the comparison has meaning. For instance, the peak irradiance of this work is 80% higher in one case and 425% higher in the other case than the earlier work done in our own lab.

In any case, we have shown that long (42 cm) rod Nd:glass amplifiers can produce output irradiances of more than 4 GW/cm^2 in a nearly collimated beam without damage. There is every reason to believe that even higher irradiances could be produced by shorter rods and/or larger diameter beams (greater preamplification).

Recent work with picosecond Nd:glass rod amplifier systems has also established irradiances of several GW/cm^2 as the threshold irradiance for self-focusing effects.[2] Our findings agree with these and show that, in these types of systems, surface damage need not be the weak link in the system. Surface damage thresholds > 5 GW/cm^2 (see Section I) have been demonstrated at normal incidence. By going to Brewsters angle, one can expect even higher thresholds. In the case of Brewster angle disk amplifiers, it is not quite so clear whether self-focusing effects or surface damage is the limiting effect. At the risk of oversimplifying, it seems that self-focusing thresholds are functions only of irradiance while surface damage thresholds are (yet unspecified) functions of irradiance and pulse length. Surface damage thresholds greater than 30 GW/cm^2 have been reported for picosecond pulses.[4] In picosecond systems, self-focusing is the most limiting factor.

II-5.2. Conclusions and discussion

This research did not establish exactly what effect longitudinal or spatial mode control had on practical damage thresholds. Indications were, however, that single-mode operation is not necessary to avoid damage in laser amplifiers for 10^{-8} second pulses. Using 15 ns

TEM_{oo} mode pulses, we obtained $\gtrsim$ 70 J/cm^2 operation with both temporally smooth (single longitudinal mode) pulses and temporally irregular (many longitudinal modes). We also obtained 70 J/cm^2 operation using 30 ns pulses with no mode control (many spatial and longitudinal modes). Due to limited preamplification, we could not attempt energy irradiances higher than these (70 and 59 J/cm^2) except by focusing the beam more sharply. This always led to self-focusing damage. The preamplification was limited either by the total gain available (multimode experiments) or by the onset of amplified spontaneous emission (single-mode experiments). Given more equipment, higher preamplification could be achieved. This would allow larger beam diameters which would make it easier to note whether the self-focusing was whole-beam or small scale.

We found that large errors resulted from estimating energy irradiances by dividing total energies by areas calculated from the FWHM of the beam profile. We developed a method for accurately measuring high energy irradiances in any plane. We found an infrared sensitive TV/videotape system to be very useful for studying the qualitative spatial and spectral characteristics of the beam in near real time.

The lens used after the preamplifier to recollimate the beam through the final amplifier was the weak link in all our experiments. In the one case in which no such lens was used, self-focusing occurred in the final amplifier - but this self-focusing damage may have been aggravated by the focusing of the beam into the final amplifier. We believe that damage-resistant lenses can be made, but we did not address ourselves to this problem soon enough due to the lack of such damage in our early experiments.

Our attempts at eliminating diffraction rings led to the invention of the total internal reflection (TIR) apodizer. This invention did not occur soon enough to be used in this research, but we think the concept is worth pursuing. We also pointed out the problem of the twice-reflected focus of any positive lens.

The question as to the effect of normal electric fields on surface damage thresholds is still not settled. Once this issue is settled, one can consider the design of damage-resistant components, oscillators and systems.

It has been demonstrated that the gain and efficiency of rod amplifiers can be increased by the use of claddings. Claddings also reduce the danger of damage from pulses reflected from the amplifier exit face and focused by reflection from the barrel of the rod. We believe that further improvements in the cladding of Nd:glass lasers will be demonstrated, and that this will aid in the development of all kinds of laser amplifiers by increasing our understanding of the effects of parasitic oscillations.

In general, we feel that more research is warranted on Nd:glass lasers because Nd:glass lasers are the most studied, most versatile, and highest peak power lasers. As such, continued research on Nd:glass lasers is most likely to lead to new understandings and improvements that will aid other laser and optical systems, as well as further improve Nd:glass lasers.

II-5.3. Suggestions for future research

Listed below are several areas we feel warrant further investigation. We note that none of these subjects is restricted to Nd:glass lasers - all have a wide range of applicability.

1. Investigate whether normal and tangential surface electric fields have the same effects on surface damage. This knowledge would allow the more intelligent design of high damage threshold optical components, oscillators, and amplifiers.
2. Investigate the effect of longitudinal and spatial mode control of self-focusing and surface damage for both picosecond and nanosecond pulses. If multimode beams can be used for damage studies, a significant savings would result.
3. Pursue the design, development, and testing of total internal reflection (TIR) apodizers. Such high damage threshold apodizers may be of use in a wide variety of laser systems.
4. Investigate the forward scattering of laser pulses by the amplifiers with a view to understanding its cause, measuring its magnitude, and possibly using it as an indicator or precursor of damage.
5. Investigate the effects of parasitic oscillations in rod amplifiers and the design of rod amplifiers that will have higher efficiencies and be less prone to damage.
6. Continue the search for a precursor of optical damage.

II-6. References

1. See for example, M. D. Crisp, N. L. Boling, and G. Dubé, Appl. Phys. Letters, 21, 364 (1972) or R. W. Beck, NBS Spec. Publ. 341, p. 11 (1970).

2. E. Bliss, paper presented at the International Quantum Electronics Conference, San Francisco, Calif., 1974.

3. See for example, J. B. Trenholme, The Design of a Large Laser System for Fusion, paper presented at the 1973 CLEA Conference, Washington, D.C.

4. J. Soures, S. Kumpan, and J. Hoon, A High Power Nd:Glass Laser for Fusion Applications, in press.

5. J. E. Swain, R. E. Kidder, K. Pettipiece, F. Rainer, E. D. Baird, and B. Loth, J. Appl. Phys., 40, 3973 (1969).

6. G. Dubé, Appl. Phys. Letters, 18, 69 (1971).

7. P. L. Kelley, Phys. Rev. Letters, 15, 1005 (1965).

8. See for example, J. Marburger, Damage in Laser Material 1971, NBS Spec. Publ. 356, p. 51.

9. See for example, J. R. Jokipii and J. Marburger, Appl. Phys. Letters, 23, 69 (1973).

10. D. M. Shetterly, private communication.

11. D. M. Shetterly, private communication.

12. G. Dubé, Appl. Opt., 13, 699 (1974).

13. J. McMahon, paper presented at the Boulder, Colorado, Damage Symposium, 1974.

14. M. D. Crisp, IEEE J. Quantum Electronics, QE-10, 57 (1974), also ref. 1.

15. See for example, R. G. Schell and G. Tyras, J. Opt. Soc. Amer., 61, 31 (1971), or G. O. Olaofe, J. Opt. Soc. Amer., 60, 1654 (1970), or J. P. Campbell and L. G. DeShazer, J. Opt. Soc. Amer., 59, 1427 (1969), or A. L. Buck, Proc. IEEE, 448 (March 1967).

16. P. Jackquinot and B. Roizen-Dossier, Prozus in Optics (North-Holland Publishing Co., Amsterdam, 1964), Vol. III, p. 31.

17. See for example, F. A. Jenkins and H. E. White, Fundamentals of Optics (McGraw-Hill Book Co., Inc., New York, 1957), 3rd ed., Ch. 18.

18. See for example, J. M. McMahon, IEEE J. Quantum Electronics, QE-5, 480 (1969), or D. C. Hanna, B. Luther-Davies and R. C. Smith, Opto-electronics, 4, 249 (1972).

19. See for example, M. V. R. K. Murtz, Appl. Opt., 3, 531 (1964).

20. W. J. Smith, Modern Optical Engineering (McGraw-Hill Book Bo., New York, 1966), Section 2.10.

21. N. L. Boling and G. Dubé, Damage Threshold Studies of Glass Laser Materials, ARPA Semi-Annual Technical Report of 31 Dec 1972 (DAHC 15-72-C-0170).

22. See for example, R. W. Wood, Physcal Optics (The Macmillan Co., New York, 1934), Chap. 1.

23. J. M. McMahon, J. L. Emmett, J. F. Holzrichter, and J. B. Trenholme, IEEE J. Quantum Electronics, QE-9, 992 (1973).

24. N. L. Boling, L. Spanoudis, and P. R. Wengert, Damage Threshold Studies of Glass Laser Materials, ARPA Semi-Annual Technical Report of 31 July 1971 (DAHC 15-69-C-0303).

25. H. Baumnacker, "Neodymium Glass Laser System," March 1971 report from Max-Planck Institut fur Plasmaphysik (available from National Technical Information Service, U. S. Dept. of Commerce).

26. Quantel Inc., private communication.

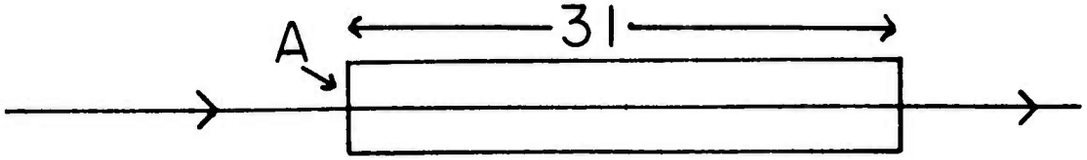

(a) long rod

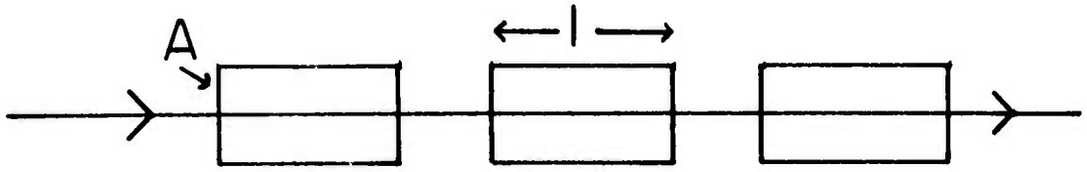

(b) series rods

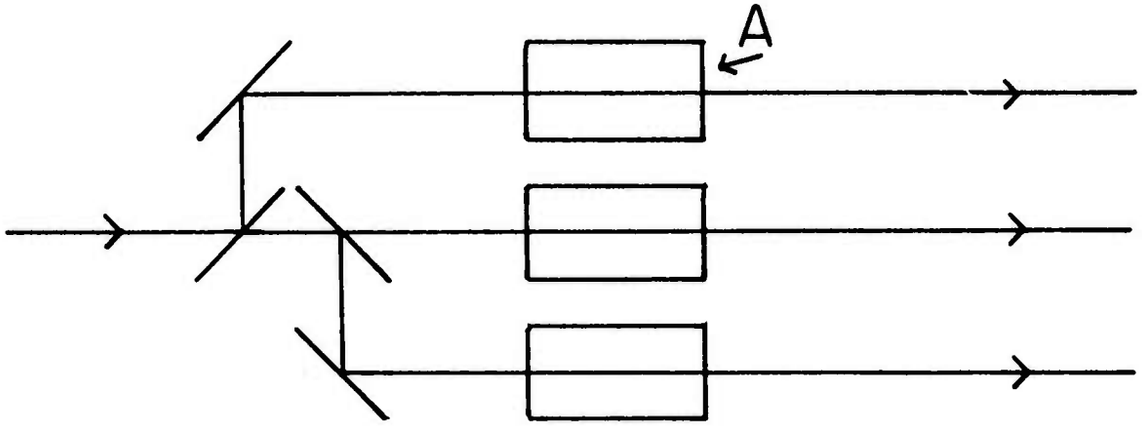

(c) parallel rods

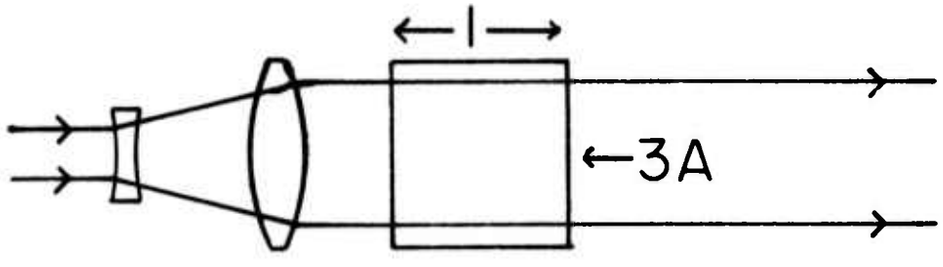

(d) large aperture

FOUR AMPLIFIERS OF EQUAL VOLUME

FIGURE II-1

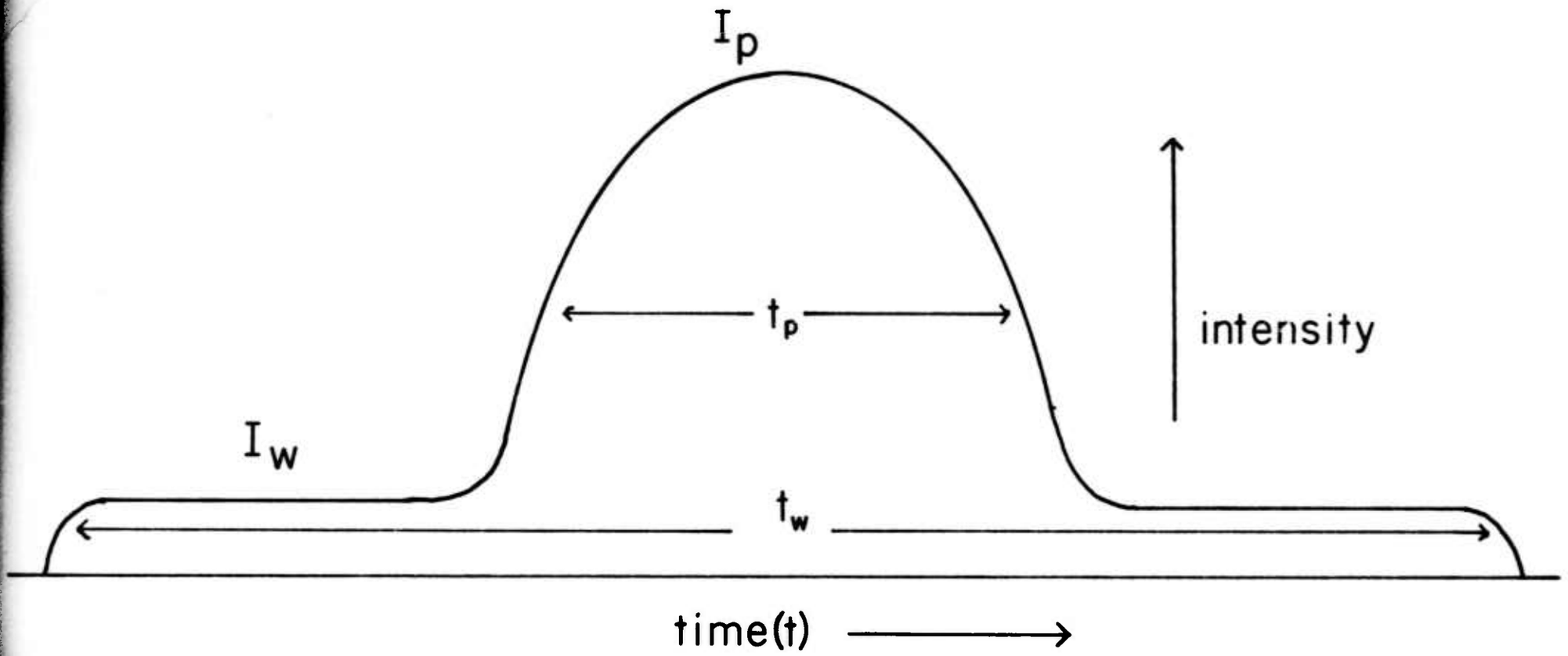

FIGURE II-2

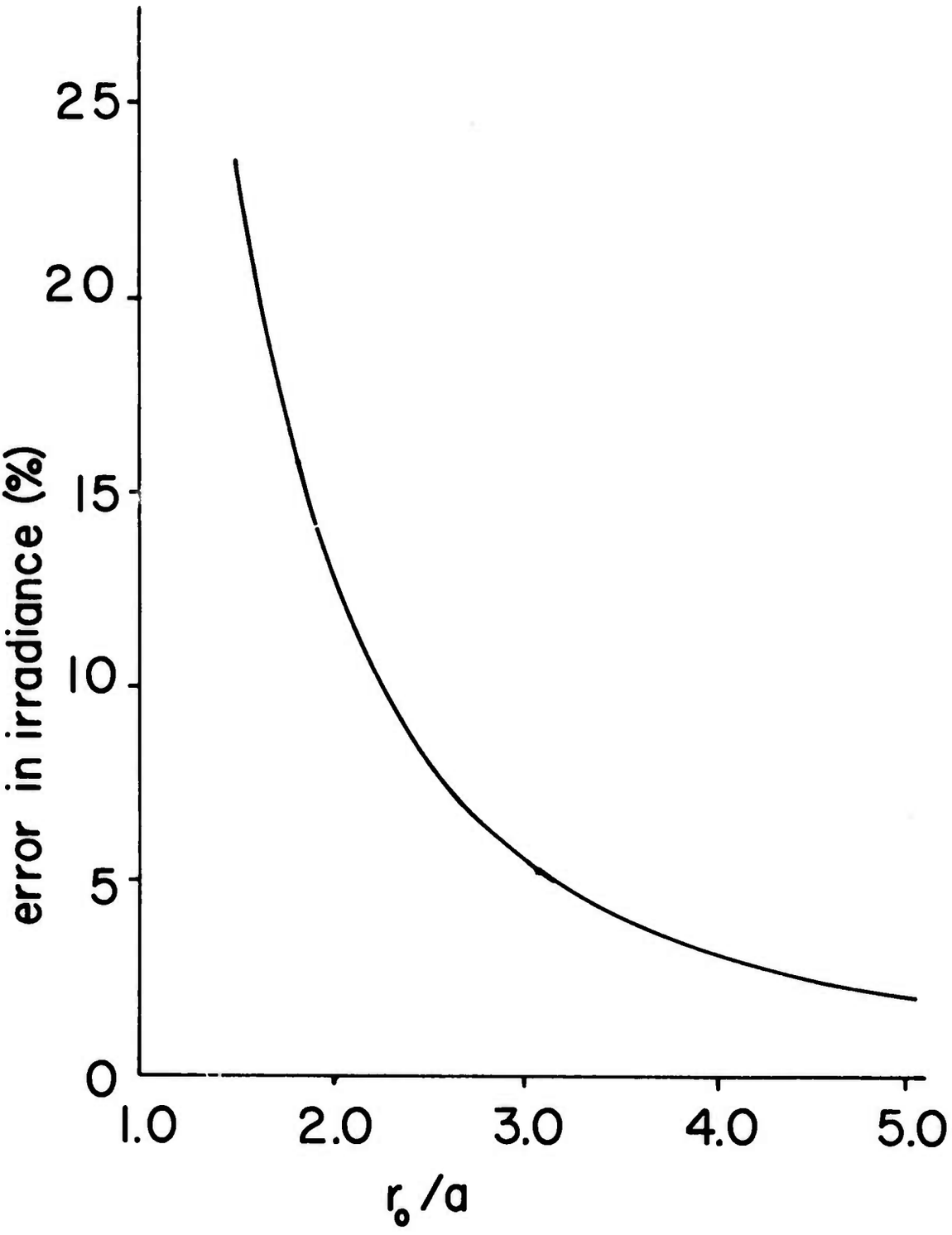

FIGURE 11-3

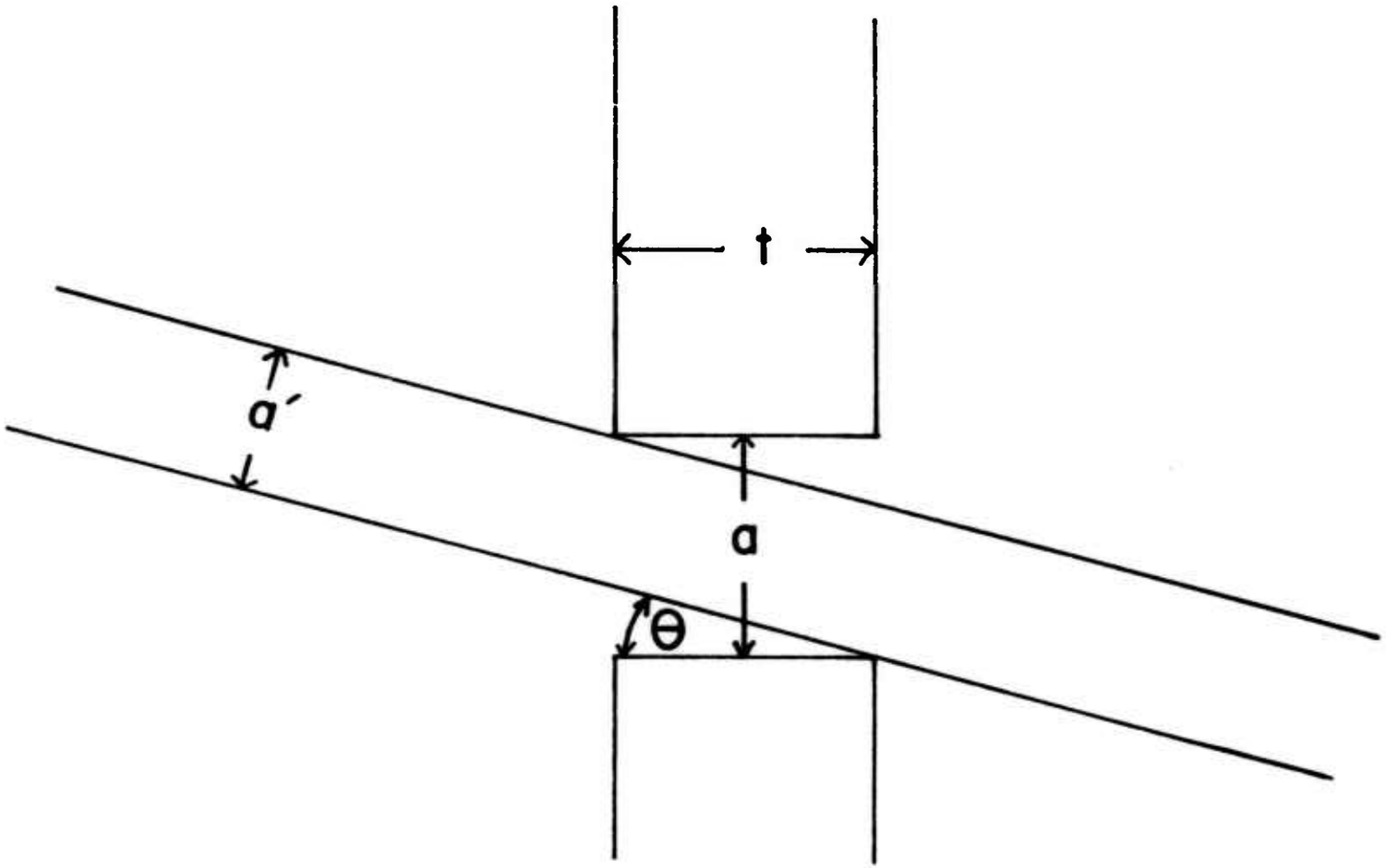

A MISALIGNED APERTURE

FIGURE II-4

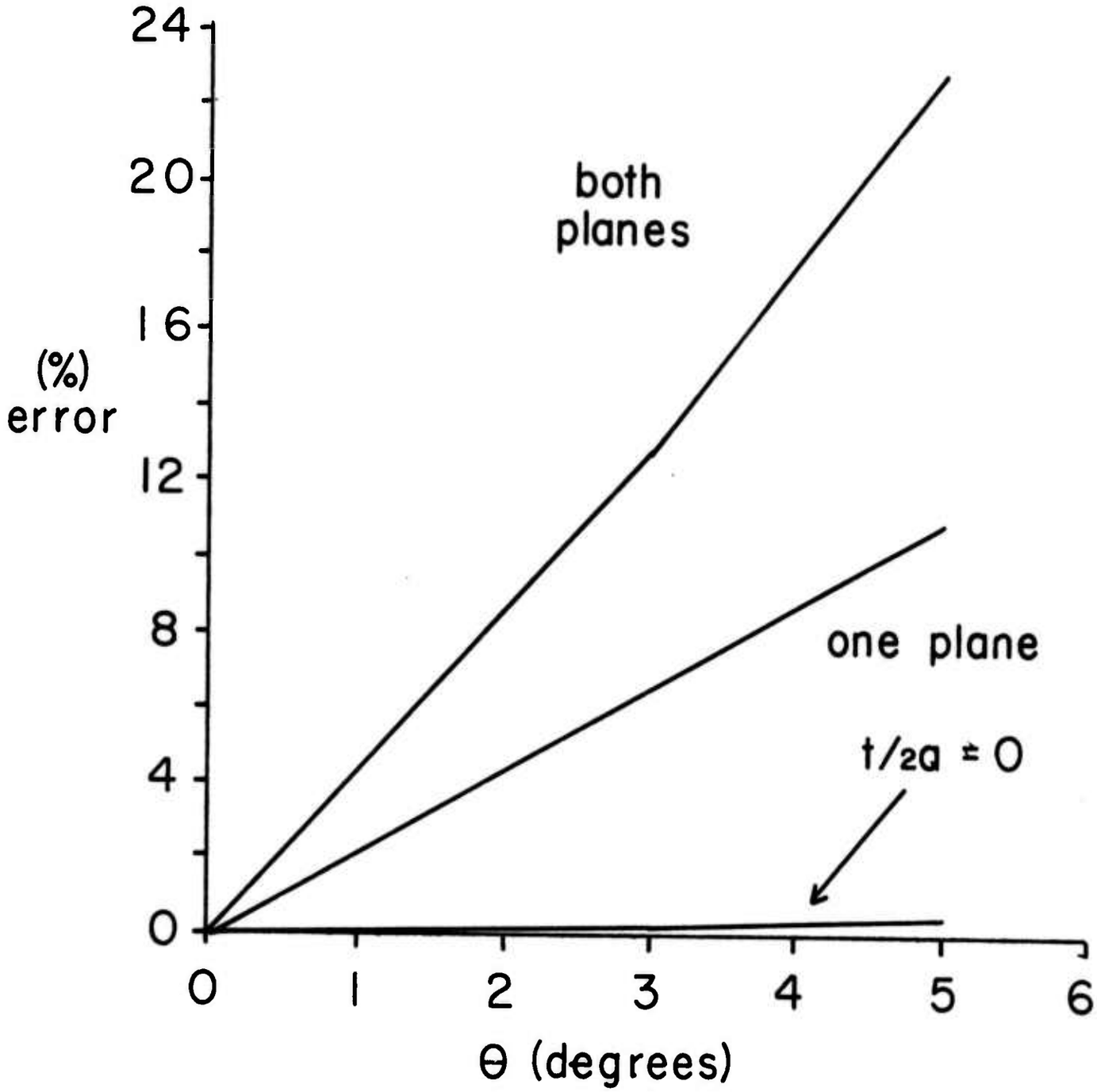
24
20
16
12
8
4
0
(%)
error
both
planes
one plane
t/2a ≈ 0
0
1
2
3
4
5
6
θ (degrees)

FIGURE 11-5

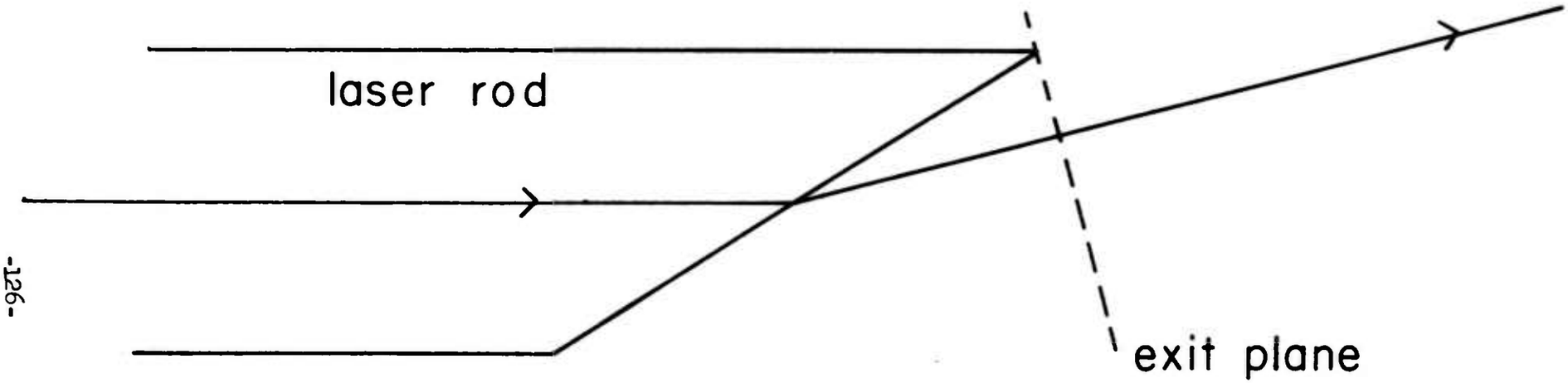

FIGURE II-6

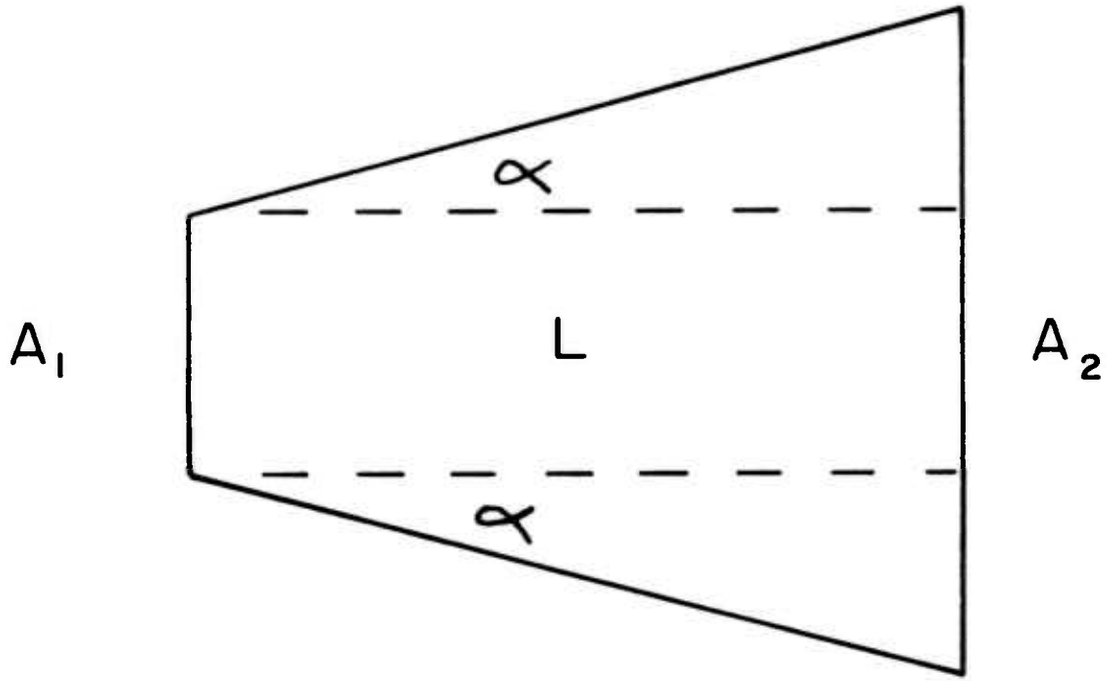

BEAM DIVERGENCE

FIGURE II-7

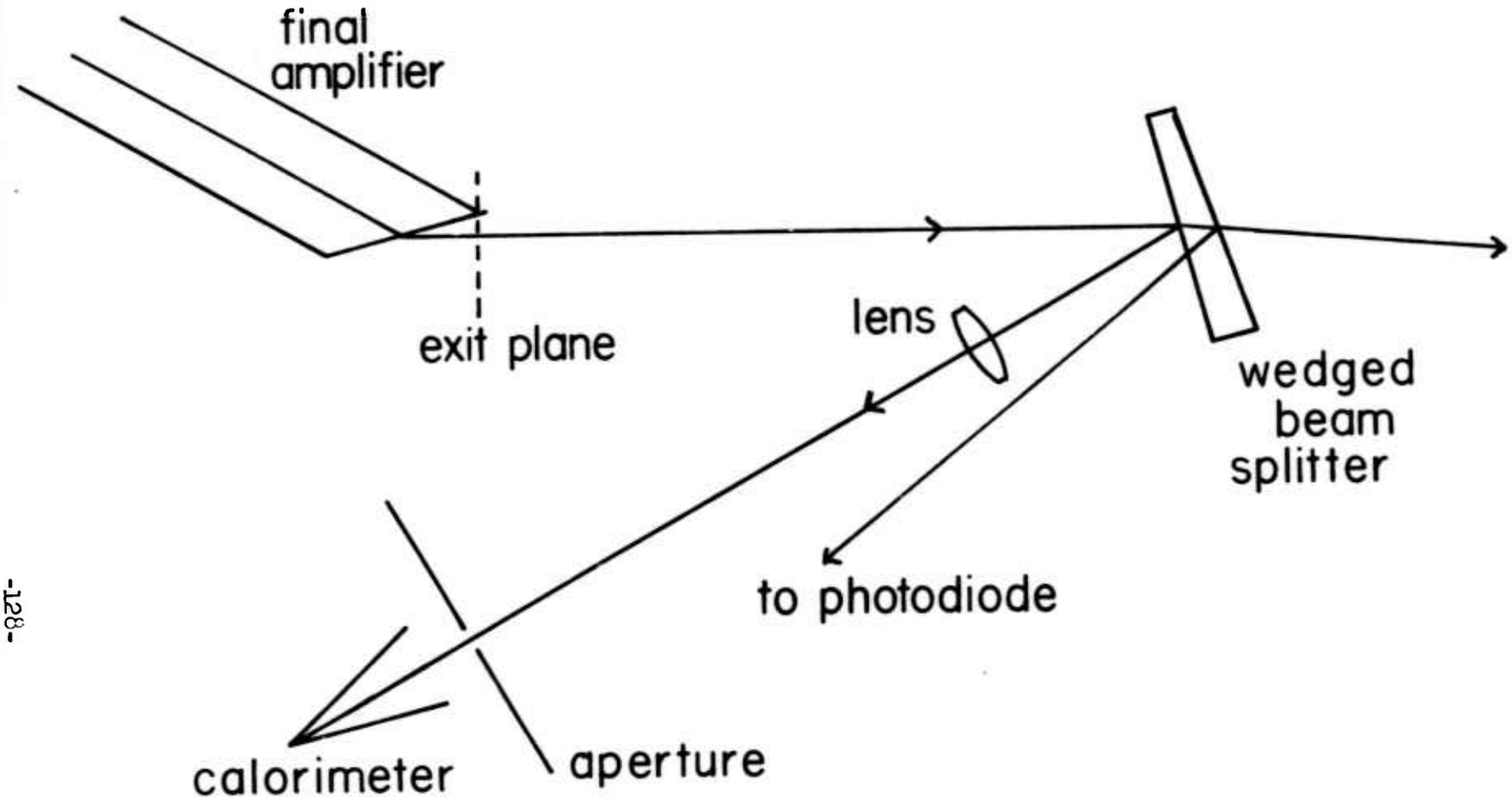

MONITORING SYSTEM

FIGURE II-8

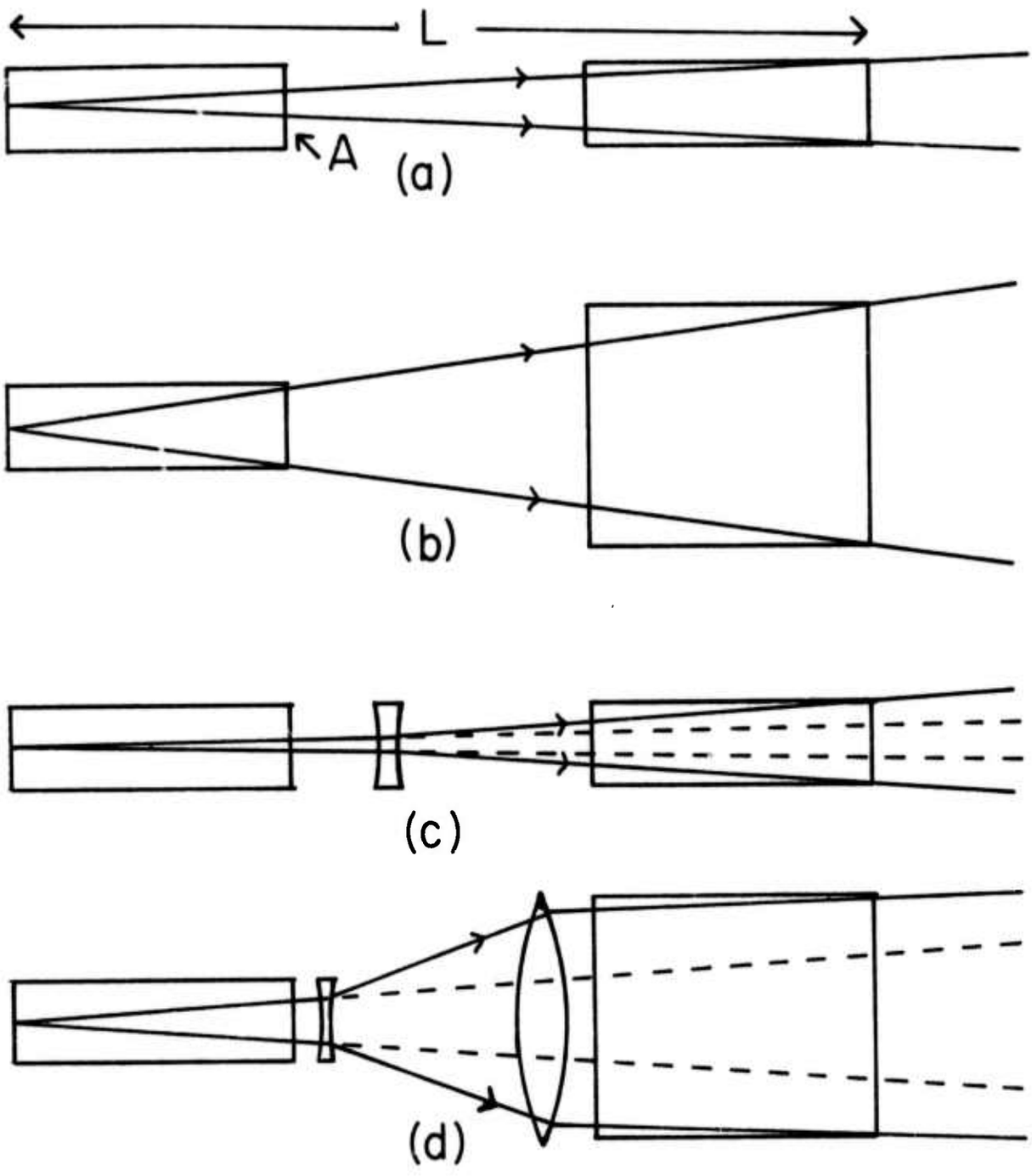

AMPLIFIED SPONTANEOUS EMISSION

FIGURE II-9

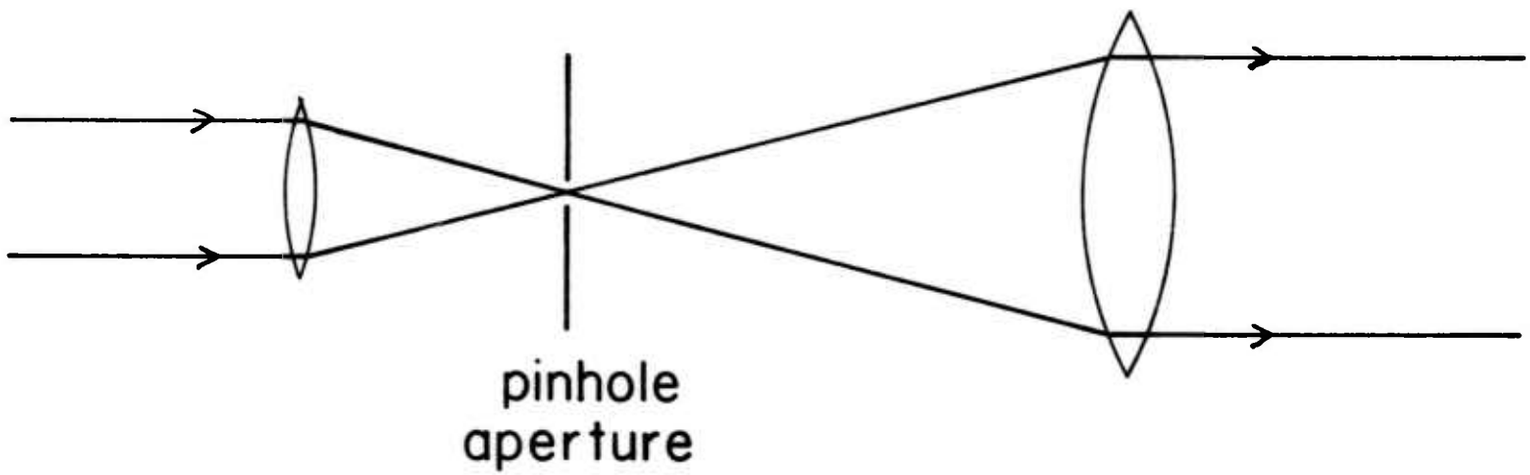

FIGURE II-10

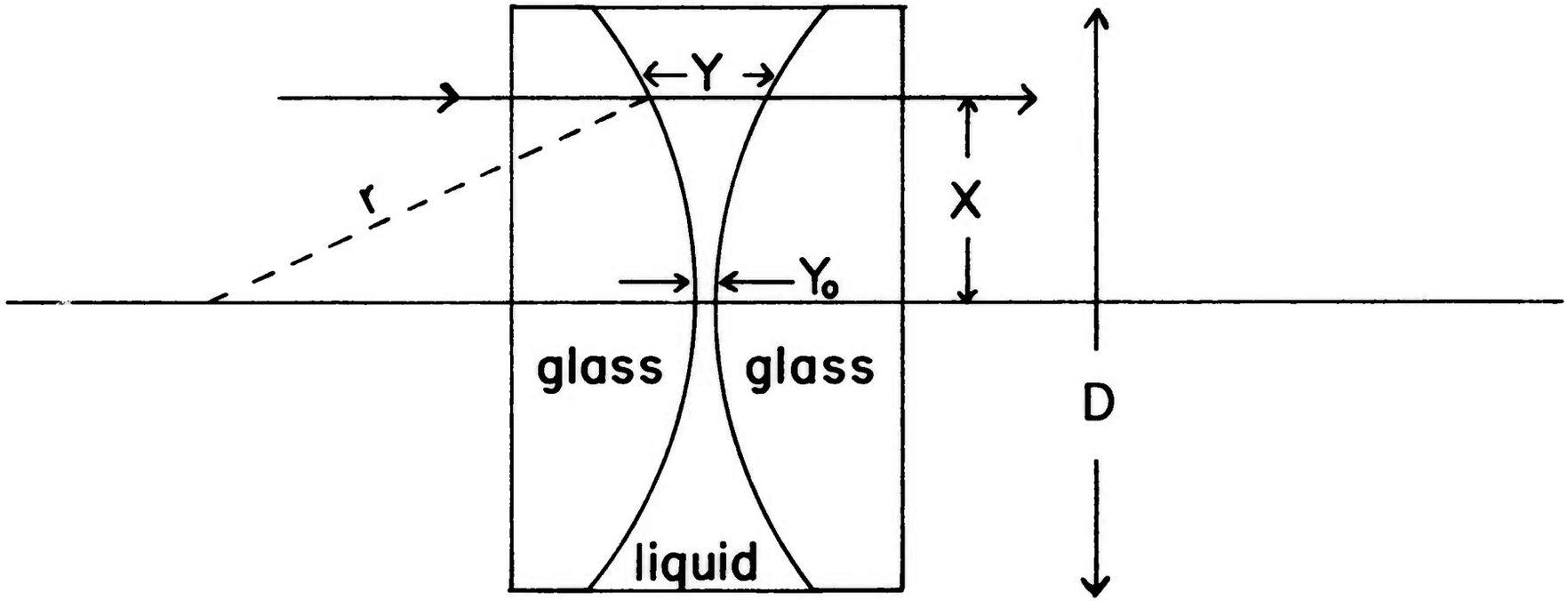

NONPLANAR DYE CELL APODIZER

FIGURE II-II

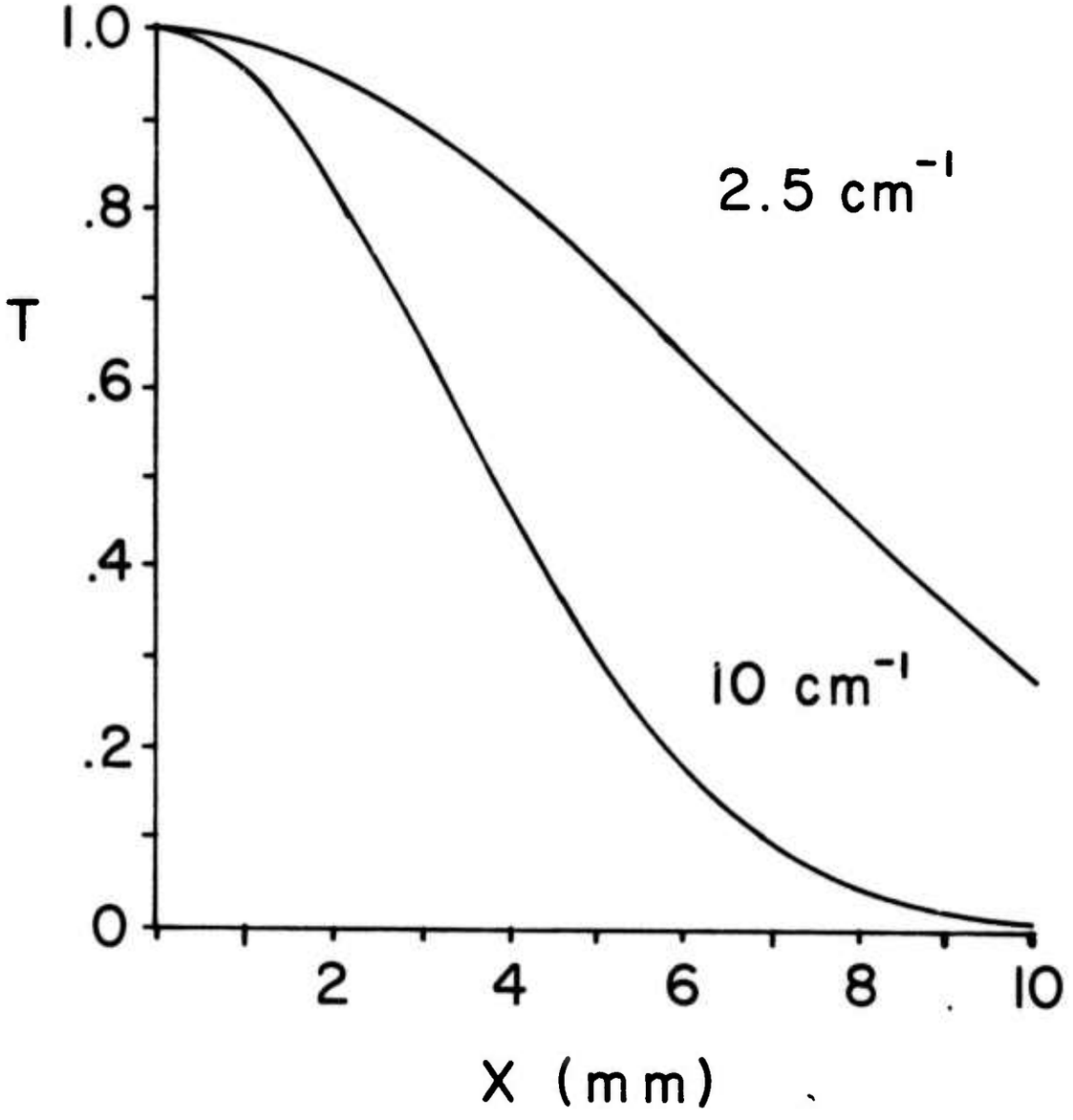

TRANSMISSION OF DYE CELL APODIZER

FIGURE 11-12

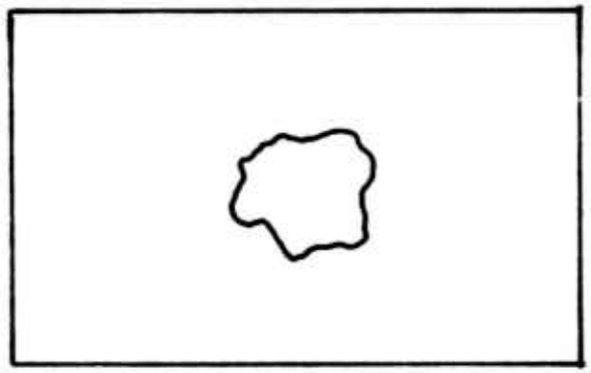

A TYPICAL RANDOM APERTURE

FIGURE II-13

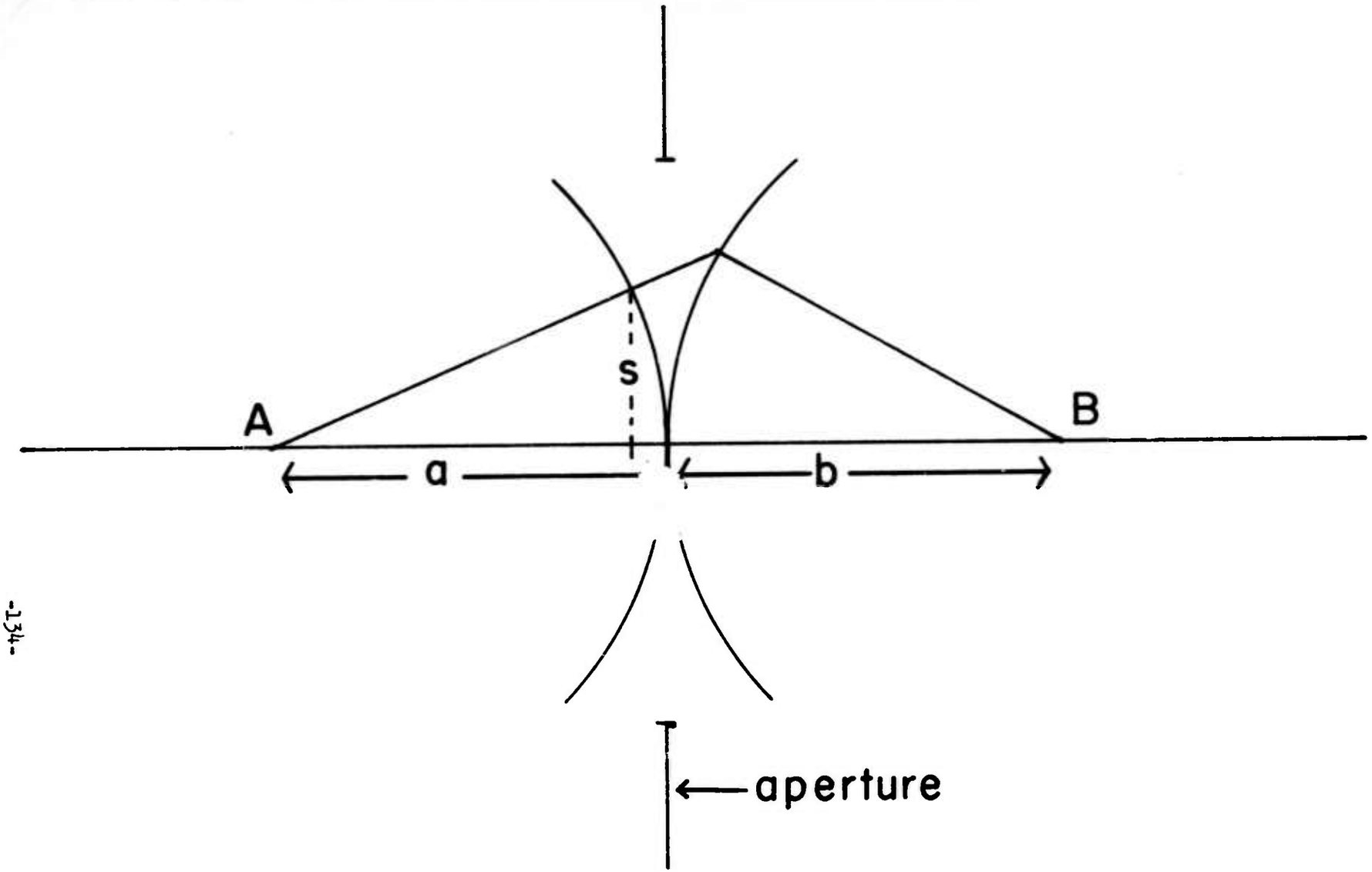

FIGURE 11-14

FRESNEL DIFFRACTION PATTERN

$a = \infty$

$b = 847$ cm

$s = 1.0$ mm

$S_2 - S_1 = 0.96$ mm

FIGURE 11-15

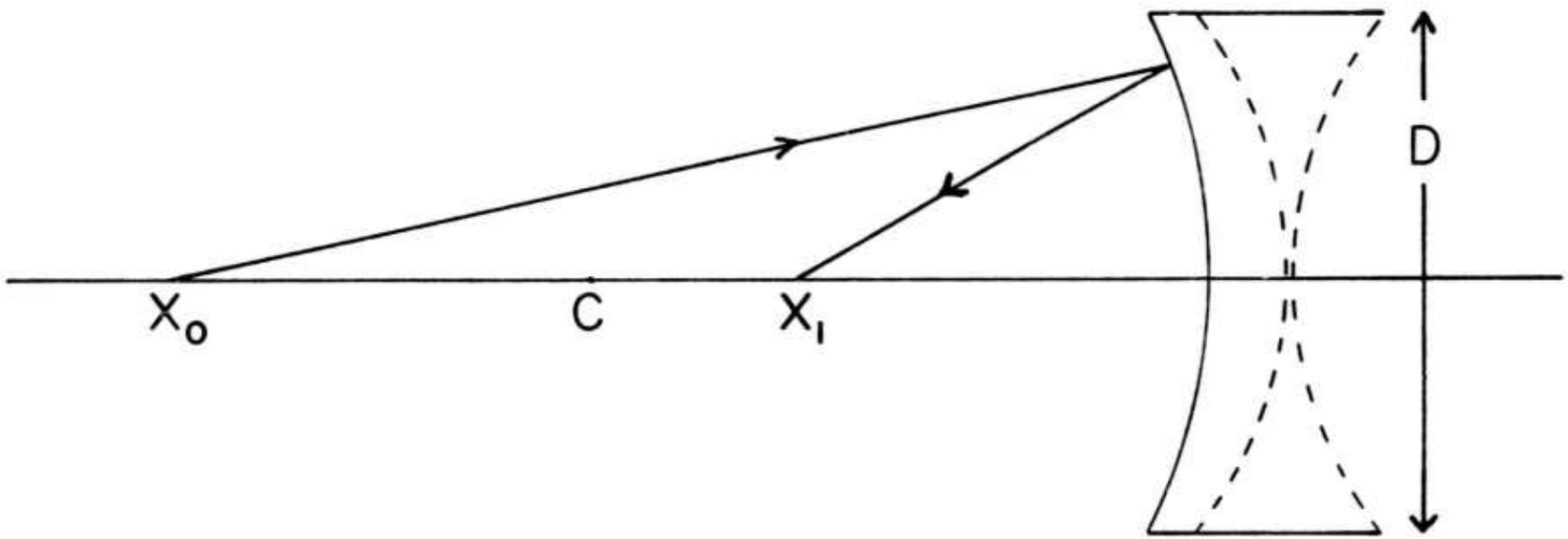

REFLECTION FROM CONCAVE FIRST SURFACE

FIGURE 11-16

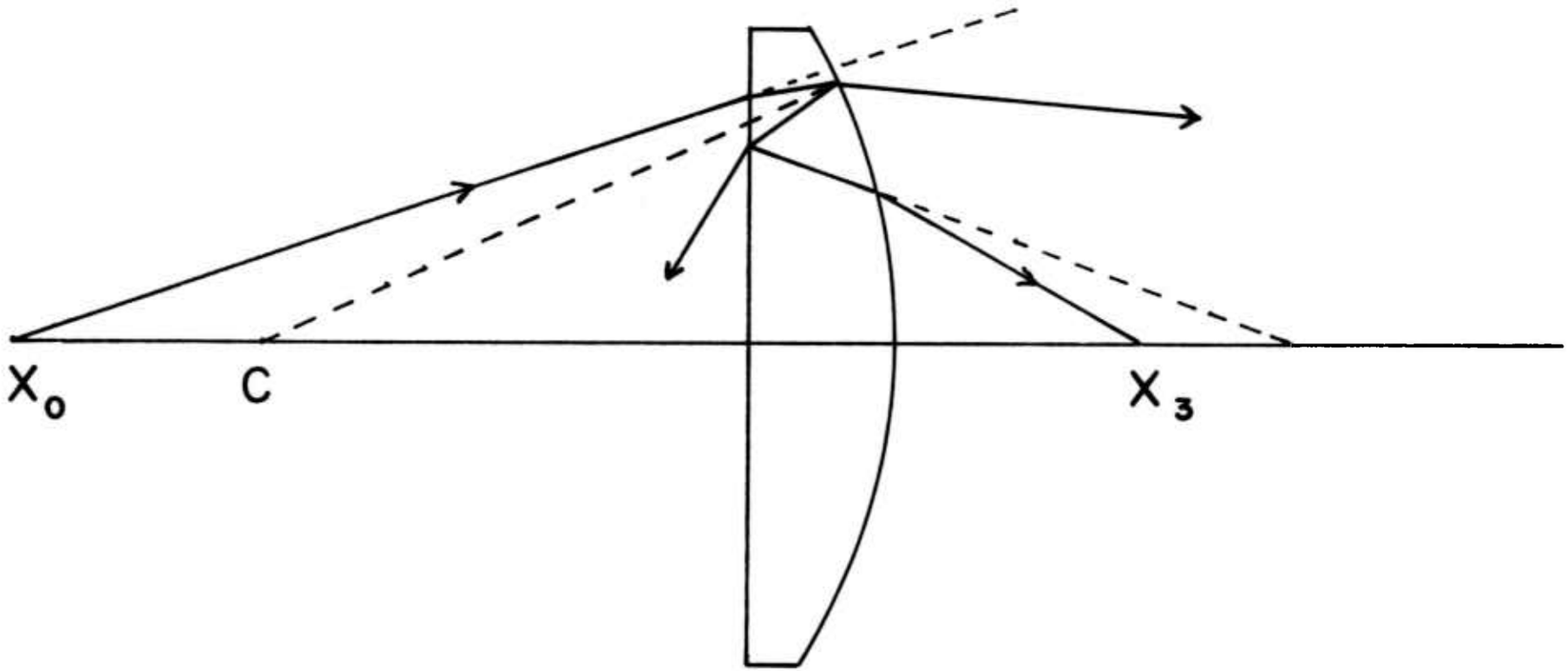

TWICE REFLECTED FOCUS OF PLANO-CONVEX LENS

FIGURE II-17

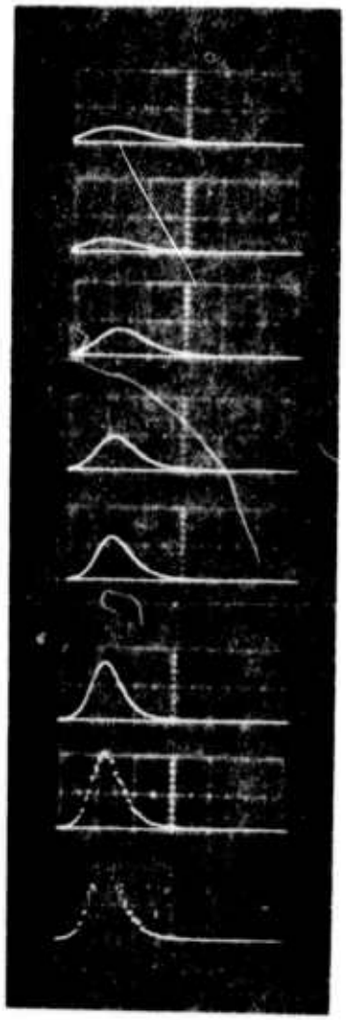

OSCILLATOR OUTPUT AT DIFFERENT POCKELS CELL VOLTAGES (20 ns/div)

FIGURE 11-18

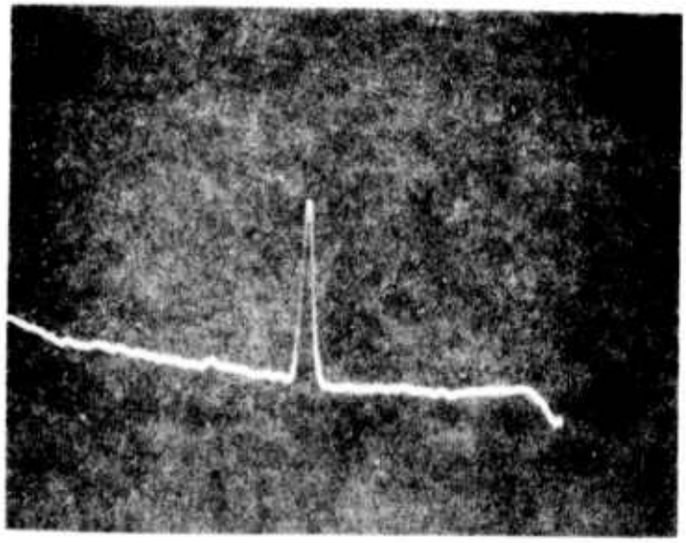

(a) narrow band (possibly single mode)

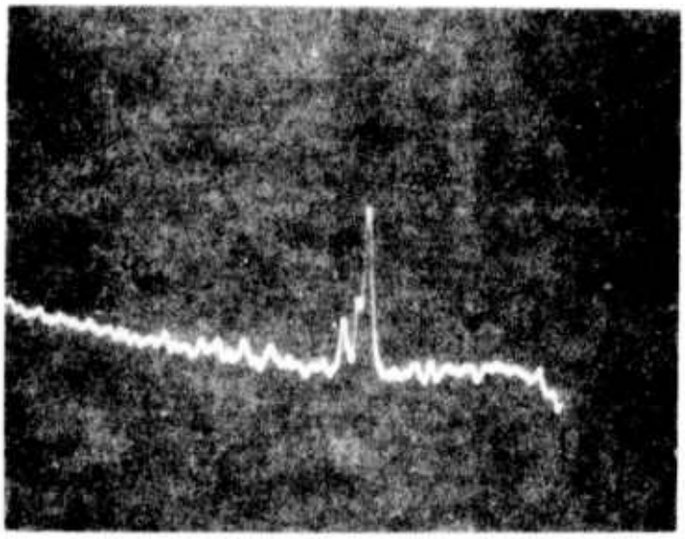

(b) broad band

TYPICAL SPECTROGRAPH DISPLAYS

FIGURE II-19

OVERHEAD VIEW OF LABORATORY

FIGURE II-20

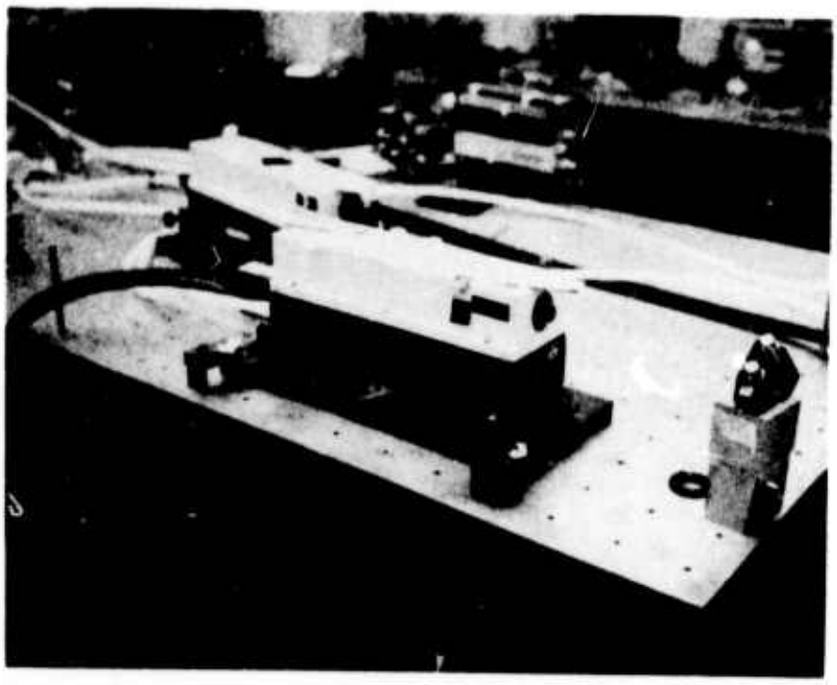

FIRST TWO AMPLIFIERS

FIGURE 11-21

FINAL AMPLIFIER

FIGURE 11-22

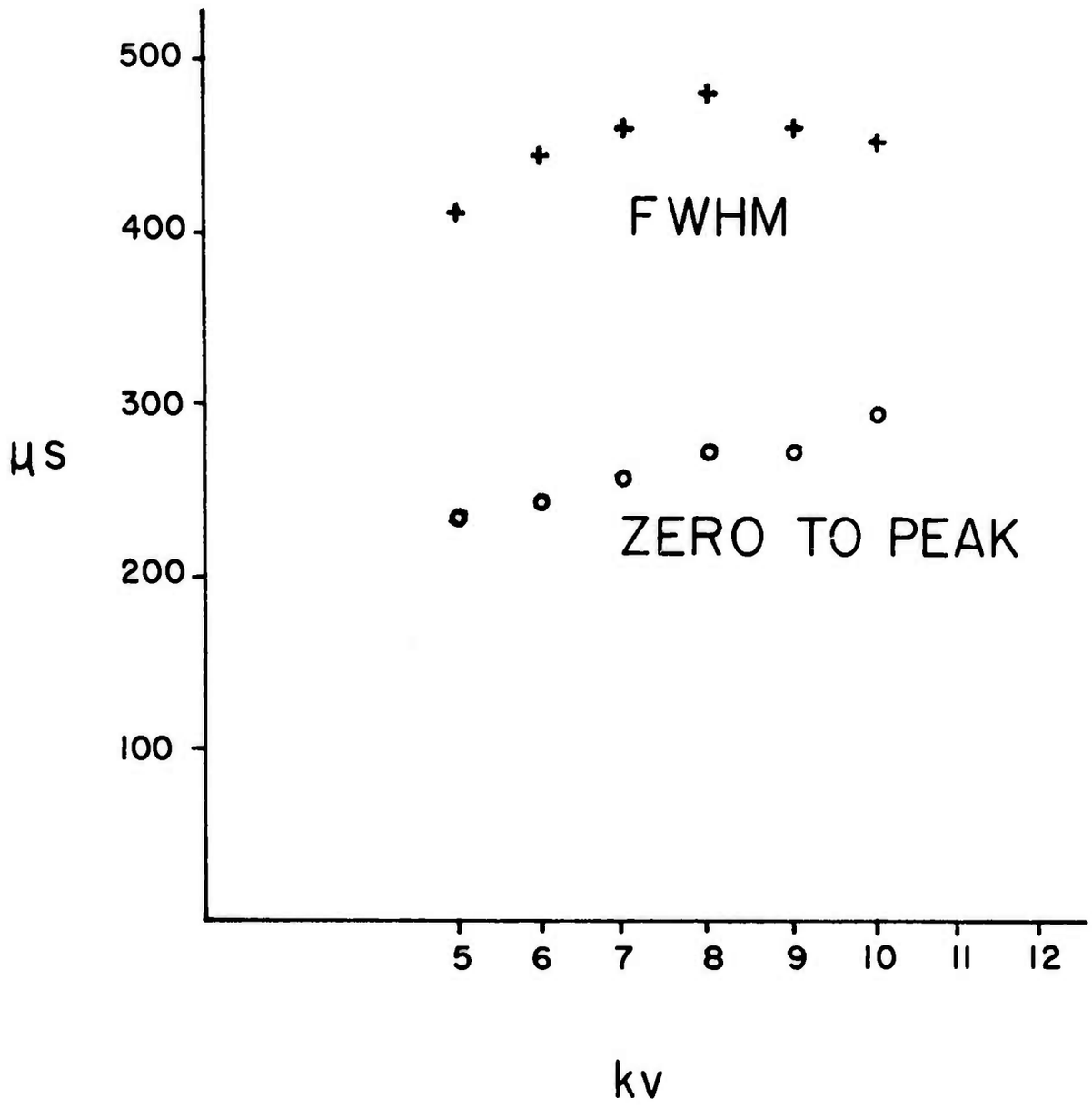

FLASHLAMP PULSE SHAPES

FIGURE II-23

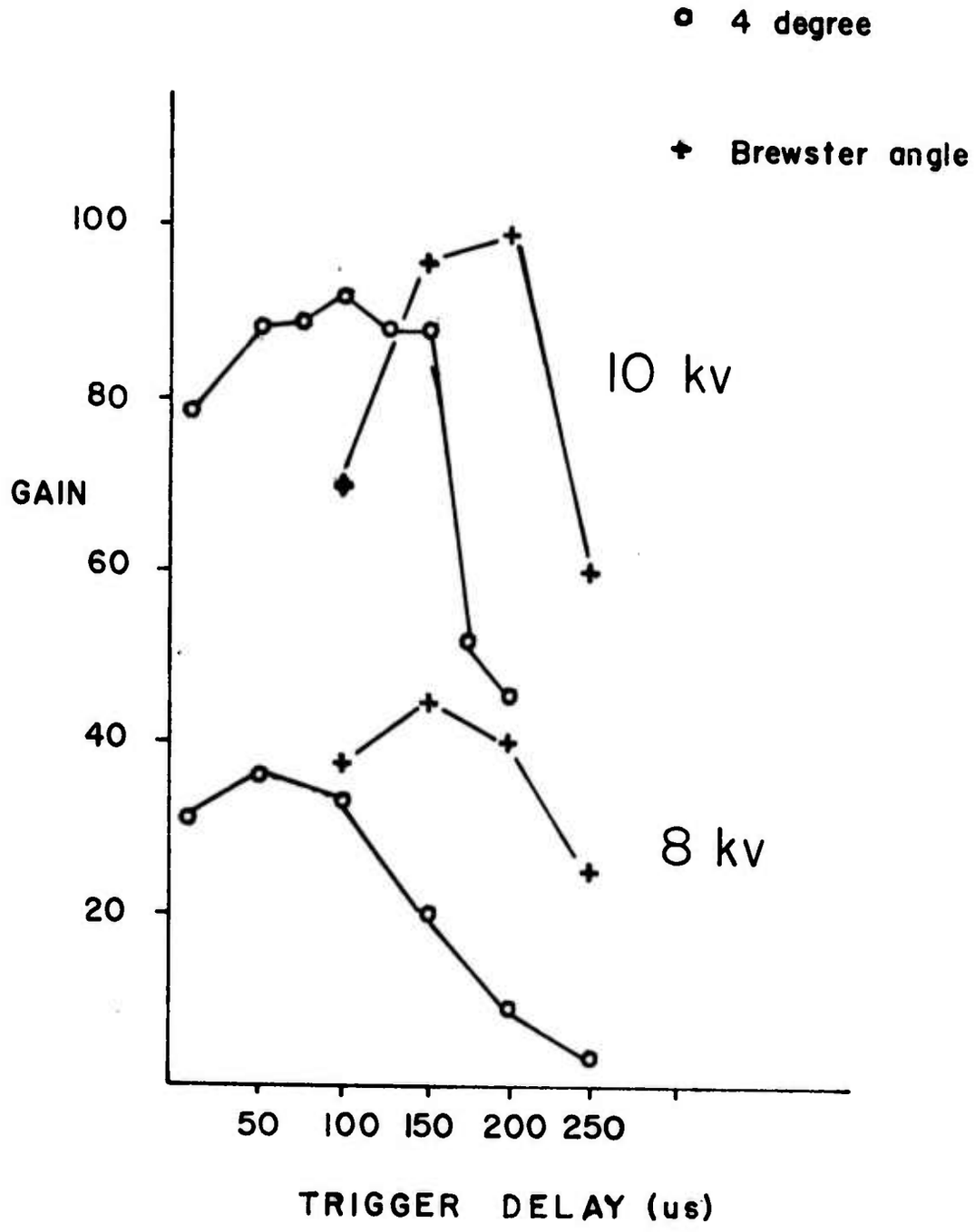

AMPLIFIER GAIN

FIGURE 11-24

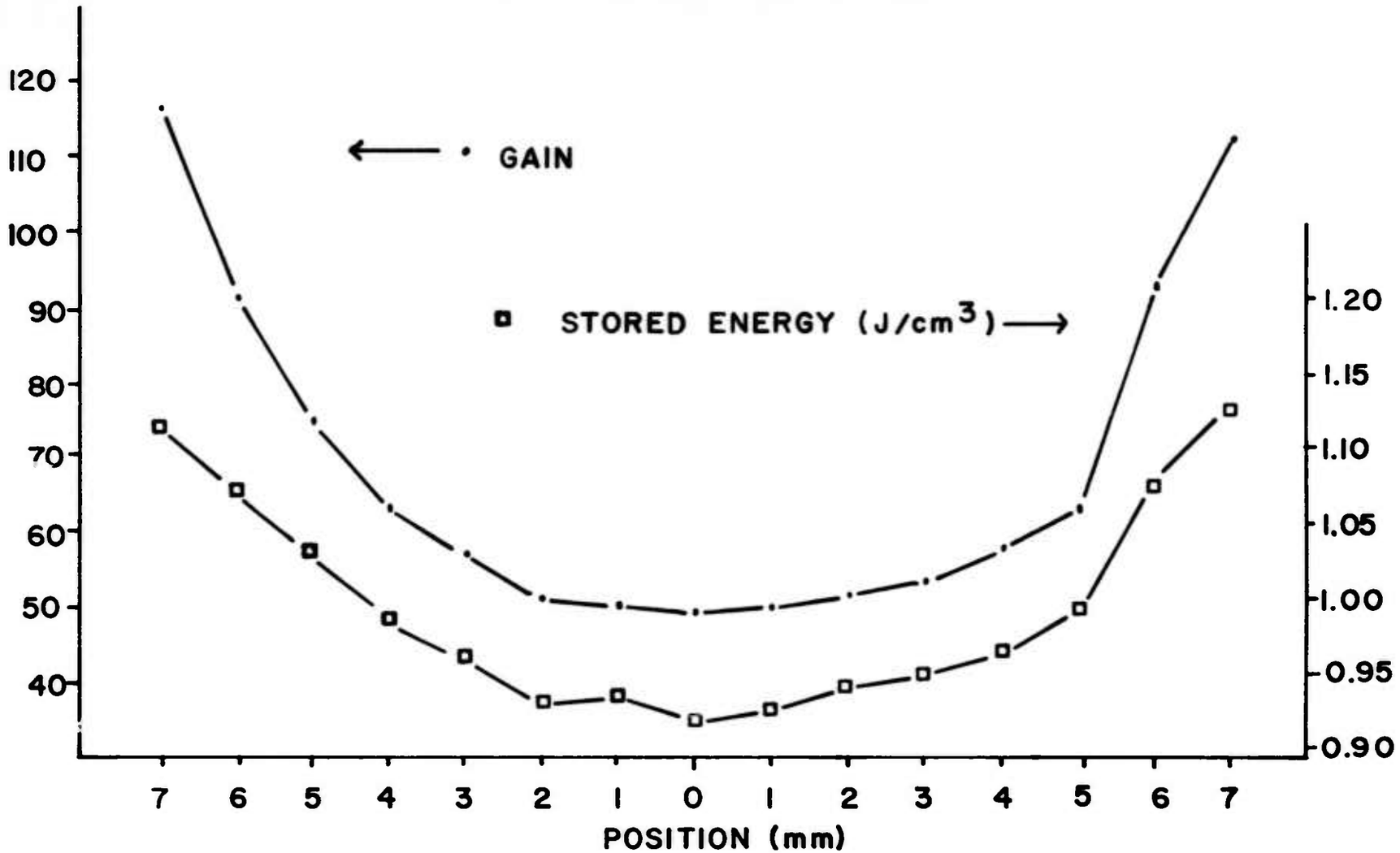

UNIFORMITY OF GAIN

FIGURE II-25

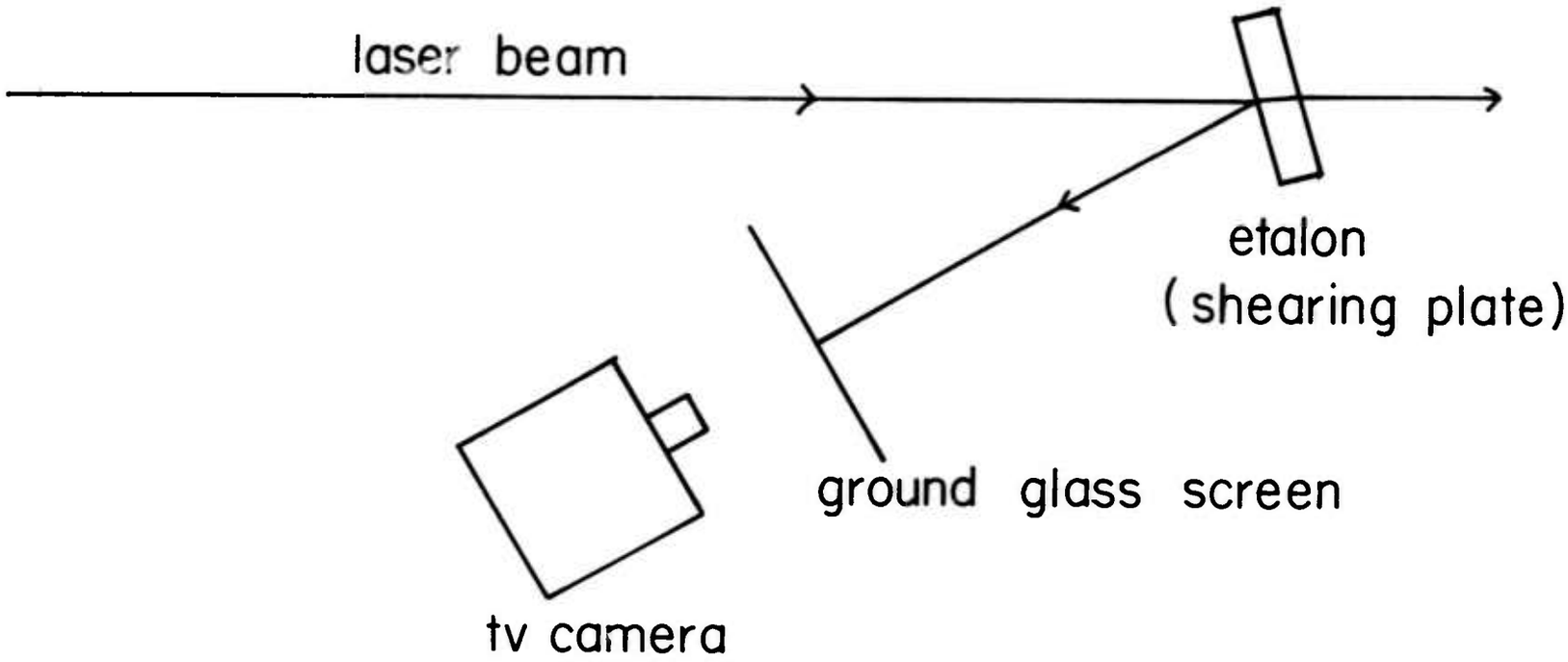

SHEARING PLATE INTERFEROMETER

FIGURE 11-26

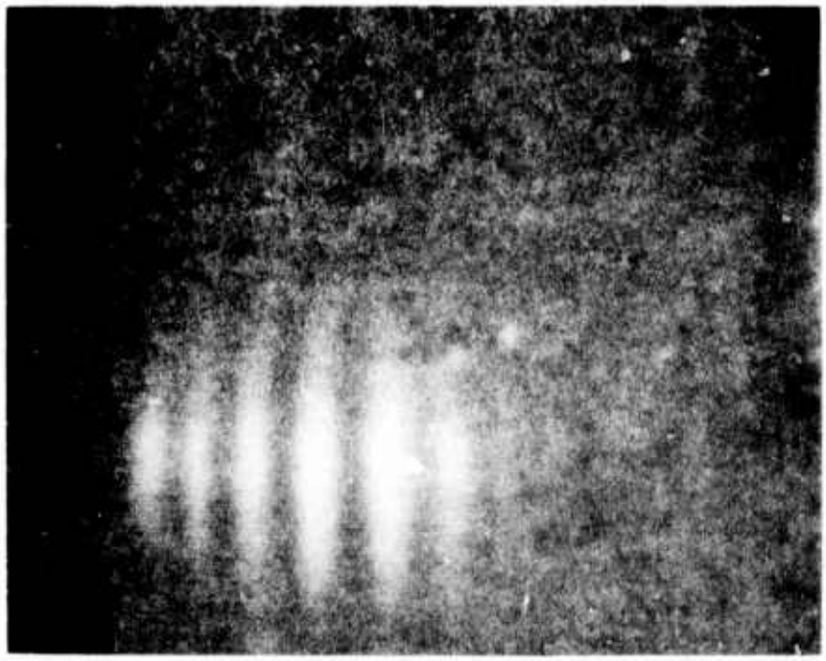

(a) tv screen display

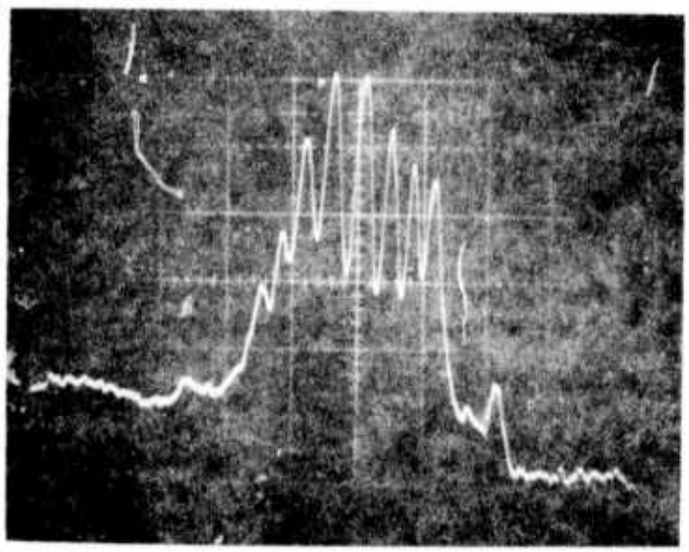

(b) oscilloscope display

TYPICAL SHEARING INTERFEROGRAMS

FIGURE II-27

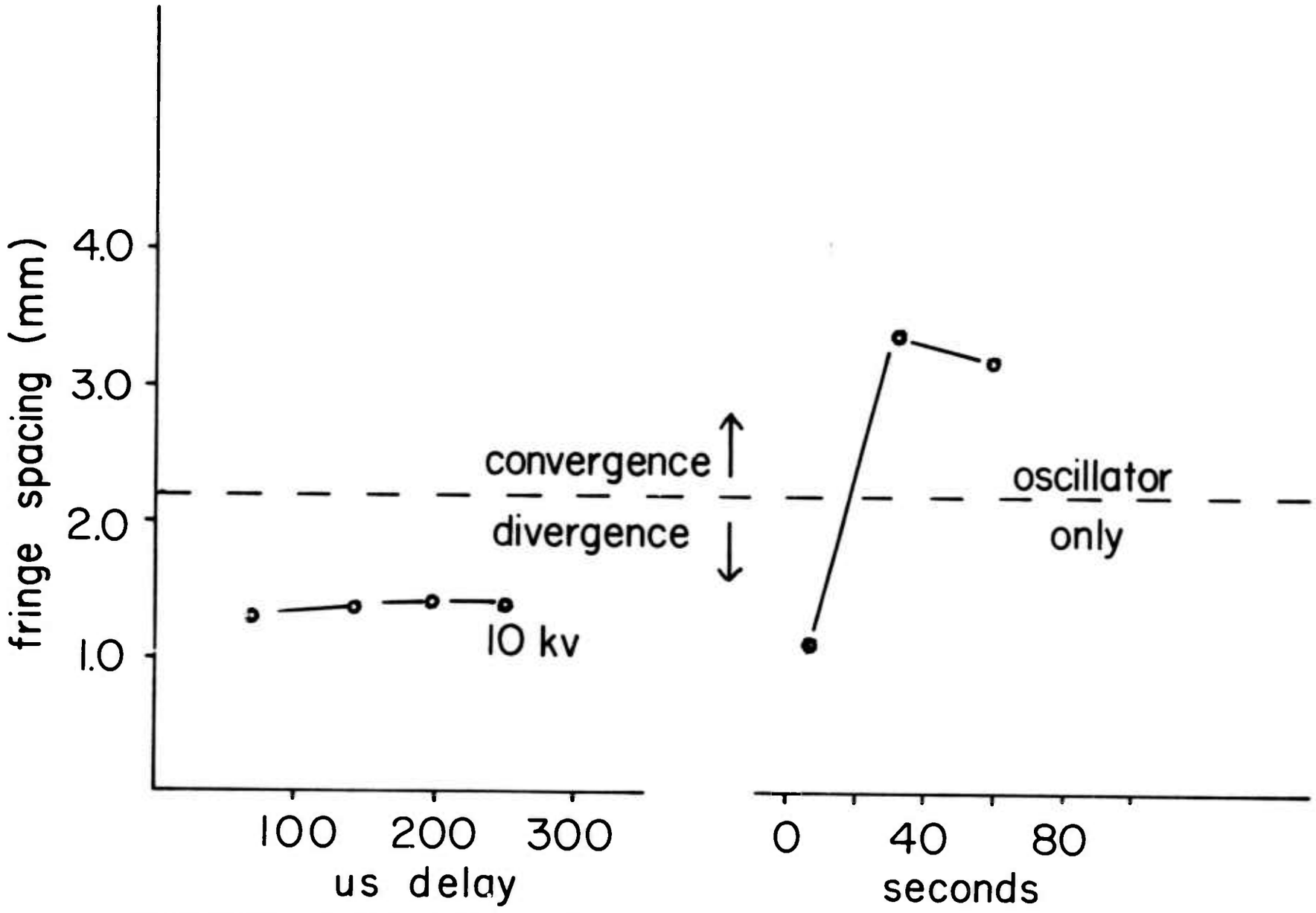

FRINGE SPACING VERSUS TIME

FIGURE 11-28

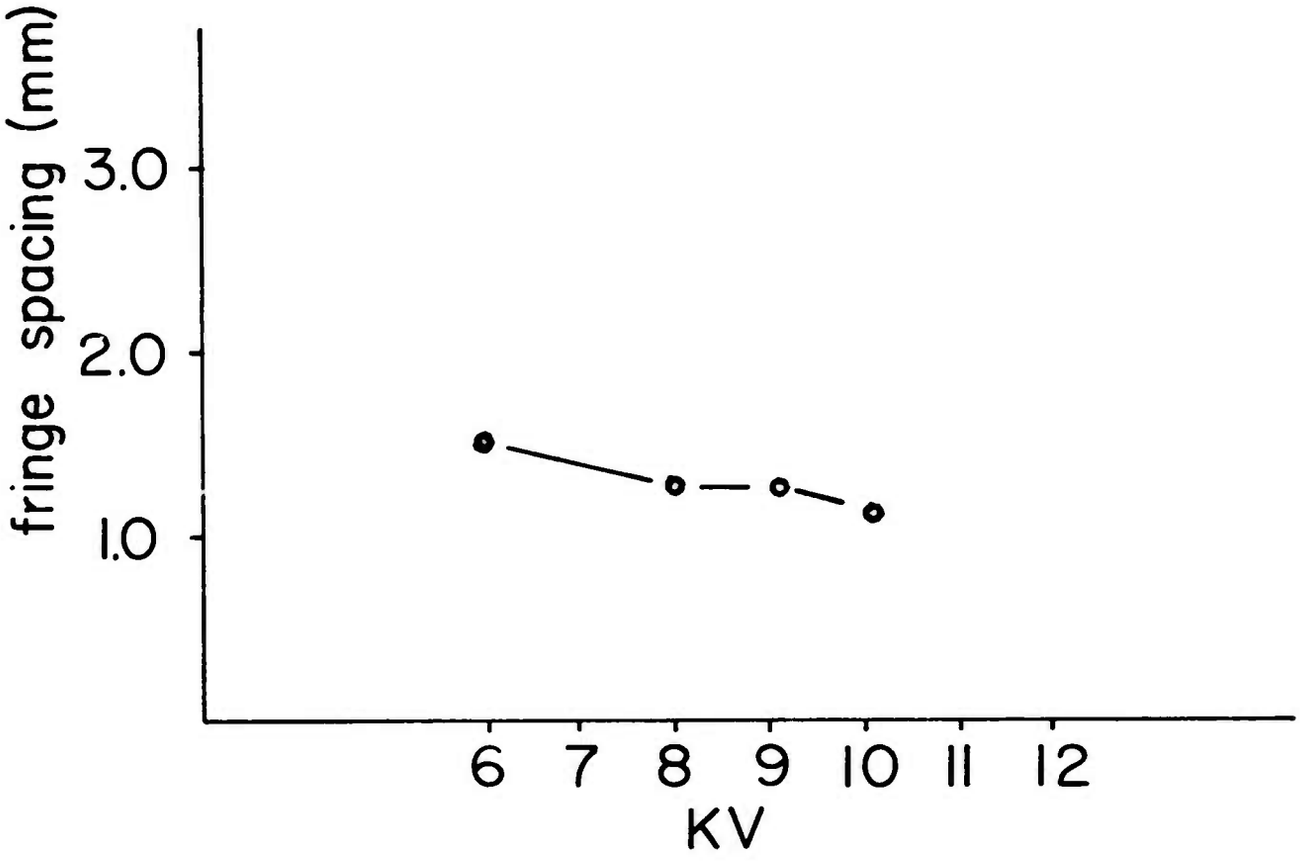

FRINGE SPACING VERSUS PUMPING INTENSITY

FIGURE 11-29

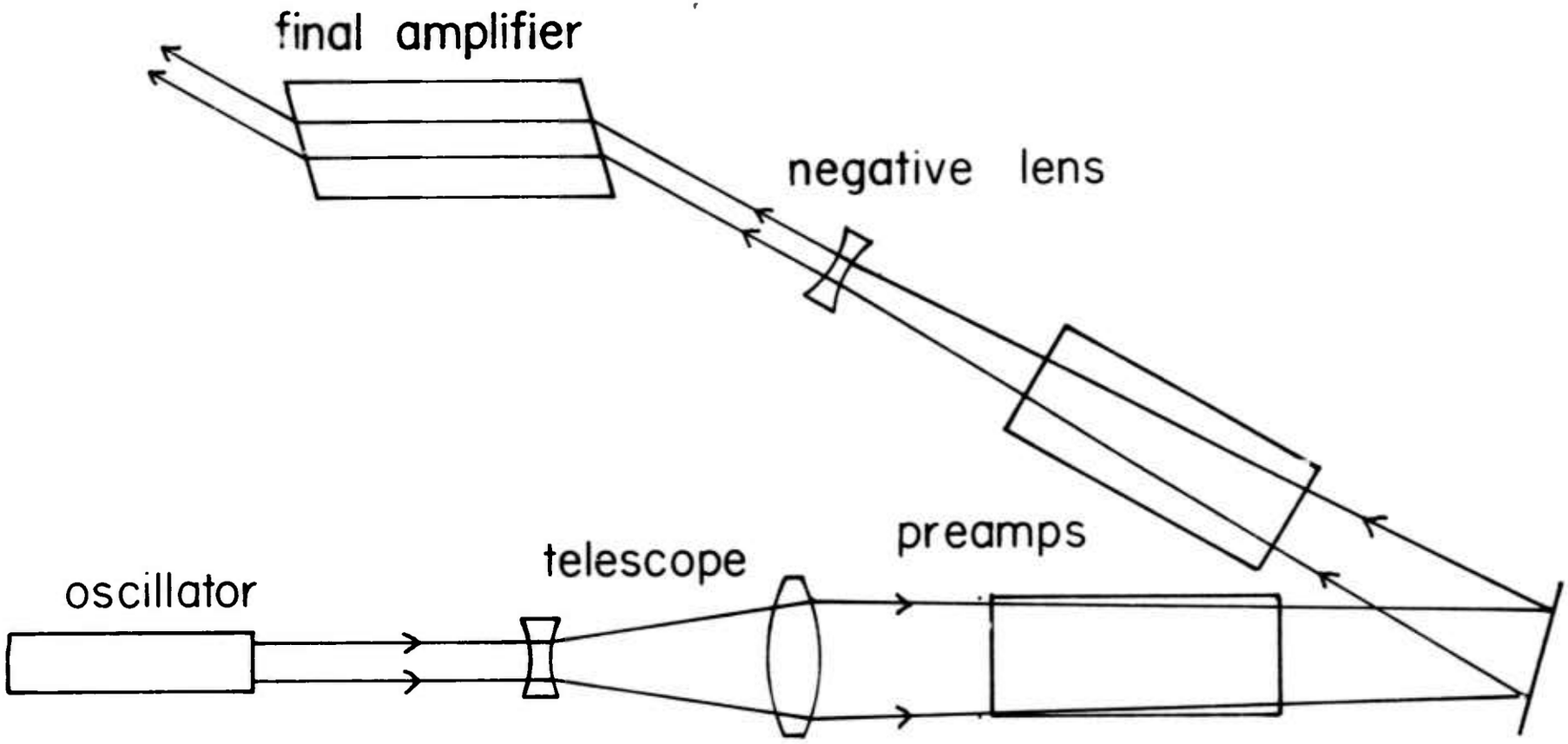

POSITION OF LENSES

FIGURE 11-30

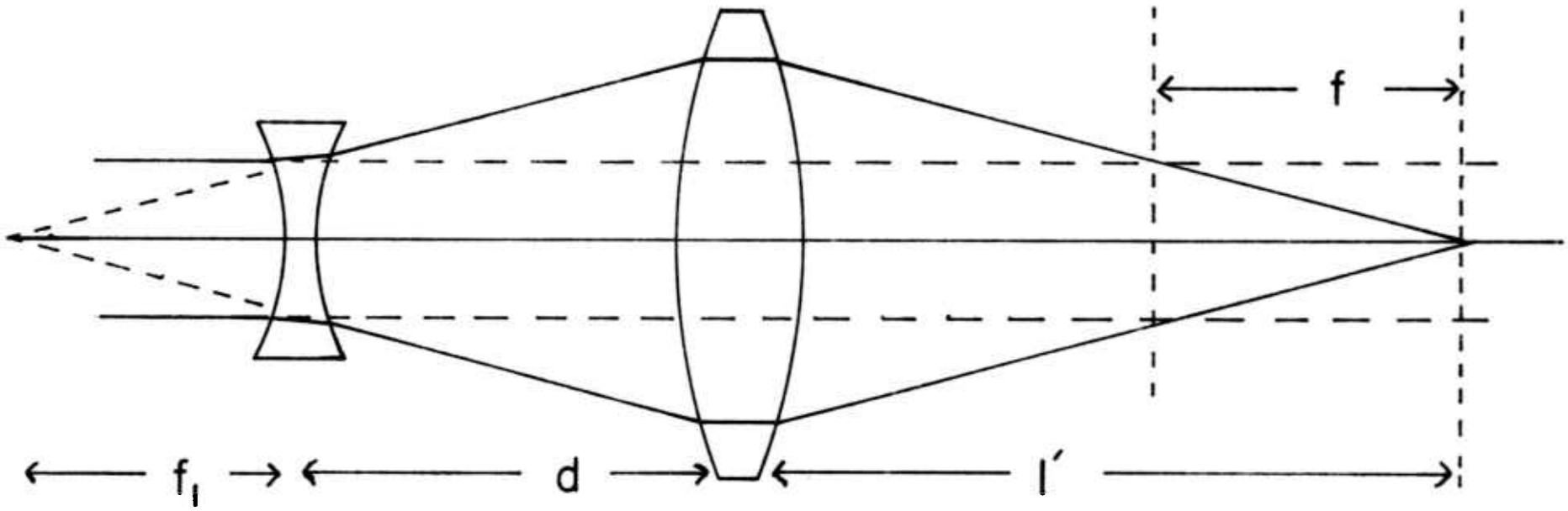

BEAM EXPANDING TELESCOPE

FIGURE 11-31

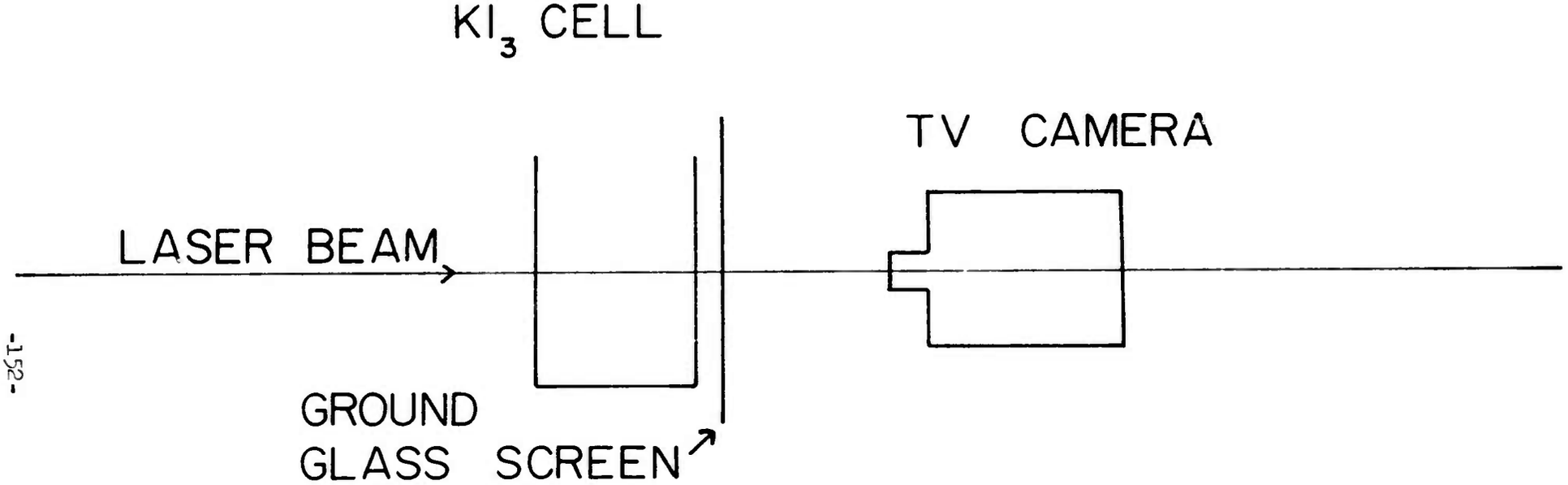

TV MONITORING SYSTEM

FIGURE II-32

BURN PATTERN AFTER FIRST AMPLIFIER

FIGURE II-33

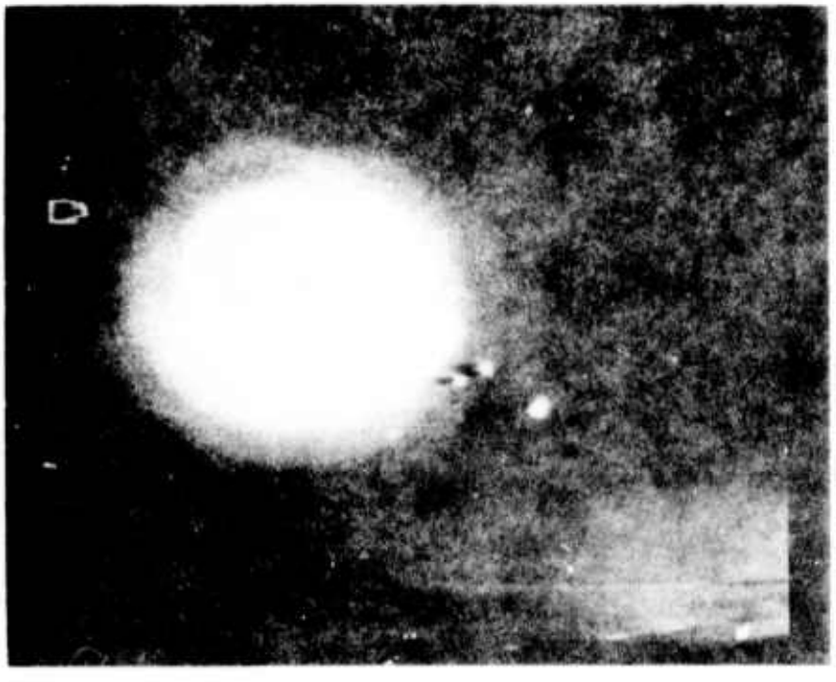

TV SCREEN DISPLAY OF
DIFFRACTION RINGS
(small spots are due to damaged
tv tube)

FIGURE II-34

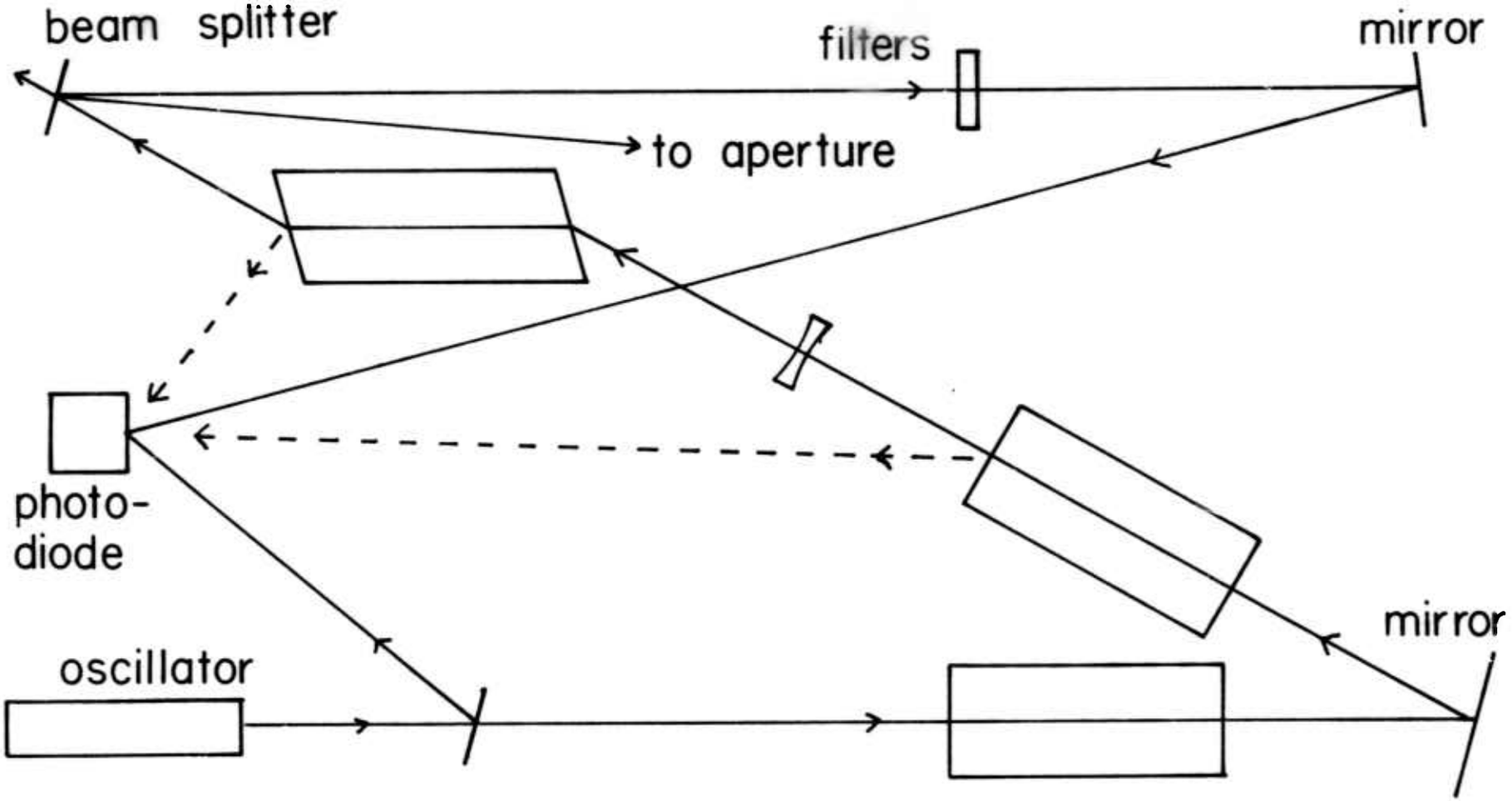

EXPERIMENTAL ARRANGEMENT

FIGURE II-35

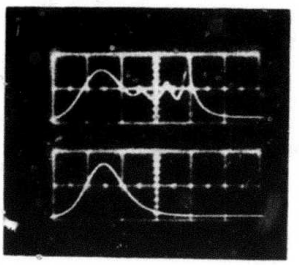

damage

no damage

OSCILLOGRAM OF OSCILLATOR OUTPUT SHOWING BACKSCATTER FROM LASER INDUCED DAMAGE IN FINAL AMPLIFIER

FIGURE II-36

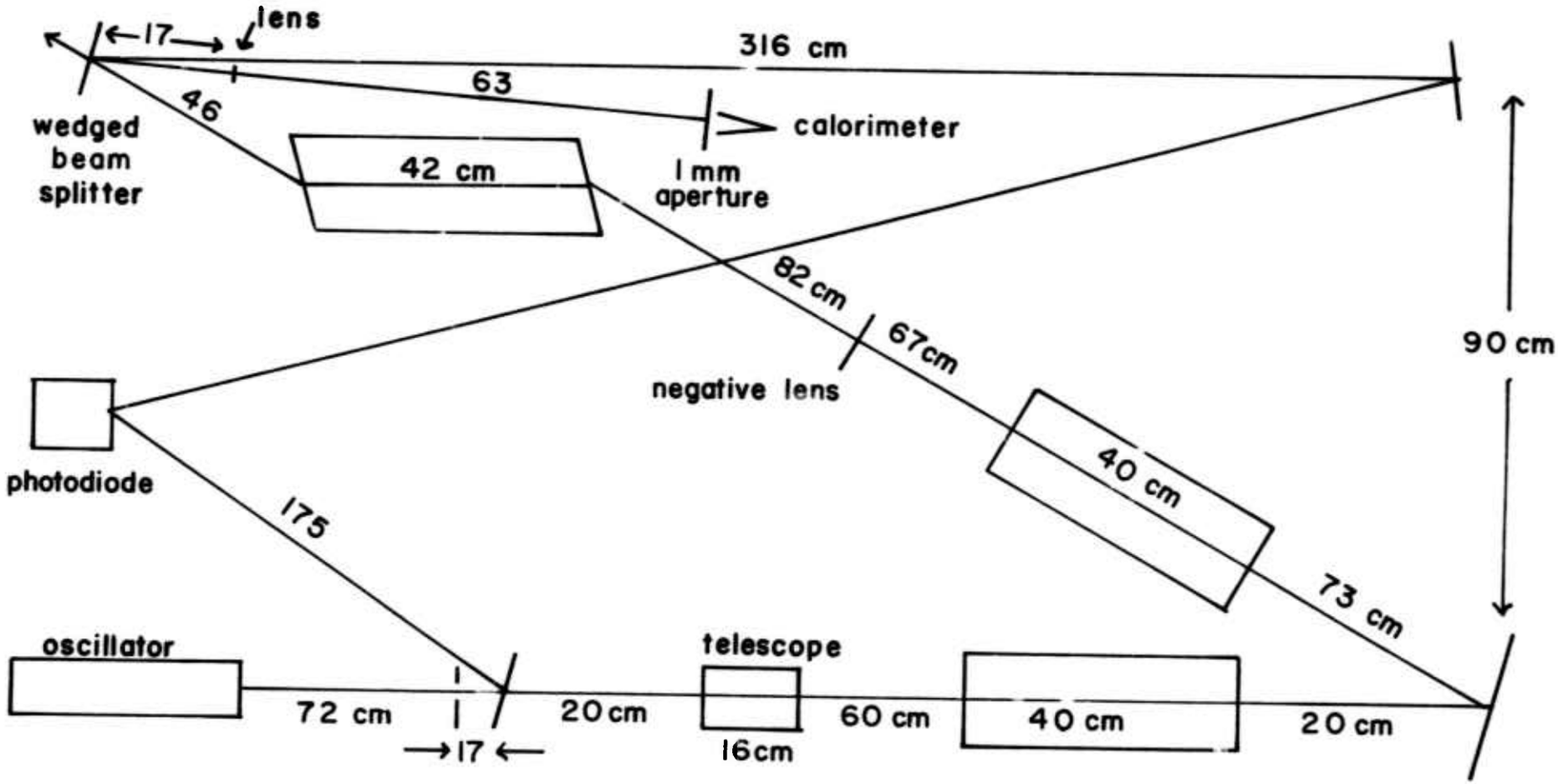

FINAL EXPERIMENTAL ARRANGEMENT

FIGURE 11-37

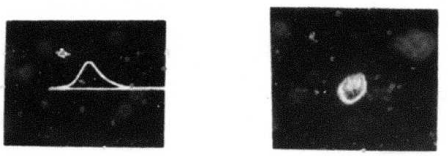

70.7 J/cm^2

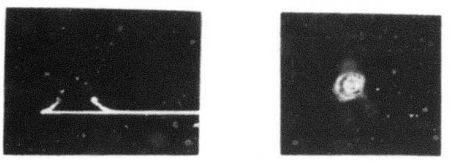

72.8 J/cm^2

OSCILLOGRAMS AND BURN PATTERNS AT MORE THAN 70 J/cm^2

FIGURE II-38

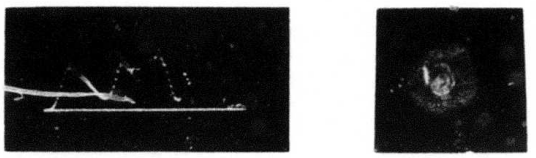

50.0 J/cm^2

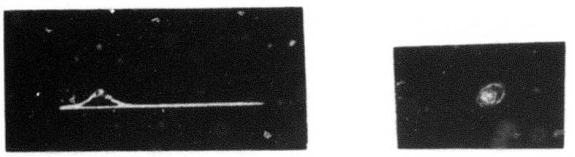

91.5 J/cm^2

OSCILLOGRAMS AND BURN PATTERNS OF PULSES THAT CAUSED SELF-FOCUSING DAMAGE

FIGURE II-39

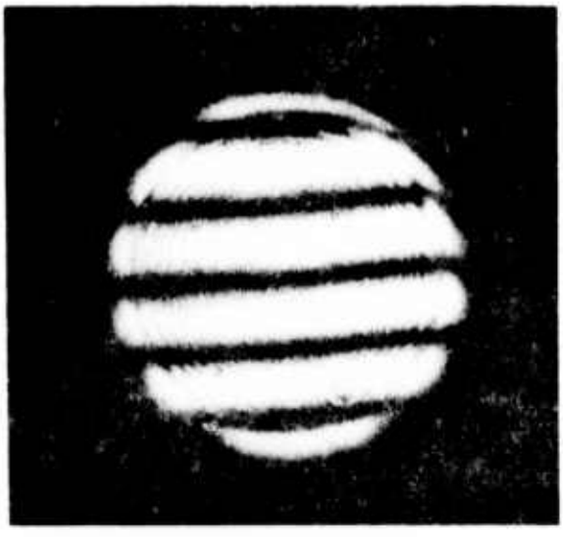

before

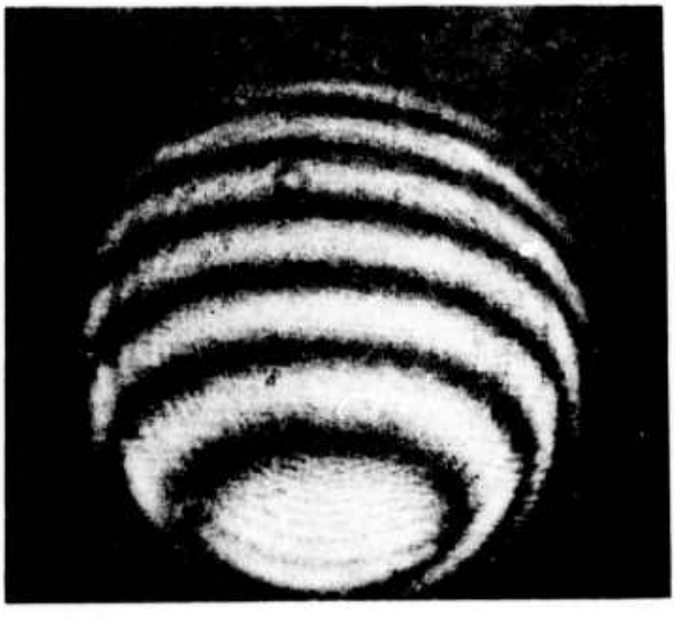

after

INTERFEROGRAMS OF THE
FIRST AMPLIFIER ROD

FIGURE 11-40

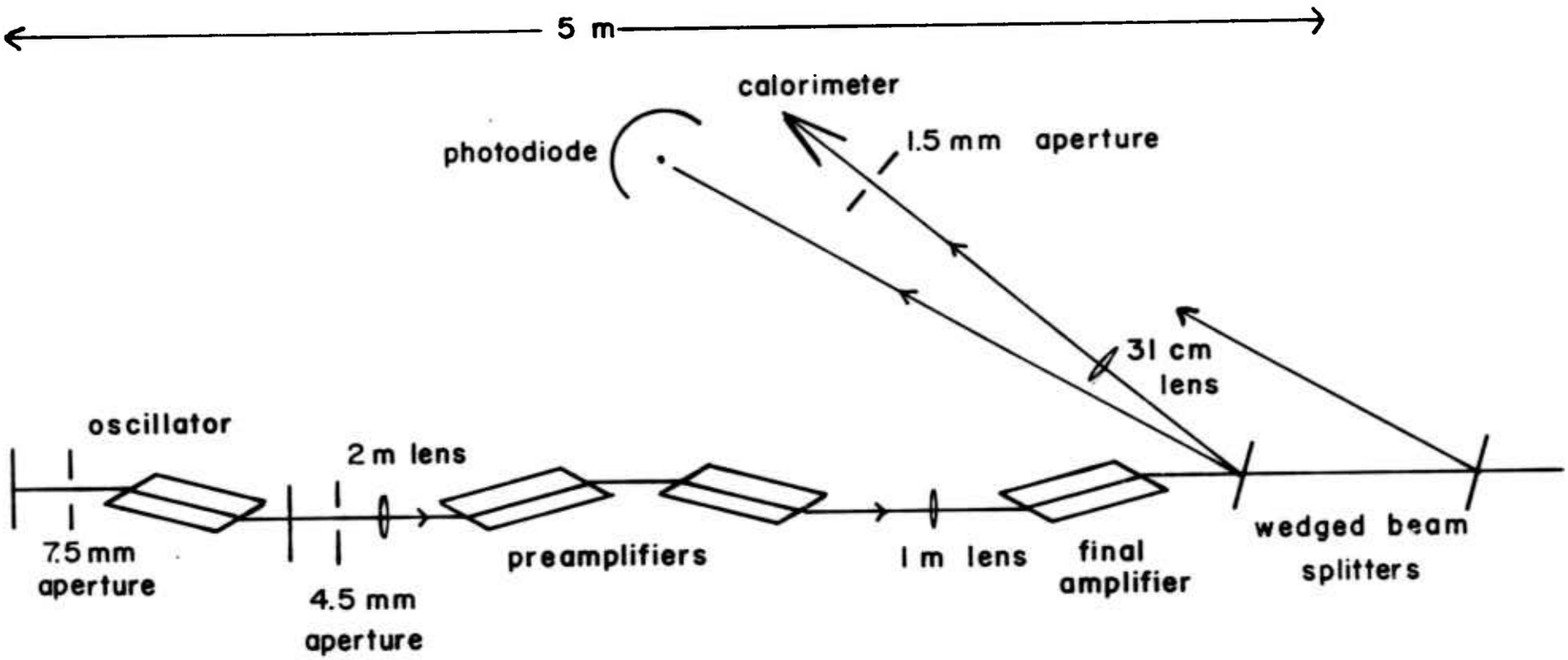

MULTIMODE EXPERIMENTAL ARRANGEMENT

FIGURE II - 41

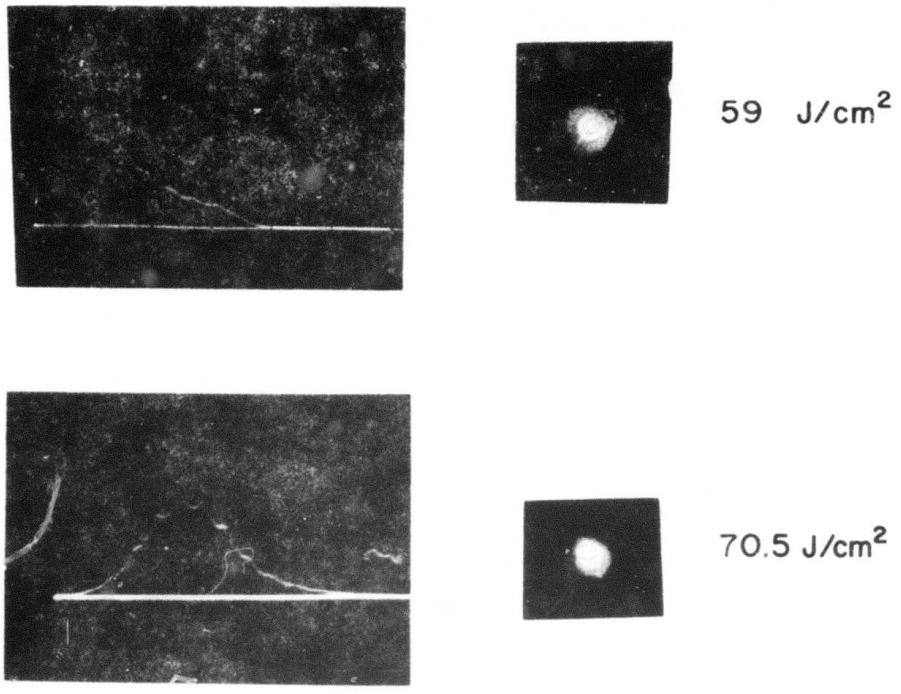

OSCILLOGRAMS AND BURN PATTERNS FROM MULTIMODE EXPERIMENTS

FIGURE II-42

Table II-1

Output of Four Amplifier Configurations of Equal Volume

Case		
(a)	$(E_o + 3\,W_o)(1 - s)^2\, e^{-3\gamma \ell}$	= 106.84 J/cm^2
(b)	$(E_o + 3\,W_o)(1 - s)^6\, e^{-3\gamma \ell}$	= 106.41 J/cm^2
(c)	$(E_o + 3\,W_o)(1 - s)^{5.33}\, e^{-\gamma \ell}$	= 107.77 J/cm^2
(d)	$(E_o + 3\,W_o)(1 - s)^{6.0}\, e^{-\gamma \ell}$	= 107.70 J/cm^2

Table II-2

Limits of Energy Irradiance for Rods and Disks

	Rods	Disks
S	1.07 J/cm^3	0.3 J/cm^3
ℓ	30 cm	3.0 cm
q	0.0005	0.0005
γ	0.002 cm^{-1}	0.002 cm^{-1}
ρ_c	491.8 J/cm^2	128.6 J/cm^2
γ	0.005	0.005
ρ_c	198.7	56.2

Table II-3

Intensity of Twice-Reflected Foci

	f = 15 cm D = 3 cm	f = 700 cm D = 10 cm
R = 0.04	3.3×10^5	1.88×10^4
R = 0.001	225.4	12.78

$\frac{I_{x_3}}{I_o}$ for four lenses

Table II-4

Output Irradiances of Various Lasers

	$\rho(J/cm^2)$	$t_p(ns)$	GW/cm^2
A.O.[25]	< 13	10-30	< 1.2-0.4
O-I (1969)[25]	60	55	1.03
Hadron[25]	15	30	0.47
NRL[25]	16	30	0.50
AFWRL[25]	20	40	0.47
LRL[25]	20	?	?
Sandia[25]	18	30	0.56
IPP[25]	8	25	0.30
Quantel (1973)[26]	5.7	10	0.53
	4	4	0.94
	3	2	1.41
O-I (multimode)	45	30	1.4
	59a	30	1.85
	70b	30	2.2
O-I (TEM_{oo})	70	15	4.4

(a) One shot only

(b) One shot only - damage to passive elements

APPENDIX A

NON-LINEAR INDEX STUDIES

This appendix is a paper submitted for publication to the Journal of Quantum Electronics. The final form will be somewhat modified.

AN EMPIRICAL RELATIONSHIP FOR PREDICTING NONLINEAR REFRACTIVE INDEX CHANGES IN OPTICAL SOLIDS

N. L. Boling,[+]

Owens-Illinois Technical Center, Toledo, Ohio 43601

Alexander J. Glass[*]

Lawrence Livermore Laboratory, Livermore, California 94550

and

Adelbert Owyoung[*]

Sandia Laboratories, Albuquerque, New Mexico 87115

ABSTRACT

It is shown that the electronic contribution to the third order nonlinear susceptibility of an isotropic material can be obtained directly from the refractive index dispersion data for the material. The phenomenon of index nonlinearity is shown to be intimately related to the optically induced quadratic Stark shift. Data obtained by ellipse rotation measurement on several glasses and crystals are seen to be in good agreement with the expression obtained.

---

[*]This work was performed under the auspices of the U. S. Atomic Energy Commission

[+]This work was partially supported by the Advanced Research Projects Agency under contract DAHC 15-72-C-0170.

In this paper we propose a simple relationship for the electronic contribution to the nonlinear susceptibility in transparent dielectrics, based on parameters obtained solely from the magnitude and dispersion of the refractive index $n(\omega)$. The model employed relates the index nonlinearity to the optically induced, quadratic Stark shift of the uv absorption edge of the material, and includes the local field corrections. This model gives good agreement for a variety of materials, including laser glasses, cubic crystals, and optical glasses of refractive index from 1.4 to 1.9, using data obtained by the ellipse rotation technique. The third order nonlinear susceptibility is shown to be given by the expression

$$\chi^{(3)}_{1221}(-\omega,\omega,\omega,-\omega) = \frac{1}{4}\left(\frac{n(\omega)^2+2}{3}\right)^2\left(\frac{n(\omega)^2-1}{4\pi}\right)^2\frac{1}{N\hbar\omega_o} \qquad (1)$$

where the parameters N and ω_o are obtained from the dispersion data for the material. $\chi^{(3)}_{1221}$ is the component of the third order susceptibility tensor relevant to ellipse rotation [1].

As is discussed in [1], for isotropic media, the susceptibility component relevant to self focusing is $\chi^{(3)}_{1111}$ which is related to the nonlinear refractive index by the expression $n_2 = 12\pi\chi^{(3)}_{1111}/n$.

In arriving at (1), we assume that the transparent dielectric is adequately described as a molecular solid made up of several constituent types. Each constituent exhibits a unique linear polarizability α^i, and a mean second hyperpolarizability γ^i [2]. Under the influence of a local

harmonic field of frequency ω, given by $E_\ell \cos \omega t$, the microscopic polarization induced in the i^{th} constituent is given by

$$p^i = \alpha^i E_\ell \cos \omega t + \frac{1}{6} \gamma^i (E_\ell \cos \omega t)^3 \tag{2}$$

We can define an average polarizability $\bar{\alpha}$, and hyperpolarizability $\bar{\gamma}$ as

$$\bar{\alpha} = \sum_i \alpha^i N^i / \sum_i N^i \tag{3}$$

$$\bar{\gamma} = \sum_i \gamma^i N^i / \sum_i N^i \tag{4}$$

where N^i is the concentration of the i^{th} constituent. Then the macroscopic induced dipole moment takes the form

$$P = \sum_i N^i p^i$$

$$= N \left[\bar{\alpha} E_\ell \cos \omega t + \frac{\bar{\gamma}}{24} E_\ell^3 (3\cos \omega t + \cos 3\omega t) \right] \tag{5}$$

where $N = \sum_i N^i$. Applying the local field correction factor

$$f = (n^2 + 2)/3 \tag{6}$$

we can write[3]

$$P = fN\bar{\alpha} E \cos \omega t + N \frac{\bar{\gamma}}{24} f^4 E_\ell^3 (3\cos \omega t + \cos 3\omega t) \tag{7}$$

where E cos ωt is the macroscopic field in the medium. From the customary definition of the nonlinear susceptibility [1], for a relation of the form given by (7) we would write

$$P(\omega) = \chi^{(1)}_{11}(-\omega,\omega)\ E(\omega) + 3\chi^{(3)}_{1111}(-\omega,\omega,\omega,-\omega)\ E^3(\omega)$$

and

$$P(3\omega) = \chi^{(3)}_{1111}(-3\omega,\omega,\omega,\omega)\ E^3(\omega) \tag{8}$$

where

$$\chi^{(1)}_{11}(-\omega,\omega) = fN\bar{\alpha} = \frac{n^2(\omega) - 1}{4\pi} \tag{9}$$

and

$$\chi^{(3)}_{1111}(-\omega,\omega,\omega,-\omega) = \frac{f^4}{24}\ N\bar{\gamma}. \tag{10}$$

It is well established from perturbation theoretic arguments [4],[5] that the hyperpolarizability $\bar{\gamma}$ and the linear polarizability $\bar{\alpha}$ are related for a polarizable electronic system by a relation of the form

$$\bar{\gamma} = q\ \bar{\alpha}^2 \tag{11}$$

where q is a parameter to be determined. Accordingly, we write (10) in the form

$$\chi^{(3)}_{1111}(-\omega,\omega,\omega,-\omega) = \frac{f^4}{24}(N\bar{\alpha})^2\left(\frac{q}{N}\right) = \frac{1}{24}\left(\frac{n^2+2}{3}\right)^2\left(\frac{n^2-1}{4\pi}\right)^2\left(\frac{q}{N}\right). \quad (12)$$

Thus, the explicit dependence of the third order susceptibility on the refractive index is expected to follow (12) for all nominally transparent dielectrics in which the Lorentz-Lorenz local field corrections are expected to apply, i.e., isotropic and cubic materials.

The ratio q defined in (11) has been defined in terms of perturbation theoretic quantities in [4] and [5]. We choose to give a semiclassical derivation of this parameter, first, to represent the problem in terms of quantities of more immediate physical significance than those accessible via perturbation theory; and second, to show explicity the connection with the optical Stark shift. We take as a model the classical nonlinear oscillator described by the equation

$$\frac{d^2x}{dt^2} + \omega_o^2(x - \lambda x^3) = s\,\frac{eE}{m}\cos\omega t, \quad (13)$$

where s is the effective oscillator strength, and λ represents the nonlinear coupling. The model indicated in (13) has been used previously to represent the nonlinear response of ionic motion. It is the simplest model which represents motion in a symmetric, non-parabolic potential. To zero order in λ the solution of (13) is given by

$$x = x_0 \cos \omega_0 t + s \frac{eE}{m(\omega_0^2 - \omega^2)} \cos \omega t \tag{14}$$

where x_0 is the amplitude of the free oscillation, and the second term represents the forced oscillation. The first term cannot be ignored, even though we assume that the free oscillations add up with random phase and make no contribution to the refractive index. This can be seen if we go to the first order in λ. It is well known that the naive iteration of the solution (14), in (13), will give rise to secular terms. Instead, we employ the method of Linstedt [6] to eliminate secular terms.

In this method we introduce a "stretched" time variable in the form

$$t = \theta(1 + \lambda a_1 + \lambda^2 a_2 + \ldots). \tag{15}$$

The differential equation is then written as

$$\frac{d^2x}{d\theta^2} + (1 + \lambda a_1 + \lambda^2 a_2 + \ldots)^2 \left[\omega_0^2(x - \lambda x^3) - s \frac{eE}{m} \cos \bar{\omega}\theta \right] = 0 \tag{16}$$

Here the effective driving frequency $\bar{\omega}$ is given by

$$\bar{\omega} = \omega(1 + \lambda a_1 + \lambda^2 a_2 + \ldots). \tag{17}$$

The zero order solution to (16) is given by

$$x = x_0 \cos \omega_0 \theta + s \frac{eE}{m(\omega_0^2 - \bar{\omega}^2)} \cos \bar{\omega}\theta. \tag{18}$$

Thus we see that although the driven oscillation is identical to that

obtained above, the free oscillation occurs at a frequency shifted from the natural resonance, $\omega_o/(1 + a_1\lambda + a_2\lambda^2 + \ldots)$.

Solving (16) in first order and eliminating secular terms, we determine the coefficient a_1 to be

$$a_1 = \frac{3}{4} s^2 \frac{e^2E^2}{m^2(\omega_o^2 - \omega^2)^2} \tag{19}$$

Thus the free oscillation of the system occurs at the Stark shifted frequency

$$\omega_o \left[1 - \frac{3}{4} \lambda \frac{s^2e^2E^2}{m^2(\omega_o^2 - \omega^2)^2} \right] \tag{20}$$

while the induced dipole moment is given by

$$p = s \frac{e^2E \cos \omega t}{m(\omega_o^2 - \omega^2)} + \frac{1}{4} \lambda \frac{s^3e^4E^3\omega_o^2}{m^3(\omega_o^2 - \omega^2)^3} \left[\frac{3\cos \omega t}{\omega_o^2 - \omega^2} + \frac{\cos 3\omega t}{(\omega_o^2 - 9\omega^2)} \right]. \tag{21}$$

The third harmonic term is identical to that obtained by Armstrong, Bloembergen, Ducuing, and Pershan [3]. The linear polarizability of the system is then given by

$$\alpha = \frac{Se^2}{m(\omega_o^2 - \omega^2)} \tag{22}$$

and, from (2), the hyperpolarizability is given by

$$\gamma = \frac{6\lambda s^3e^4\omega_o^2}{m^3(\omega_o^2 - \omega^2)^4} \tag{23}$$

The parameter q, defined in (11), is thus given by

$$q = \frac{6\lambda s\omega_o^2}{m(\omega_o^2 - \omega^2)^2} \xrightarrow{\omega << \omega_o} \frac{6\lambda s}{m\omega_o^2} \tag{24}$$

The significance of these results is clear. The effect of the applied field is to distort the charge distribution of the polarizable atom or ion so as to extend it further into the region of nonlinearity. If the nonlinearity is characterized by $\lambda > 0$, then the effective force constant is reduced by the nonlinearity, lowering the resonant frequency and increasing the polarizability. On the other hand, for $\lambda < 0$ the nonlinearity leads to a stiffer force constant, raising the resonant frequency and leading to a lower polarizability. Both the Stark shift and the nonlinear susceptibility $\chi^{(3)}$ arise as a direct consequence of the nonlinearity in the potential.

It remains to evaluate the nonlinear parameter λ. Let us consider a potential well which is parabolic near the center, but which has a finite ionization energy, or well depth, V_o. Two potential functions which satisfy this criterion are the quartic well

$$V = m\omega_o^2\left(\frac{x^2}{2} - \lambda_Q \frac{x^4}{4}\right), \qquad \lambda_Q = \frac{m\omega_o^2}{4V_o}, \tag{25}$$

and the Gaussian well,

$$V = V_o[1 - \exp(-\lambda_G x^2)], \qquad \lambda_G = \frac{m\omega_o^2}{2V_o} \tag{26}$$

These represent the simplest forms of potential well which are parabolic near the center and exhibit a finite well depth. The nonlinear parameter $\lambda > 0$ in each case. We see that the relation of the nonlinearity parameter to the well depth and the resonant frequency is not greatly dependent on the model assumed, and exhibits the same functional form. For the Gaussian well we can write the factor

$$q = \frac{6\lambda s\omega_o^2}{m(\omega_o^2 - \omega^2)^2} = \frac{6\omega_o^4 s}{2(\omega_o^2 - \omega^2)^2 V_o} = 6g\left(\frac{\omega_o^3}{\hbar(\omega_o^2 - \omega^2)^2}\right), \tag{27}$$

where the coefficient $g = s\hbar\omega_o/2V_o$ for the Gaussian well and $s\hbar\omega_o/4V_o$ for the quartic well. For the Gaussian well, the Stark shift is then written in the form

$$\frac{\Delta\omega}{\omega_o} = -\frac{3}{4} q \frac{\alpha E^2}{V_o} \tag{28}$$

Substitution of (27) in (12) in the limit as $\omega << \omega_o$, leads to the result

$$\chi^{(3)}_{1111}(-\omega,\omega,\omega,-\omega) = \frac{g}{4}\left(\frac{n^2+2}{3}\right)^2\left(\frac{n^2-1}{4\pi}\right)^2 \frac{1}{N\hbar\omega_o} . \tag{29}$$

This expression corresponds to the perturbation theoretic expressions obtained in [4] and [5] with the local field corrections stated explicitly. We find that a value g = 3 leads to the best agreement with experimental data.

The parameters N and ω_o are obtained from fitting available refractive index data to the Lorentz-Lorenz equation,

$$\left(\frac{n^2 - 1}{4\pi}\right)\left(\frac{3}{n^2 + 2}\right) = \frac{Ne^2}{m(\omega_o^2 - \omega^2)}, \tag{30}$$

assuming an oscillator strength of unity. This differs from the procedure followed by Wemple and DeDomenico [7] who fit refractive index data without considering the local field corrections. This accounts for the discrepancy between results obtained here and those obtained from Wang's equation (2).

The experimental apparatus used to perform the ellipse rotation measurements for this work has been described in detail in previous papers [8],[9]. These measurements were facilitated with the use of a TEM_{ooq} near-Gaussian mode ruby laser system. The values reported in [8] were determined to ±7%. Subsequent measurements have been carried out to a precision of ±10%. In Table I the results of these measurements have been tabulated for a number of silicate glasses of widely varying composition. The result which was obtained for the symmetric combination $1/6(\chi^{(3)}_{1111} + \chi^{(3)}_{1221} + 2\chi^{(3)}_{1122})$ for crystalline YAG has also been included for comparison since it is the only crystalline material on which ellipse rotation data is presently available. Also in Table I are the values of $\chi^{(3)}_{1221}$ computed from (1) using available refractive index data. For further comparison, computed values for CCl_4 and ruby are included, along with experimental values obtained from ellipse rotation [10] and self-focusing [11] measurements.

These data are presented graphically in Fig. 1. We see that, although as a general trend $\chi^{(3)}$ increases with increasing index, no simple scaling law would suffice to predict the variation. With the exception of the two heavy flint glasses, SF-7 and LaSF-7, the agreement between theory and

experiment is quite satisfactory. It should be emphasized that a value of $q = 3$ was used in all the calculations, and that no other free parameters were involved in fitting the data.

The value of q used in the calculation is somewhat larger than expected. Wang [5] pointed out that a value of 1.2 would be expected from calculations performed on the hydrogen atom, a case which can be solved exactly. On the basis of the model potentials introduced in (25 and (26), we would expect a value of q less than unity, assuming the strongest uv transition (unit oscillator strength) lies not far below the ionization level for the material.

In every case except ruby and LaSF-7, the computed value is equal to or less than the measured value. The measured value can contain contributions from "nuclear" effects [9] as well as electronic effects, whereas the computed value is purely electronic.

The greatest source of uncertainty for the computed values is the fit of the refractive index data to a single oscillator. In each case, using published values of refractive index [12], the quantity $(4\pi/3)(n^2 + 2)/(n^2 - 1)$ was fit to a linear function of the form $(\omega_0^2 - \omega^2)/N(e^2/m)$, using least-squares fitting over the frequency range corresponding to $0.365\ \mu m < \lambda < 1.014\ \mu m$. In all cases the fit reproduced the index value to one or two parts per thousand over the range of the fit yielding a 1% uncertainty in the fitted parameters.

As a further check on the theory, the cluster of parameters measured at a single frequency, $(n^2 - 1)^2(n^2 + 2)^2/4(12\pi)^2\chi^{(3)}_{1111}$, was plotted versus the parameters obtained from refractive index data, $N\hbar\omega_0$ for each of the

materials measured. The results are shown in Fig. 2. All materials which satisfy (1) are expected to fall on the 45° line on such a plot. It is seen that over a variation of a factor of four, the data for several crystalline and amorphous solids, and a liquid, all fall very near the theoretical line. (The data for ruby are included, for comparison, divided by a factor of 2 on each axis, to provide a more compact plot.)

It is noteworthy that these simple considerations yield a result which is so broadly applicable. In glasses, we expect contributions to the index nonlinearity from a variety of ions, and the averaging process by which (11) is obtained may not be valid. For (11) to apply, either all the ions must make similar contributions to $\bar{\alpha}$ and $\bar{\gamma}$, or one species dominates entirely. It is unlikely that the latter is the case, since the indices vary so greatly for the glasses measured. This implies that the parameter q is essentially the same for all the contributing species.

In conclusion, it is seen that (1) yields good agreement with accurate experimental results on the third order, electronic hyperpolarizability for a large class of glasses and crystals. The intimate relation between the optical Stark effect and the index nonlinearity has been shown, by appeal to a classical model. There is satisfactory agreement with perturbation theory results. The expression (1) provides a useful scaling relation to allow the accurate estimation of index nonlinearities of electronic origin in transparent dielectrics, assuming that refractive index data are known. Although there is a general trend for materials of lower index to exhibit lower values of $\chi^{(3)}$, the details of the dispersion curve must be included to obtain an accurate value for the nonlinearity.

The authors wish to acknowledge the aid of Dr. George Dube for several invaluable discussions, and of Dr. John Emmett for suggesting the interrelation between the Stark shift and the index nonlinearity.

TABLE I

Material	n	$10^{15}\ \chi^{(3)}_{1221}$ (esu) Measured	Calculated
FK-6	1.446	1.45 ± 0.15	1.15
FS (Fused Silica)	1.456	1.28 ± 0.09	1.17
BK-7	1.517	1.96 ± 0.20[a]	1.58
LSO	1.519	1.92 ± 0.13	1.95
FD-4	1.567	2.39 ± 0.16	2.42
EY-1	1.635	2.93 ± 0.21	3.40
SF-7	1.640	8.45 ± 0.85[a]	6.32
LaK-3	1.694	3.85 ± 0.39	3.86
YAG	1.829	6.62 ± 0.46	6.60
LaSF-7	1.914	10.5 ± 1.0	14.2
CCl_4	1.460	3.2 ± 0.3[a]	2.62
Ruby	1.75-1.76	2.1 ± 0.2	3.26

[a] The values of $\chi^{(3)}$ taken from [9] and [10] have been reduced by 15% to compensate for the calibration error alluded to in [8].

REFERENCES

[1] P. D. Maker and R. W. Terhune, "Study of optical effects due to an induced polarization third order in the electric field strength," Phys. Rev., vol. 137, pp. A801-A818, 1965.

[2] C. A. Coulson, A. Maccoll, and L. E. Sutton, "The polarizability of molecules in strong electric fields," Trans. Faraday Soc., vol. 48, pp. 106-113, 1952.

[3] J. A. Armstrong, N. Bloembergen, J. Ducuing, and P. S. Pershan, "Interactions between light waves in a nonlinear dielectric," Phys. Rev., vol. 127, pp. 1918-1939, 1962.

[4] S. S. Jha and N. Bloembergen, "Nonlinear optical susceptibilities in group-IV and III-V semiconductors," Phys. Rev., vol. 171, pp. 891-898, 1968.

[5] C. C. Wang, "Empirical relation between the linear and the third order nonlinear optical susceptibilities," Phys. Rev. B, vol. 2, pp. 2045-2048, 1970.

[6] R. Bellman, Perturbation Techniques in Mathematics, Physics, and Engineering. New York: Holt, Rinehart and Winston, 1964, part 2.

[7] S. H. Wemple and M. DiDomenico, Jr., "Optical dispersion and the structure of solids," Phys. Rev. Lett., vol. 23, pp. 1156-1160, 1969.

[8] A. Owyoung, "Ellipse rotation studies in laser host materials," IEEE J. Quantum Electron., vol. QE-9, 1064-1069, Nov. 1973. Also, A. Owyoung, "Nonlinear refractive index measurements in laser media," in Laser Induced Damage in Optical Materials. NBS Special Publication 387, A. J. Glass and A. H. Guenther, Editors, U.S. Govt. Printing Office, 1973.

REFERENCES (cont)

[9] Adelbert Owyoung, R. W. Hellwarth, and Nicholas George, "Intensity induced changes in optical polarizations in glasses," Phys. Rev. B, vol. 5, pp. 628-633, 1972.

[10] R. W. Hellwarth, Adelbert Owyoung, and Nicholas George, "Origin of the nonlinear index of liquid CCl_4," Phys. Rev. A, vol. 4, pp. 2342-2347, 1971.

[11] R. L. Carman, M. Moran, and C. Y. She, to be published.

[12] Index data taken from the following sources: Schott glasses from Catalog 3053 and supplements. YAG from W. L. Bond, "Measurement of the refractive indices of several crystals," J. Appl. Phys., vol. 36, pp. 1674-1677, 1965. Laser Glasses from R. M. Waxler, G. W. Cleek, I. H. Malitson, M. J. Dodge, and T. A. Hahn, J. Res. Natl. Bur. Stand. (U.S.) A., "Optical and mechanical properties of some neodymium doped laser glasses," vol. 74, pp. 163-174, 1971. Others from American Institute of Physics Handbook. New York, McGraw-Hill, 1972, 3rd Edition.

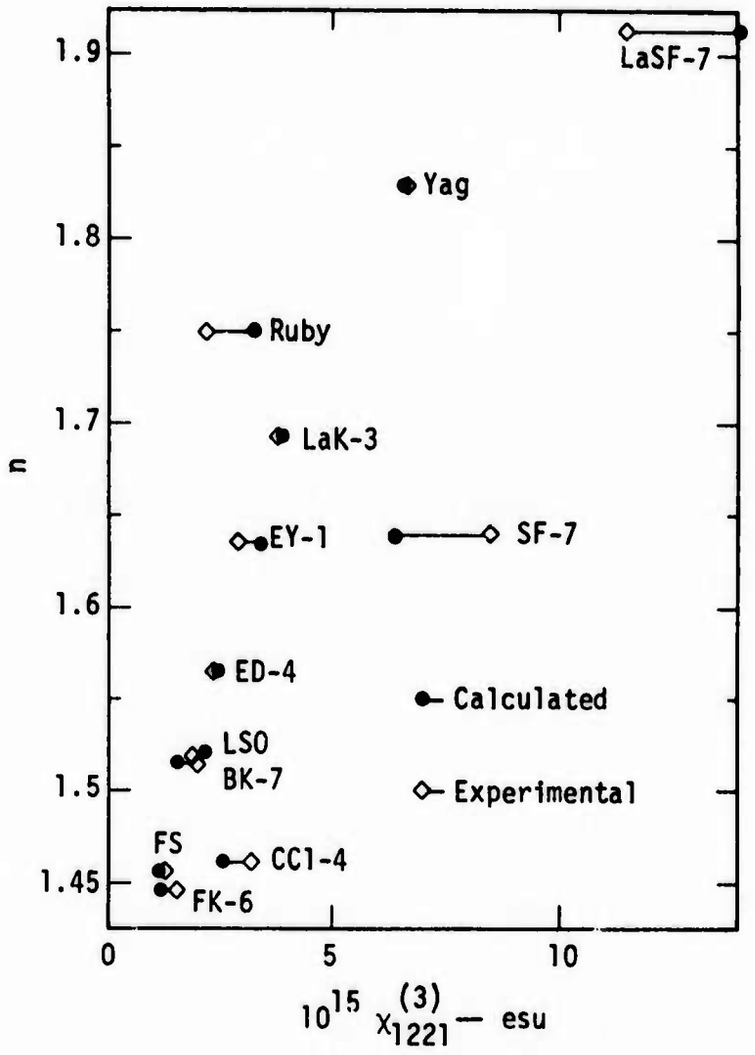

Fig. 1. $10^{15}\ \chi^{(3)}_{1221}$ vs refractive index (n) for several transparent dielectrics. For Comparison, the electronic contribution to the nonlinear susceptibility for CCl_4 is included [10].

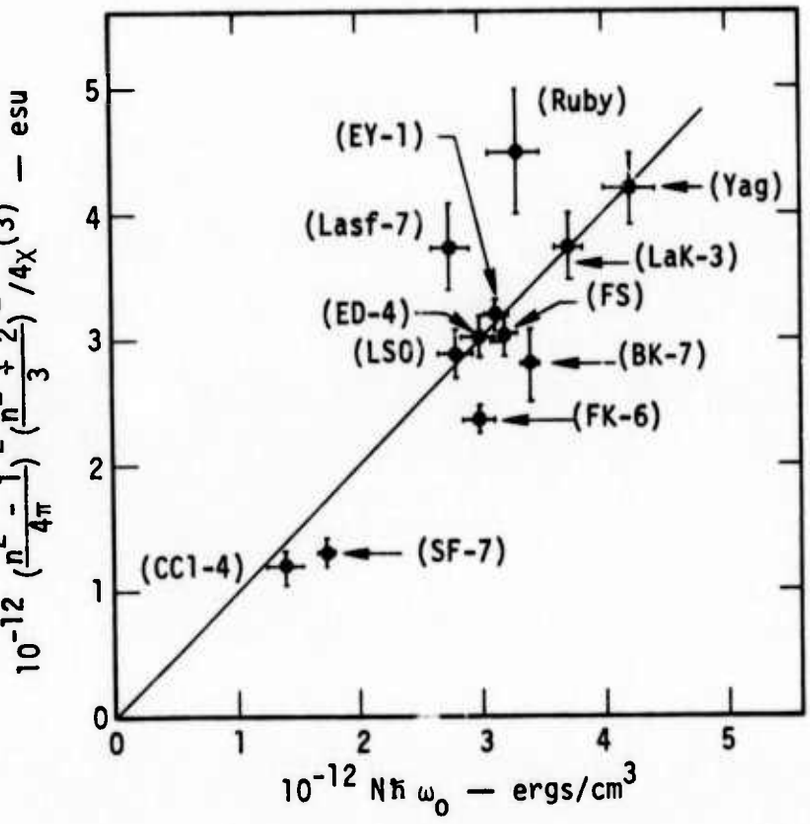

Fig. 2. Measured parameters vs fitted parameters, corresponding to (1). (The data for ruby have been divided by 2 on each axis for comparison with the other materials measured.)

APPENDIX B

TOTAL INTERNAL REFLECTION APODIZERS

by

G. Dubé

ABSTRACT

A novel type of apodizer using total internal reflection is suggested for use in high-power laser systems.

Recently, there has been a great deal of interest in developing apodizers or soft apertures for use in high-power laser amplifier systems.[1-6] The purpose of the apodizer is to reduce the depth of modulation in diffraction patterns associated with the truncation or aperturing of the laser beam. By eliminating or reducing the diffraction rings, the effects of nonlinear laser light-amplifier interactions can be reduced, allowing the propagation of more powerful laser beams.

A suitable apodizer should be capable of handling high-power laser beams without being damaged. To efficiently extract energy from the laser amplifiers, the transmission of the apodizer should be near one from its center to perhaps 3/4 of the full aperture. The rotationally symmetric transmission should then decrease smoothly to less than 10^{-4} at the edge (full aperture).[2] The apodizer should not introduce any irregular phase changes (as stepped dielectric coatings do) because the diffraction pattern will be affected by both phase and amplitude (transmission) variations. The real requirement, of course, is that the transmission of the incident laser beam through the apodizer produce a spike-free diffraction pattern in propagating through the amplifier chain.[7]

Many types of apodizers have been considered by various researchers. Radial variations in transmission have been demonstrated or contemplated in devices utilizing photographic film,[1,4] nonplanar dye cells,[8] pinhole spatial filters,[9] dielectric coatings,[5] metallic coatings,[3] electrooptical effects,[6,8] and magnetooptical effects.[6] The purpose of this letter is to suggest another type of apodizer that seems worthy of further investigation.

The apodizers described here utilize internal reflection to apodize and truncate the beam. Consider the plano-concave (negative) and plano-convex (positive) elements shown in Figure 1. The first elements (lenses) have diameter D, refractive index n, and second surface radius R. We consider the incident light to be collimated and parallel to the optic axis. Any ray in this beam can be identified by its distance from the axis r and its angle from the vertical φ (cylindrical coordinates in a plane perpendicular to the optic axis). If the incident light is linearly polarized, we arbitrarily consider the E vector to be horizontal (azimuth angle $\varphi = \pm 90°$). With this convention, the linearly polarized light will have zero reflection only at the two points given by $\varphi = \pm 90°$ and r = R sin (arctan 1/n). All rays with $r > R/n$ will experience total internal reflection (TIR) and thus have zero transmission. Figure 2 shows the predicted transmission T(r) as a function of r of linearly polarized light through the second surface for $\varphi = 0$ (T_s) and $\varphi = 90°$ (T_p). These transmissions were calculated from Fresnel's equations[10] and assumed a refractive index of 1.5. If linearly polarized light is used, the greater than zero transmission is not independent of φ. We will return to this problem later. We notice, however, that the (average) transmission of unpolarized or circularly polarized light (T_{av}) is independent of φ (rotationally symmetric) and seems qualitatively to be as desired for an apodizer. We have not calculated the diffraction patterns produced by any of these apodizers, but we feel that the possible advantages of TIR apodizers warrant further investigation.

Among their advantages are the following. Because there is no absorption, the TIR apodizer should be able to handle high-power laser beams. The attenuation at full aperture is complete ($T < 10^{-4}$) and no irregular phase changes are introduced. TIR apodizers are scalable to beams of almost any diameter, the only limits being imposed by the difficulty of fabricating very small or very large optical elements. Being passive elements, TIR apodizers do not require any additional power supplies and there is no danger of malfunctioning due to electrical failures. TIR apodizers do not require linearly polarized light as electrooptical and magnetooptical devices do. With electrooptical and magnetooptical devices, the transmission is a minimum only for one particular r value and increases for r greater than this value, unless additional apertures on apodizers are used. The transmission of TIR apodizers stays at zero for any r greater than R/n. Also, the T(r) function seems well suited for reducing diffraction effects while efficiently utilizing most of the clear aperture of the laser amplifiers. The chief disadvantages of the TIR apodizer would seem to be its sensitivity to (and effect on) the polarization of the incident light, and the severe spherical aberration of the second surface of the first element if used as a conventional lens.

The TIR apodizers are also lenses and normally the beam must be recollimated for propagation through an amplifier chain. One way to recollimate the beam would be to use the TIR element as the first lens in an afocal telescope. However, the steep angles of incidence required for TIR cause the TIR surface to introduce severe spherical aberration into the transmitted wavefront. Constructing a second lens to eliminate this spherical aberration probably will be impractical. The aberration can be reduced

by placing an approximately complimental lens near to, but not in contact with, the TIR element (Figure 1). The distance between the two elements (d) should be small to reduce the beam expansion and aberration, but at least a few wavelengths so the TIR is not frustrated. (This distance is shown greatly enlarged in Figure 1.) The figure of the first, third, and fourth surfaces could be used to reduce the aberrations (and curvature) introduced by the second surface. Note that the second element need not have the same refractive index as the first element. Anti-reflection coating of the second and/or third surface(s) would eliminate any Newton's ring type interference patterns in the transmitted beam.

If the incident light is linearly polarized, the greater than zero transmission is not rotationally symmetric and the azimuth angle of the plane of polarization (ψ) is altered by an amount that depends on both r and φ. Transmission through the second (TIR) surface changes ψ less than 8°. The third surface has a similar effect, so the $\cos^2(\Delta\psi)$ loss through a later polarizer would never be more than 8%. This maximum loss occurs only for large r where T is already low. An exact and complete calculation of $T(r,\varphi)$ for a TIR apodizer would require knowledge of all surface figures, coatings, spacings, refractive indices, and the polarization of the incident beam. There should be no TIR at the other surfaces, but near the edge there may be steep angles of incidence that result in large (polarization dependent) reflection losses. A computer program could calculate the position and direction of the beam (ray trace), transmission, and state of polarization for all r and φ. Once the transmission is known, a computer could calculate the diffraction pattern for any specified incident beam of the same polarization.

We have not calculated the exact details of the asymmetry in the transmission of linearly polarized light, nor the effect of this asymmetry on the diffraction patterns. If the asymmetry is objectionable, it could be reduced or eliminated in three ways. One way uses two similar TIR apodizers and places between them a device that rotates the plane of polarization by 90°. Such a system would have a rotationally symmetric transmission and no effect on the state of polarization for incident light of any polarization. The transmission would be given by $T_s T_p$ and is probably the most suitable of the T(r) functions shown in Figure 2. Using one concave (Figure 1b) and one convex (Figure 1a) TIR apodizer might also reduce any aberrations inherent in one TIR apodizer. A second way that might reduce the asymmetry in the transmission of linearly polarized light through one TIR apodizer would be to apply a special dielectric coating to the second and/or third surfaces. This coating would be designed to have a polarization sensitive transmission that would eliminate the polarization sensitivity of the complete TIR apodizer. A third way would be to use a specially made photographic film (or other type of apodizer) also designed to result in a rotationally symmetric transmission when used with one TIR apodizer. Because no portion of the film would have to be strongly (> 30%) absorbing, it should be possible to maintain a high damage threshold. Note that although the transmission of circular and/or unpolarized light through one TIR apodizer is rotationally symmetric, the polarization of the transmitted beam is altered in a way that is not rotationally symmetric.

With the concave TIR apodizer (Figure 1b), the diameter D would have to be carefully chosen so the extreme edge rays ($\omega' \approx 90°$) escape without intersecting the TIR surface at more outward points. No such problem exists

with the convex TIR apodizer. In this case D can be any value large enough to insure TIR ($D > 2R/n$). If modest changes in the $T(r)$ function are desired, one could consider using aspheric TIR surfaces, curving the three other surfaces appropriately, or using special dielectric coatings. If diffraction calculations show that the truncation produced by TIR apodizers is still too severe, it may be advantageous to use TIR apodizers in conjunction with other apodizers so as to take advantage of the best features of both apodizers.

In summary, we have suggested a new type of apodizer that, with further development, may prove useful in high-power laser systems. This development should include the calculation of minimum aberration configurations, detailed calculation of the transmission and state of polarization, and calculation of the diffraction patterns produced by the apodizer. By adjusting the curvatures, coatings, spacings, and refractive indices of the elements, it should be possible to make high damage threshold TIR apodizers for use in high-power laser systems.

The author appreciates helpful discussions with J. Ringlien of Owens-Illinois, Inc., and J. Forsyth of the University of Rochester, Rochester, New York.

REFERENCES

1. A. J. Campillo, B. Carpenter, B. E. Newnam and S. L. Shapiro, Opt. Comm., 10, 313 (April 1974).

2. A. J. Campillo, J. E. Pearson, S. L. Shapiro, and W. J. Terrell, Jr., Appl. Phys. Letters, 23, 85 (July 15, 1973).

3. D. H. Gill, R. C. Hyer, P. N. Mace, J. McLeod, J. E. Perry, C. H. Reed, R. H. Robertson, W. J. Terrell, and B. E. Watt, paper presented at the VIII International Quantum Electronics Conf., San Francisco, California, 1974.

4. J. Soures, Laboratory for Laser Energetics, University of Rochester, Rochester, N.Y., private communication.

5. V. Costisch, Coherent Radiation, Inc., Palo Alto, California, private communication.

6. W. W. Simmons, G. W. Leppelmeier and B. C. Johnson, Appl. Opt., 13, 1629 (July 1974).

7. J. A. Fleck, Jr. and C. Layne, Appl. Phys. Letters, 22, 467 (May 1, 1973).

8. G. Dubé, Ph.D. Thesis, University of Rochester, 1972, unpublished.

9. W. F. Hagen, J. Appl. Phys., 40, 511 (Feb. 1969).

10. See for example, F. A. Jenkins and H. E. White, Fundamentals of Optics (McGraw-Hill Book Co., Inc., New York, 1957), 3rd ed., Chap. 25.

FIGURE CAPTIONS

Figure 1. TIR apodizers, (a) convex, (b) concave. The separation of the two elements (d) is shown greatly exaggerated.

Figure 2. Transmission as a function of normalized radius (r/R) through the second surface of a TIR apodizer with refractive index 1.5.

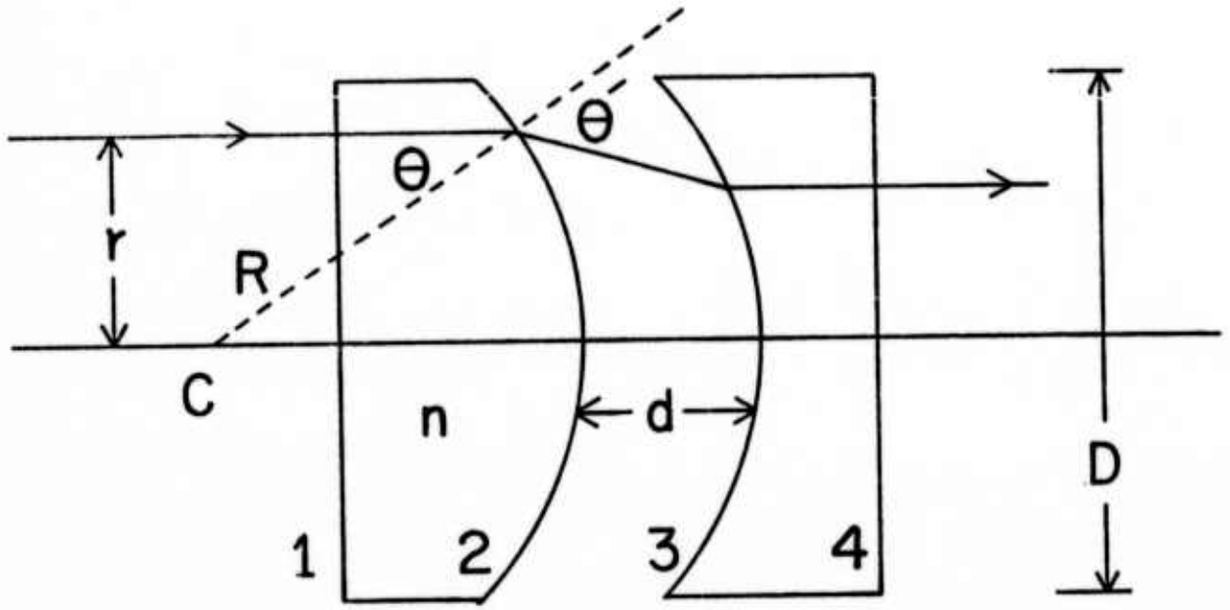

(a)

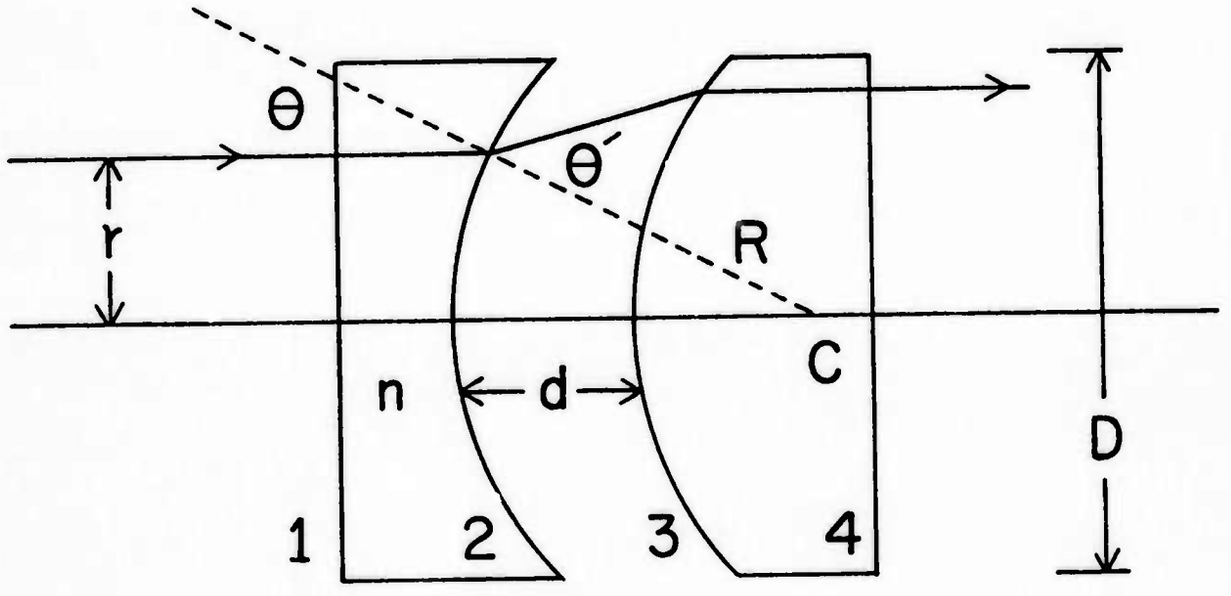

(b)

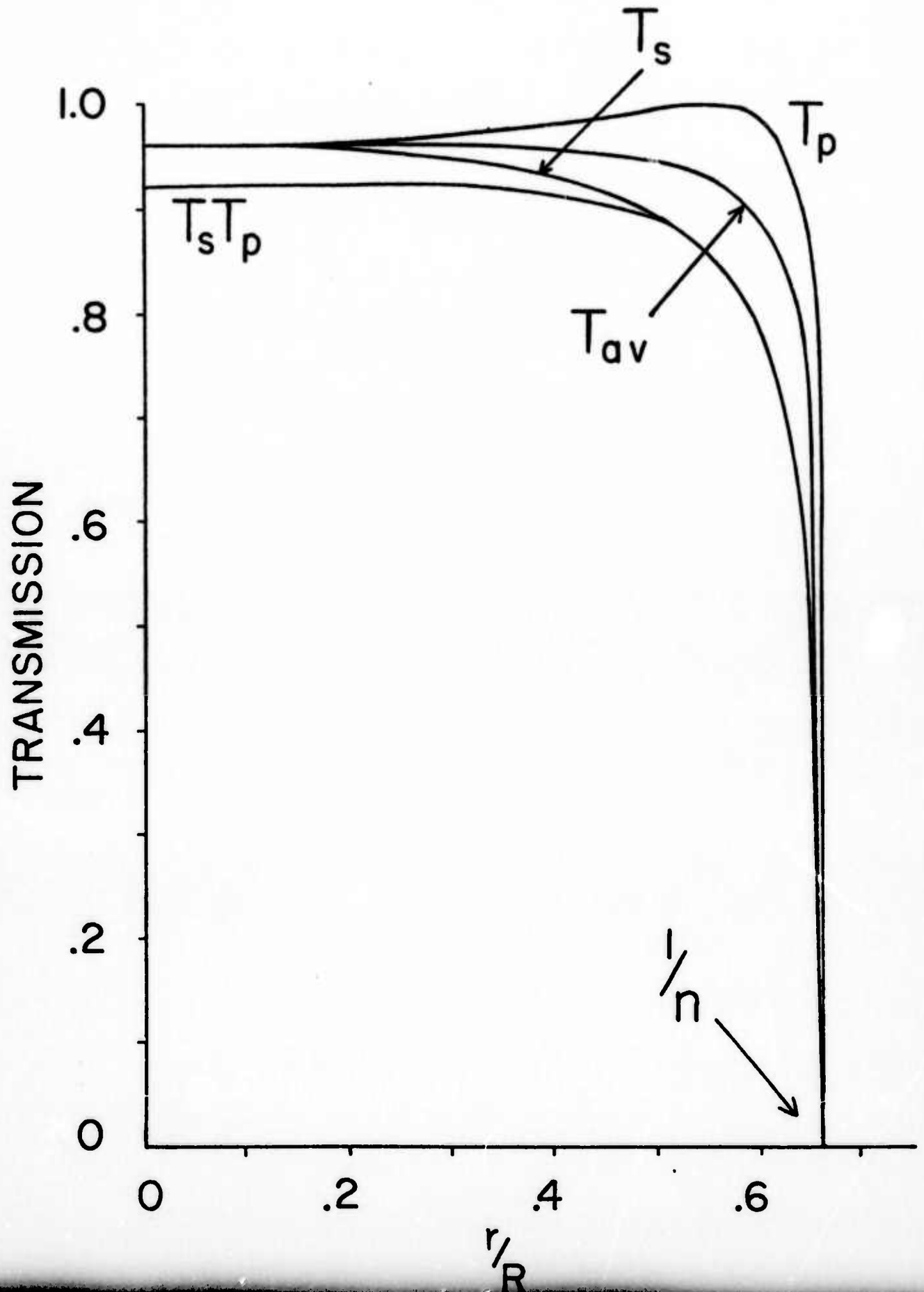
T_s
T_p
$T_s T_p$
T_{av}
1/n
1.0
.8
.6
.4
.2
0
TRANSMISSION
0
.2
.4
.6
r/R